NORWEGIAN UNIVERSITY OF SCIENCE AND TECHNOLOGY

MASTER'S THESIS

The Sensory Role of Motile Cilia

Author:
Ingrid Reiten

Supervisor:
Nathalie Jurisch-Yaksi

Kavli Institute for Systems Neuroscience / Centre for Neural Computation

Trondheim, June 2016

NTNU
Faculty of Social Sciences and Technology

Abstract

The structure of all cilia is remarkably well conserved from single-celled organisms to mammals, and they have well-established roles as motile and sensory organelles in various species. The propulsive motility of beating cilia serves high-impact biological functions in the tissues where they are located. Mutations in ciliary genes, which impair the function and presence of motile cilia, can lead to various human pathologies, known as ciliopathies. Significant advances have been made the last twenty years in understanding the importance of cilia, but much is yet unknown about the physiological role these organelles play in most tissues. Thus, more research addressing ciliary biology and function is needed to eventually bring about better ways to cure or treat people whose lives are impacted by defective cilia. Zebrafish is a unique model organism to study the role of cilia in human diseases and vertebrate development, due to their high amenability to genetic engineering techniques and the genetic and developmental similarities between humans and zebrafish. They develop multiciliated cells (MCCs) and olfactory receptor neurons (ORNs) in the olfactory pit early in embryogenesis, establishing the zebrafish olfactory epithelium as an easily accessible ciliated organ for high-throughput studies of ciliary characteristics.

In the first part of my work, I characterized cilia morphology and physiology by investigating ciliary beating in the olfactory epithelium of zebrafish larvae and discussing potential regulatory mechanisms. To do this, we developed and automated a method that allows analysis of ciliary beating frequency (CBF) from high-speed video recordings. Various stimuli were tested for a potential effect on the CBF. The frequency of beating increased upon shear force induced by water flow and upon exposure to higher temperatures (up to 32°C). Larvae were also treated with different chemicals, namely denatonium (20mM), KCl (40mM) and forskolin (25µM), but CBF was not affected in either of the treatments. Neither an optogenetic activation of ORNs modified ciliary beating. Furthermore, my findings suggest that calcium (Ca^{2+}) is not involved in regulating the CBF of motile cilia in the olfactory pit, as opposed to what has been shown for many other MCCs.

Genetic mutants with ablated or defective cilia are suited to investigate the function of motile cilia in the olfactory pit of zebrafish larvae. I characterized 5 mutant lines, with emphasis on the distribution of cilia in the olfactory pit and their beating properties, to provide new tools for future ciliary research. The zebrafish *schmalhans* (*smh*) mutant have

a mutation in *ccdc103*, which only affect motility and no other aspects of cilia, and is therefore suitable for investigation of early developmental effects solely induced by ciliary beating. Potentially, this mutant will ultimately allow us to understand the function of motile cilia in the olfactory pit and identify whether they are important for olfactory responses. By the characterization of mutant lines and adequate methods to detect ciliary beating and other ciliary properties, we hope this work will lead forth to an establishment of zebrafish genetic mutants as a toolkit for identification of molecules and pathways curing ciliopathies.

Acknowledgements

This work was carried out at the Kavli Institute for Systems Neuroscience at the Norwegian University of Science and Technology (NTNU), under the supervision of Nathalie Jurisch-Yaksi. First, I would like to thank Nathalie for giving me the opportunity of doing this project and for introducing me to this fascinating world of science. Thank you for your infinite patience, never giving up on me and for all your valuable time. Your encouraging smile and the passion you show for what you do have truly inspired me. Thank you for showing me that not all knowledge is found in books, but mostly by continuously asking questions and being curious. I would like to thank Emre, whose smile, enthusiasm and generosity is truly one-of-a-kind and which has made me feel warmly welcomed and appreciated. Also, I would like to thank Robbrecht, who has several times had to come to rescue. Thank you for always having a solution and never rolling your eyes at me. And to Filip, for breeding the *OMP:Chr2-YFP* larvae (Fig. 3.17 is thanks to you), always complimenting my singing and for "having a disco" in the lab (even though I constantly turn the radio off). A great thanks to all the members of the Yaksi lab whose companionship, eagerness to work and cooperation across nationality and scientific background is truly inspiring. You are weird and I like every one of you very much. Thank you for all your help and encouragement the last year.

Then, I would like to thank Cecilia. I am so glad our paths crossed and that I got to know you. You are an invaluable source of sugar and laughter. And, of course, Ida, who is always so kind, consoling and down to earth for the both of us. Thank you both for sharing this experience with me.

Finally, I would like to thank my family, who do not fully understand what I am doing, but still has faith in me and my work. Thank you for your unconditional support and for being there when I need you to. Anna and Silje, thank you for keeping me sane. Your conversations, support and presence have been (and are) invaluable. To Jarl, who is always online and has had to deal with a whole lot of heart-related issues the last year, and for correcting my English grammar. And to you, Jacob, for keeping me company while working on this thesis.

Table of contents

List of figures

List of tables

Abbreviations

AC	Adenylyl cyclase
ADPKD	Autosomal dominant polycystic kidney disease
AKAP	A-kinase anchor protein
BBEC	Bronchi bovine epithelial cells
Ca^{2+}	Calcium
cAMP	Cyclic adenosine monophosphate
CBF	Ciliary beating frequency
cGMP	Cyclic guanosine monophosphate
ChR	Channelrhodopsin
COPD	Chronic obstructive pulmonary disease
CP	Central pair
Dpf	Days post fertilization
DRC	Dynein regulatory complex
ENU	N-ethyl-N-nitrosourea
EtOH	Ethanol
FFT	Fast Fourier transform
GECI	Genetically encoded indicators
GFP	Green Fluorescent Protein
GPCRs	G protein-coupled receptors
HCO_3^-	Bicarbonate ion
Hh	Hedgehog
Hpf	Hours post fertilization
Hz	Hertz
IFT	Intraflagellar transport
IP3	Inositol triphosphate
MCC	Multiciliated cell
MOs	Morpholino antisense oligonucleotides
N-DRC	Nexin-dynein regulatory complex
NH_4Cl	Ammonium chloride
NO	Nitric oxide
OE	Olfactory epithelium
OMP	Olfactory marker protein
ORN	Olfactory receptor neurons
PC	Polycystin
PCD	Primary ciliary dyskinesia
PCP	Planar cell polarity
pH_i	intracellular pH
PKD	Polycystic kidney disease
ROI	Region of interest
sAC	Soluble adenylyl cyclase
TEM	Transmission electron microscopy
TRPV	Transient-receptor potential vanilloid
Vangl2	Van Gogh-like protein 2

Chapter 1.

Introduction

1.1 The rediscovery of cilia

Cilia are slender, microscopic, hair-like structures that extend from the surface of cells. The structure of all cilia is remarkably well conserved from single cell organisms to mammals, and at present they have well-established roles as motile and sensory organelles in various species. For a long time, they were thought to only function as oars for small organisms to propel through water. In fact, cilia are the oldest known cellular organelles, first described in 1674 by Antony van Leeuwenhoek. He composed several letters with descriptive tales about these small, peculiar animals with "incredibly thin feet" (Toledo-Pereyra, 2009). The Danish naturalist Otto Müller coined the term cilium (Latin for 'eyelash') a century later, in 1786 (Beales and Jackson, 2012). Since then, the structure and beating of motile cilia and flagella have fascinated biologists. A century of investigation led to the observance of cilia lining the epithelia of brain ventricles, spinal canal, respiratory tract and the fallopian tube, and the high clinical importance of the propulsive motility of multiciliated cells (MCCs) was eventually acknowledged.

Zimmerman discovered the immotile cilium in 1898 as he observed non-motile, solitary cilia on epithelial cells lining the kidney tubules. He proposed a name and even a sensory function (Bloodgood, 2010), but this was soon forgotten and immotile cilia were assumed to be a vestigial cellular feature serving no purpose (Webber and Lee, 1975). The name 'primary cilium' was first used in 1968 as an immotile cilium was observed to emerge in early stages of all cells, including MCCs before multicilia assembly (Sorokin, 1968). An explosive interest in primary cilia arose in the beginning of the 21st century as it was clearly demonstrated that they exhibited sensory functions and in fact enabled us to see, hear and smell, as well as being crucial for normal development and organs to function properly (Muhammad et al., 2012). A duality within the ciliary research field had emerged, which separated immotile and motile cilia. Suddenly the interest in primary cilia had eclipsed that of its motile counterpart.

Within a decade, the picture of 'cilia' expanded into a brand new field of biomedical research as evidence by a net increase in publications since 1998. At this time, seminal publications led to new insights in ciliary function and biology, in particular focusing olfactory receptor neurons (ORNs) and the primary cilia protruding from the dendritic knob. New discoveries unraveled the molecular basis of the intraflagellar transport (IFT) complexes, which are essential for assembly and maintenance of cilia and flagella, and it was revealed that a specialized cilia in embryos are critical for nodal flow and organ asymmetry, and (Cole et al., 1998, Beales and Jackson, 2012). Cilia quickly attracted attention as it was linked to polycystic kidney disease (PKD) in humans (Pazour et al., 2000) and to vertebrate development as Hedgehog signaling was found to be controlled by primary cilia (Huangfu et al., 2003). Later, also other signaling pathways important for development were revealed to intricately depend on this forgotten sensory organelle.

As the interest in primary cilia increased, the functions of motile cilia have also elaborated. Reports from the last two decades have identified sensory reception as an attribute of not only primary, but also motile cilia. It is hypothesized that motile cilia are more intricately linked to biological functions in the body than first thought (Jain et al., 2012). Thus, the clear distinction between these two organelles will most likely blend in the coming years. Overall, publications within the field of ciliary research has increased twentyfold since the 1980s and are now represented with its own journal, Cilia. The journal covers a broad and variable field embracing a wide range of topics. It contains reports about detailed microscopy, biophysics and fluid dynamics to ciliary biology, diseases and developmental dysfunctions. Today the field continues to grow, particularly focusing on inherited diseases caused by dysfunctional cilia (Beales and Jackson, 2012).

1.2 What are cilia?

Cilia and flagella are thin protrusions of cells that extend into the extracellular environment. They mainly have two functions: to generate a regular beating waveform or to serve as a sensory compartment of the cell. The microscopic, hair-like structures house a tubulin-based axoneme, which seems to be conserved throughout evolution. The internal structure is similar in all organisms carrying cilia, ranging from the earliest unicellular organisms to humans (Vincensini et al., 2011). Unicellular organisms use motile cilia to swim and to sense nutrients or obstacles in the environment (Tamm, 1994). Evolution is however parsimonious and recycle old design to evolve new functions if it can. This is the case for the cilium, whose ancient structure has

been preserved through millennia, but acquired many different functions in higher order multicellular organisms (Breunig et al., 2010).

Cilia generate flow or play a structural, sensory or signaling role in many tissues in humans. A primary cilium is present on almost every eukaryotic cell at least at some point during the life cycle (Wheatley et al., 1996), and specialized tissues and tracts are lined with multiciliated cells to exert propulsive flow. Each class of cilia is highly linked and adapted to a biological function, which range from reproduction and fertility, clearance of pathogens from airways, sensory or developmental signal transduction, left-right patterning of embryo body-axis and more (Choksi et al., 2014). Hence, defects in cilia have the potential to affect multiple organs and induce diverse effects, such as developmental impairments, heart and kidney disease, respiratory dysfunction, anosmia and neurological disorders (Fliegauf et al., 2007a). The universal importance of cilia is apparent by the severely disrupted phenotype associated with ciliary defects that are shared by all animals which possess cilia.

1.2.1 Flagella and cilia

Flagella and cilia have earlier been separated as two different structures. Ciliates and flagellates are both subgroups of protozoans and likely represent two different evolutionary lineages as they behave differently and live in different habitats (Lee and Kugrens, 1992). In addition, cilia and flagella differ in length, number per cell and beating pattern. Motile cilia are usually short, highly numerous and beat in a coordinated whip-like pattern to provide motion (i.e. *Paramecium*) (Funfak et al., 2015). Flagella are longer, typically only 1-8 per cell and beat in more of a wave-like fashion (i.e. *Chlamydomonas*). However, since cilia and flagella are of the same origin, and both maintained and generated through similar mechanisms (Snell et al., 2004), there is no distinct border between these two terms as of today. Therefore, these two concepts will be used interchangeably in this text.

1.2.2 Model organisms and cilia diversity

A fascinating high diversity of model organisms are available for ciliary studies. Ciliates and flagellates have led forth to many major discoveries about cilia as we know it today. This is much because they are higher in numbers, smaller in size and more amenable to genetic manipulation per se than higher order model organisms. For instance, the biflagellate green algae *Chlamydomonas* led to the discovery of IFT, the main mechanism behind ciliary assembly and maintenance (Kozminski et al., 1993). Unicellular organisms are however not ideal for vertebrate studies. Neither are mammals, as cilia are not easily approached and it is necessary

to prepare for biopsies and surgeries. Cilia are also abundant in other higher order organisms, such as *C. elegans*, *Xenopus*, mice and zebrafish (Vincensini et al., 2011). These have all shown highly useful as ciliary model organisms and have provided additional insights in various aspects of ciliary biology and functions, which can more easily be extrapolated to mammals. Due to the different biological functions cilia have acquired, they exist in many different shapes and sizes dependent on tissue, species and age (Fig. 1.1)(Silverman and Leroux, 2009).

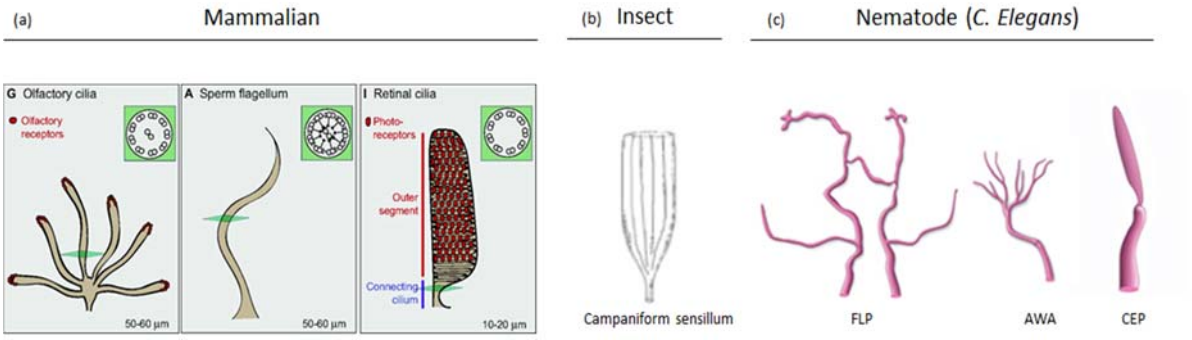

Figure 1.1. Diversity of cilia. (a) Mammalian cilia; olfactory cilia, sperm flagellum and rod photoreceptor cilia. Average length is given in the bottom right of each panel and the ultrastructure of the axoneme in the top right corner; (b) insect campaniform sensillum mechanosensor; (c) various cilia of *C. elegans*; FLP (senses touch, response: avoidance), AWA (senses volatile odorants, response: mediates attraction), and CEP (senses surface texture, response: slows down on encountering food). Modified from (Altun, 2010), (Choksi et al., 2014) and (Silverman and Leroux, 2009).

1.3 Two classes of cilia

There are two main types of cilia; namely those that can move and those that can not, referred to as motile and primary cilia respectively. Motile cilia propel water or mucus and are densely packed on specialized, terminally differentiated cells (Brooks and Wallingford, 2014). Primary cilia are solitary, immotile and a feature of nearly every mammalian cell (Wheatley et al., 1996). In fact, even MCCs develop an immotile cilium some days before the multicilia assembly (see section 1.5.2)(Sorokin 1968). In cilia, microtubules are coupled in pairs and are arranged as a circle of 9 outer doublets. Depending on the presence of a central pair (CP), the structure is referred to as either 9+0 or 9+2. Normally all motile cilia have a 9+2 structure and immotile cilia have a 9+0 structure, but there are exceptions to this rule. Per today we distinguish between four subtypes of cilia: motile 9+2 (i.e. ependymal cilia), motile 9+0 cilia (i.e. nodal cilia), sensory 9+2 cilia (i.e. kinocilium and stereocilia in the inner ear) and sensory 9+0 cilia (i.e. osteocyte cilia or photoreceptor connecting cilia)(Fliegauf et al., 2007b).

1.3.1 Motile cilia

Multiciliated cells are post-mitotic cells normally decorated with dozens of motile cilia, sometimes even several hundred (Brooks and Wallingford, 2014). In vertebrates, MCCs beat in a coordinated and polarized manner and drive a directional flow across tissues. They are found i.e. in the inner linings of the respiratory tract, important for protective mucus clearance (Chilvers and O'Callaghan, 2000); in the spinal cord and ventricles of the brain, important for circulation of the cerebrospinal fluid and neural migration (Sawamoto et al., 2006); and, in the fallopian tubes, required for ovum transport (Lyons et al., 2006, Brooks and Wallingford, 2014). The propulsive flow created by the densely packed cilia is essential for proper functioning of the respective tissues (Fliegauf et al., 2007b). A specialized class of motile cilia are solitary expressed in cells located in the embryonic node, the organizer of gastrulation in vertebrates. The specialized motile cilia are devoid of the CP (9+0 structure) and beat in a rotating fashion. This beating is thought to create a directional fluid flow that triggers asymmetric gene expression. Nodal cilia are relevant subjects of ongoing research but will not be discussed in more detail in this text (see i.e. (Essner et al., 2005)).

There is no consensus regarding a baseline rate of CBF for the various MCCs, mostly due to the numerous and varied techniques employed to measure CBF. Moreover, CBF obtained from cells in culture, *ex vivo* or *in vivo* preparations may differ by twofold (O'Callaghan et al., 2012). A wide range of frequencies from 5-20 Hz has been reported for the CBF in the human fallopian tube (Lyons et al., 2006); CBF of respiratory MCCs are normally reported below 12 Hz in culture (i.e. (Lansley and Sanderson, 1999)) and around 20-25 Hz in physiological conditions (～37°C, tissue maintained in a balanced salt solution) (Delmotte and Sanderson, 2006); and 20-40 Hz is usually reported for cilia of ependymal cells (O'Callaghan et al., 1999). The crucial role of motile cilia and the flow they generate is seen in ciliopathy patients. Patients with primary ciliary dyskinesia (PCD), in which cilia beat inefficiently or not at all, suffer from i.e. chronic cough, fatigue and shortness of breath (Bush et al., 2007).

1.3.2 Primary cilia

Primary cilia are in general shorter than their motile counterpart, measuring about 1-2μm (Muhammad et al., 2012). They serve important roles during embryonic development and are essential for many organs and tissues to function normally. First, they enable us to see, hear and smell, being an essential component of visual, auditory and odorant sensory tissues (Fliegauf et

al., 2007b), and they also serve important sensory roles in non-sensory tissues (Muhammad et al., 2012).

Primary cilia are signaling centres during vertebrate development, participating in signal transduction pathways such as Hedgehog (Hh) (Huangfu et al., 2003) and Wnt (Germino, 2005). The Sonic Hedgehog (SHH) pathway is essential for organogenesis and tumorigenesis as well as setting up the early body plan of most animal embryos. Moreover, primary cilia play a role in regulation of blood pressure and energy metabolism. In Bardet-Biedl syndrome, a rare human disorder characterized by obesity, polydactyly, hypertension and diabetes, 5 out of the 8 mutated genes discovered so far encode proteins localized to primary cilia or basal bodies (Pan et al., 2005). In addition, cilia are present on brain cells and involved in the response to leptin, a molecule involved in weight regulation (Stepanyan et al., 2003). Lastly, primary cilia are also mechanosensors that can sense flow. Defects in mechanosensation has been suggested as the cause of the human syndrome Polycystic kidney disease (PKD), an inherited disorder in which water-like fluid filled cysts develop primarily within the kidneys (Yoder, 2007). Most of the disrupted genes in human PKD have been localized to primary cilia and mutations seem to be involved in sensory transduction rather than assembly or motility.

1.4 Cilia architecture

1.4.1 Ultrastructure of the axoneme

The cilium is a highly specialized extension of the cell membrane. Cilia are slender structures, only measuring 0.2 - 0.3μm in diameter, with an internal structure made up of microtubules (Salathe, 2007). In a barrel-shaped network, the microtubules are arranged in a circle of nine outer doublets. Depending on if the cilium is motile or not there may be a central pair (CP) of microtubules (see section 1.1.3)(Lindemann and Lesich, 2010). Doublets consist of a complete A-tubule of 13 protofilaments and an incomplete B-microtubule of 10 protofilaments. They are polymerized such that the fast growing plus-end is at the tip of the axoneme and the slow-growing minus-end at the base. Further, there are intricate interactions between microtubules and other axonemal proteins, such as nexin links connecting the microtubule doublets and radial spokes reaching inward (Fig. 1.2). The CP is surrounded by a protein sheath with CP-projections that can interact with the radial spokes (Gibbons, 1961). Dynein motors connect to the A-tubule in an outer and inner row, providing ciliary motility by ATP hydrolysis (see section 1.3 for ciliary motility)(Roberts et al., 2013). The axoneme is a repetitive structure, in which a

pair of nexin links, outer and inner dynein arms, and radial spokes are arranged in distinct units along the entire length of the axoneme in a characteristic 96-nm repeat (King, 2010).

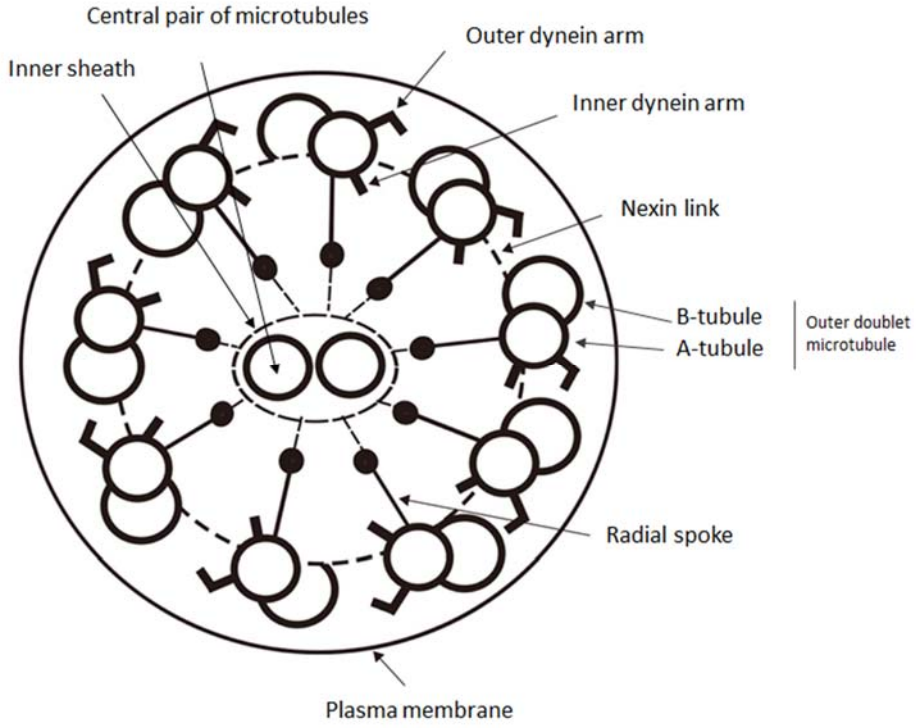

Figure 1.2. Ultrastructure of cilia. Doublet microtubules consist of a complete A-tubule and an incomplete B-tubule, lined in an outer ring. Doublets are connected by nexin links. Each A-tubule has one outer and one inner row of dynein arms, which provide motility to cilia by ATP hydrolysis. Radial spokes reach inward from the A-tubule to the inner protein sheath of the CP. Most motile cilia are of 9+2 axonemal configuration. Modified from (Horani et al., 2014).

1.4.2 Centriole formation and ciliogenesis

The assembly of axonemes occurs at the cell surface above a centriole-like structure known as the basal body. Centrioles consist of microtubules arranged in 9 sets of triplets built from A-, B- and C-tubules, where assembly of polymerized axonemal doublets occurs directly on the triplet microtubule structures (Szymanska and Johnson, 2012). The basal body consists of two centrioles, which are orthogonally positioned relative to each other (Fig. 1.3c). They differ in age and functionality and only the oldest gives rise to the extending cilium. The daughter centriole develops from fibrillar structures extending from the base of the mother centriole and remains partly attached (Sorokin, 1968). Still, both centrioles are required to nucleate a cilium. The linkage between the two is suggested to be important for tight control of ciliary assembly (Pearson and Winey, 2009). Centrioles also assemble into microtubule-organizing centres which separate chromosomes in dividing cells, but as the cell exits from mitosis and enters G0

they become the organizers of cilia and flagella (Quarmby and Parker, 2005). They migrate to the cell periphery and matures into basal bodies from which axonemal microtubules extend (Szymanska and Johnson, 2012). Basal bodies are anchored by a basal foot protruding from the side of the basal body and a striated rootlet, a prominent cytoskeleton matrix originating from the proximal side of the basal bodies (Bornens, 2008).

Multiciliated cells are terminally differentiated cells that do not divide further. They duplicate their centrioles following their last mitosis, reaching up to 200-300 per cell, in order to generate multiple cilia at the same time. These centriole duplication pathways exist only in MCCs and are not involved in regular centriole duplication observed during mitosis (Brooks and Wallingford, 2014). There are two mechanisms identified so far, namely the centriolar and the acentriolar pathway. In the centriolar pathway, several procentrioles are simultaneously produced by a mother centriole. The mechanisms underlying this pathway remain a mystery as the number of procentrioles produced varies among cells for unknown reasons and the identity of the core proteins of the machinery is not yet identified (Dawe et al., 2007). In the acentriolar pathway, procentrioles form around intermediate structures called deuterosomes. These are dense spheroidal structures residing in the cytoplasm of the cell, providing the templates for new centrioles. Later, the newly generated centrioles migrate to the apical plasma membrane and nucleate ciliary axonemes (Brooks and Wallingford, 2014).

Even though the ciliary membrane is continuous with the plasma membrane of the cell, it has a distinct protein and lipid content (Rohatgi and Snell, 2010). This is permitted by a specialized transport system dedicated to cilia and a sorting process occurring at the base of the cilium controlling which proteins may enter. Firstly, ciliary transport is mediated by the intraflagellar trafficking machinery which brings new cargo from the cell body to the tip of the axoneme and brings old material back for recycling (Kozminski et al., 1993). Secondly, cilia selectively concentrate only material that is necessary for motility and/or sensory-mediating transductions from the cell body. This is achieved by a pore-like complex made of the transition zone and transition fibers working in cooperation with the IFT machinery (Deane et al., 2001). Transition fibres anchor the microtubules to the plasma membrane of the cell, emerging from the B-tubules of the distal end of the basal body triplet. The adjacent transition zone comprise champagne-glass structured Y-links which attach the axoneme to the membrane via parallel strands of membrane particles, the ciliary necklace (Fig. 1.3)(Szymanska and Johnson, 2012).

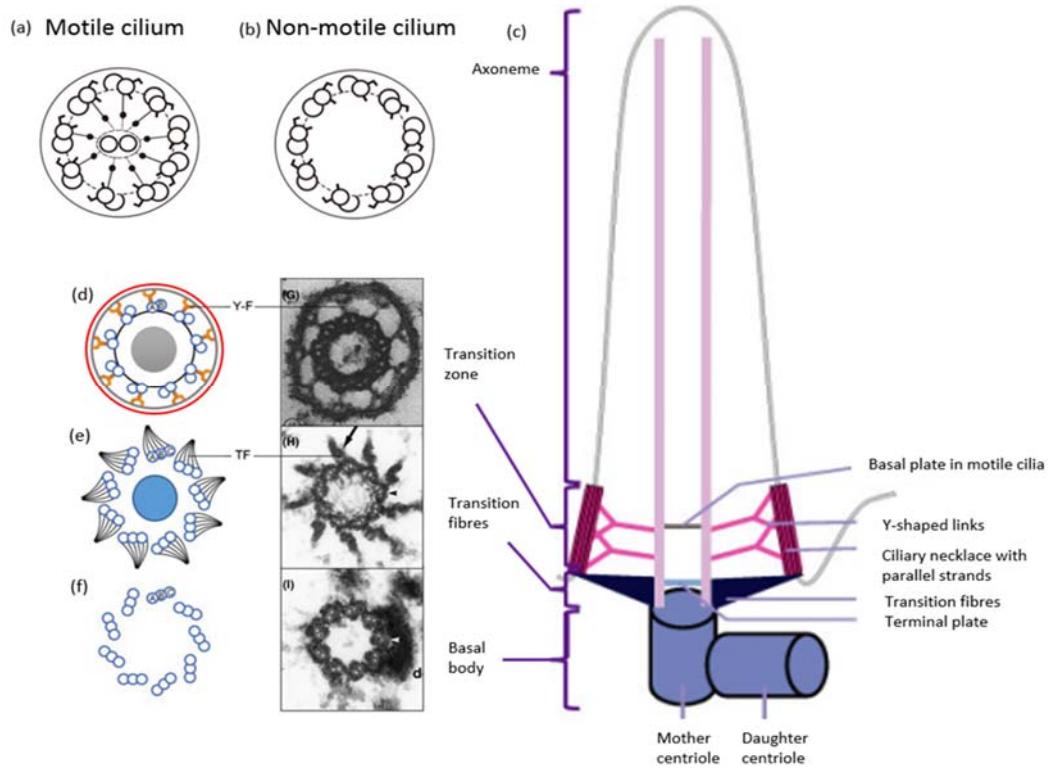

Figure 1.3. Structure of the basal body, transition zone, and ciliary axoneme. (a,b) Cross-section of axoneme in motile and non-motile cilium. In non-motile cilium the CP, radial spokes and dynein arms are absent. (c) Schematic longitudinal view of a motile cilium. Microtubular doublets of the axoneme extend from the 9 triplet microtubular structure of the mother centriole, while the daughter centriole remains attached through rootlet filaments. Illustrative and TEM cross-sections of (f,i) the nine triplet structure of the basal body (A,B,C-tubules); (e,h) the distal part of the basal body. Transition fibres (TF) attach to all three subfibres of the basal body and connect to the plasma membrane. The basal body is closed at its outer end by a terminal plate; (d,g) the transition zone, characterized by parallel strands of membrane particles, called the ciliary necklace (red outer circle). Y-links (orange) connect the membrane particles of the ciliary necklace to the axoneme. Motile cilia display a basal plate from which the CP extend. Modified from (Horani et al., 2014), (Pedersen et al., 2012) and (Szymanska and Johnson, 2012).

The first evidence of the intraflagellar trafficking system was made in *Chlamydomonas* (Kozminski et al., 1993). IFT particles move along the microtubules, loaded with cargo proteins and attached to a motor protein complex. Anterograde transport is mediated by kinesin 2 and retrograde transport is mediated by cytoplasmic dynein 1b/2 (Roberts et al., 2013). Even though the functions of cilia and flagella have evolved considerably, the same ancient process mediates the assembly and maintenance of these organelles. Interestingly, IFT machinery is not present in organisms that lack cilia, such as *Arabidopsis thaliana* and yeast (Rosenbaum and Witman, 2002). IFT particles consist of around 16 proteins divided into two complexes bridged by accessory proteins, known as complex A and B. Complex A consists of 6 subunits (IFT144, IFT140, IFT139, IFT122A, IFT122B, and possibly IFT143) and complex B consists of 10 subunits (IFT172, IFT88, IFT81, IFT80, IFT74/72, IFT57/55, IFT52, IFT46, IFT27, and IFT20)(Cole, 2003). Retrograde movement returns leftover molecules, as well as kinesin

motors, back to a large pool of IFT components at the base of the cilium, where they can be recycled (Rosenbaum and Witman, 2002). Disruptions within the IFT complexes affect ciliary assembly, maintenance and function and is often the cause of various ciliopathies (Cole, 2003).

1.5 Mechanisms behind ciliary beating

1.5.1 Axonemal dyneins

Dyneins are motor proteins with dual functions. Axonemal dyneins, which provide motility to cilia, were the first to be discovered. Later, cytoplasmic dyneins were found, which transport cargo toward the minus ends of microtubules. Each dynein is a large molecular complex that consists of one to three large polypeptide chains: heavy chains (~500 kDa), intermediate chains (~50-140 kDa) and light chains (8-45 kDa). About 70% of the heavy chains makes up a globular head domain, important for attachment to cargo. Thin stalks extend from the head domains and connect to a microtubule base by their intermediate and light chains (Roberts et al., 2013).

Dynein heavy chains are classified into nine major groups. Two exert minus end-directed transport, one in the cytoplasm (cytoplasmic dynein 1 heavy chain) and one along cilia or flagella (cytoplasmic dynein 2), while the remaining 7 function within the axoneme to provide ciliary beating (Howe et al., 2013). Fig. 1.4a illustrates the outer dynein arm of *Chlamydomonas,* which consist of three distinct heavy chains with different motor properties (α, β, γ). Each heavy chain connect to the adjacent B-tubule by a coiled-coil stalk, and the γ – heavy chain connects the dynein molecule to its base, the A-tubule, by its intermediate and light chain (King, 2010).

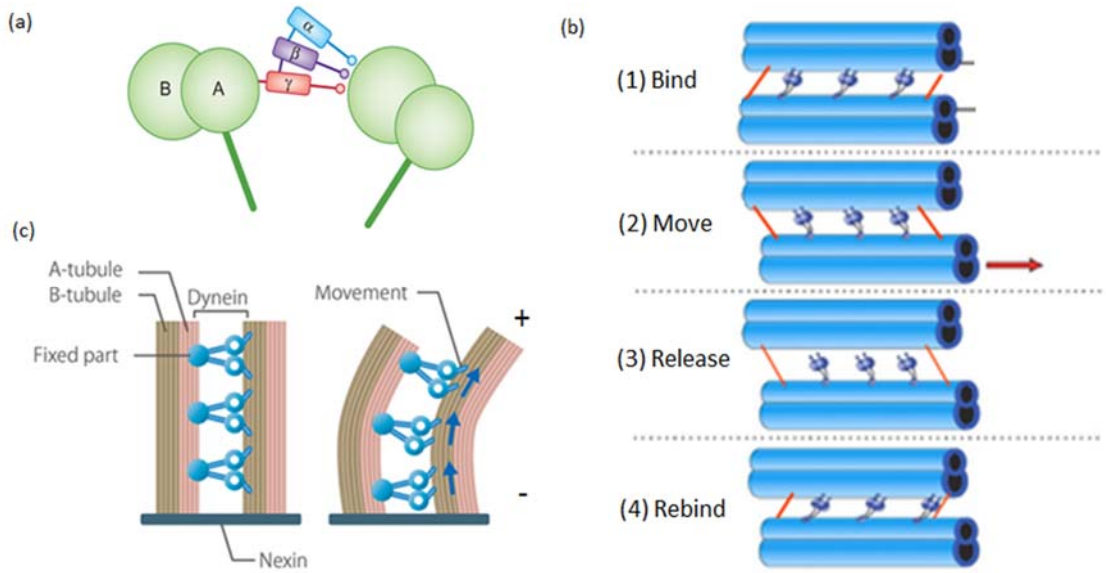

Figure 1.4. The dynein molecule and how they induce ciliary bending. (a) Schematic cross-section through two axonemal doublets connected by an outer dynein arm. In *Chlamydomonas* each outer arm contain three distinct heavy chains (α,β,γ) with different motor properties. They connect by a coiled-coil stalk to the adjacent B-tubule. (b) Illustration of how two axonemal doublets slide relative to each other through 4 steps.(1) Dynein molecules are attached to its base by light chains (bottom doublet) and heavy chains connect to cargo (top doublet). (2) Dyneins move, (3) release and (4) rebind to repeat the process. Red lines: nexin bridges. Resultantly, the cargo doublet move to the left and base doublet move to the right. (c) As doublets are firmly connected at their base and by nexin links, dynein activity leads to microtubule bending. This causes the ciliary movement. Modified from (King, 2010) and Division of Life Sciences[1].

Dynein arms form bridges between the A and B-subfibers of two adjacent doublets (Fig. 1.4a) and upon ATP hydrolysis by dyneins, they slide relative to each other (King, 2010). The conformational change of the dyneins as they attach, exert its force and release is the main motor behind any ciliary movement. If linkages between doublets are removed by proteolysis, dynein molecules activated by ATP move the A-tubule (to which it is attached) toward the base of the axoneme and the B-tubule (to which it "walks" along) toward the tip of the cilia (Fig. 1.4b). As the tubules are firmly anchored to the basal body and by nexin links, a bending deformation is the only possible outcome of local sliding of filaments (Fig. 1.4c). Sliding motions need to be tightly controlled in order to allow the cilium to beat properly (Camalet and Julicher, 2000).

1.5.2 The ciliary beat cycle

Epithelial cilia performs an active whip-like motion to propel fluid in a certain direction. The ciliary beat cycle consists of two phases: a fast effective stroke and a slower recovery stroke,

[1] Division of Life Sciences, the University of Tokyo. Found at: *http://csls-text3.c.u-tokyo.ac.jp/active/17_01.html*

separated by a resting period. A cilium is fully extended throughout the effective stroke and beats toward the cell membrane. After a short rest it swings backward almost 180° in a recovery stroke, keeping close to the cell surface (Fig. 1.5). Generally, the effective stroke is thought to be approximately 2-3 times faster than the recovery stroke (Salathe, 2007). In *Paramecium*, the effective stroke lasts 9 ms and the recovery stroke about 26ms (Guirao and Joanny, 2007). Beating can be planar, where the recovery stroke goes back in the same plane as the effective stroke, or three-dimensional, where the cilium sweeps backwards and to the side (i.e. in *Paramecium*)(Guirao and Joanny, 2007). It was thought for many years that respiratory cilia beat with a sideway recovery sweep (Sanderson and Sleigh, 1981), but by the advent of high-speed video recordings it was found that both respiratory and ependymal cilia beat with a planar stroke (O'Callaghan et al., 2012).

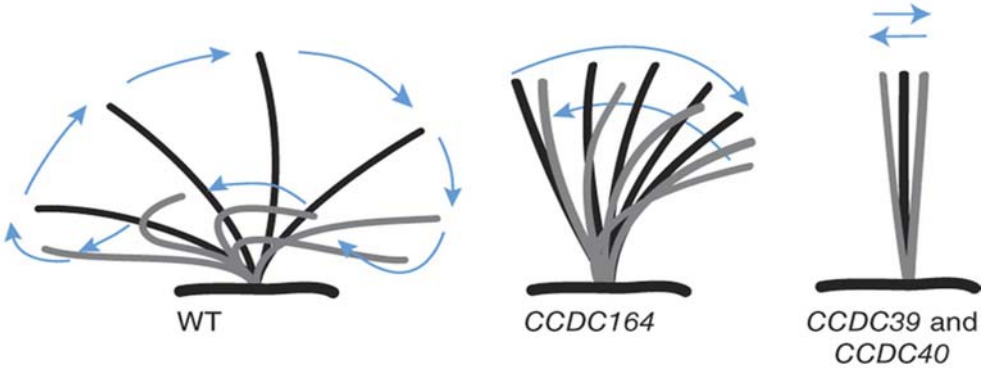

Figure 1.5. The ciliary beat cycle of human respiratory cilia.. Wild-type (WT) ciliary beating is characterized by a series of bends which originate at the base and propagate toward the tip. Beating occurs in two stages: an effective stroke (black) and the recovery stroke (grey). Cilium extend perpendicularly to the cell membrane and remains extended throughout the effective stroke. During the recovery stroke the cilia goes backward from the end-position of the effective stroke and stays near the cell surface until it reach the position to initiate another effective stroke. Mutations in genes of regulatory complex subunits essential for ciliary motility lead to impaired beating. Ciliary beat of mutants appear stiff and rigid with strongly reduced amplitude. A less severe phenotype is seen for CCDC164 mutants compared to CCDC39 and CCDC40 mutants. Modified from (Wirschell et al., 2013).

The ciliary beat pattern is highly dependent on proper functioning of axonemal subcomponents and assembly factors, such as dynein arms and radial spokes. Mutations in genes encoding axonemal subunits that are important for motility have been identified as disease-causing factors in PCD. For instance, mutation of i.e. CCDC164, CCDC39 or CCDC40 leads to severe defects in assembly of the Nexin-Dynein Regulatory Complex (N-DRC) and impair ciliary beating. Wirschell et al. demonstrated a combined defect of N-DRC and inner dynein arm assembly for CCDC39 and CCDC40 mutants, which could explain why the beating amplitude is less severe inn CCDC164 mutants than the two former (Fig. 1.5)(Wirschell et al., 2013).

1.5.3 How the cilium works as a motile organelle

It is established that bending occurs as a result of microtubule sliding by dynein activity in axonemes. How this is coordinated to produce beating is however still a matter of intense discussion. Numbering of the microtubule doublets makes the discussion easier. The nine microtubular doublets of motile cilia have distinct features so that they can be separated and assigned an index number. This was first proposed by Afzelius in 1959 and is now widely accepted within the field (Afzelius, 1988). Numbering starts with the doublet that is approximately perpendicular to the plane of the CP and continues in the direction of the dynein arms (Fig. 1.6). This numbering system can however not be directly applied to cilia whose CP rotates or twists, such as in cilia of some plants or unicellular organisms (Afzelius, 1988).

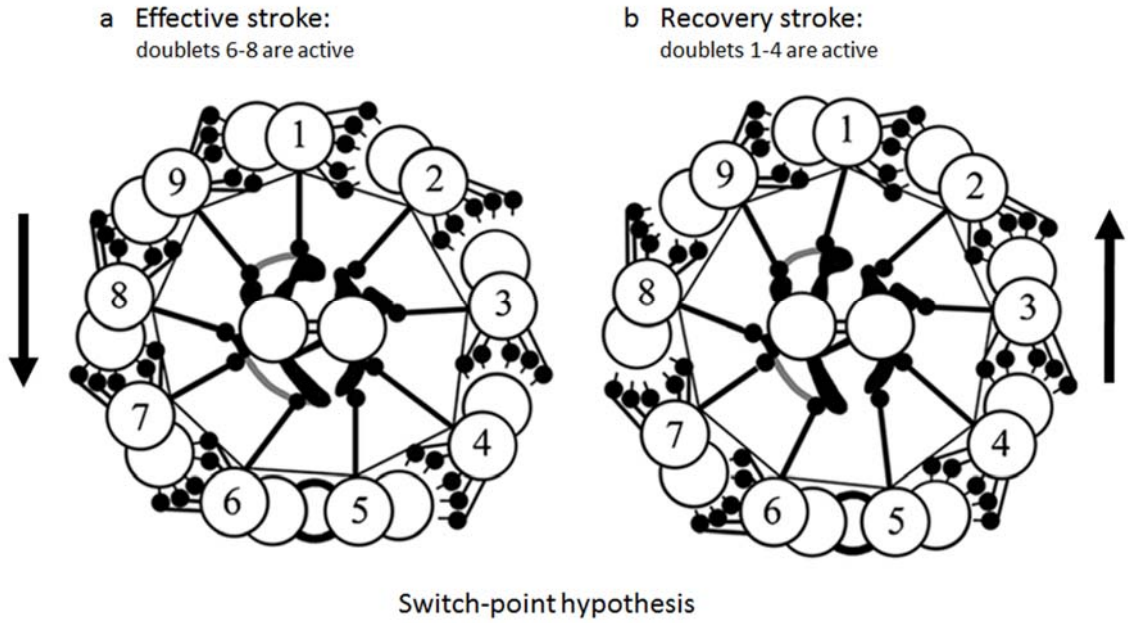

Figure 1.6. The switch-point hypothesis of ciliary motility. Doublets are numbered 1-9. Numbering starts with the doublet that is approximately 90 degrees to the plane of the CP. As illustrated, doublets 5 and 6 are permanently linked, preventing sliding. The "switch-point" hypothesis suggests that doublets 6-8 are responsible for bending of the axoneme in the effective stroke (a, directed towards doublets 5 and 6) and doublets 1-4 are responsible for bending of the axoneme in the recovery stroke (b, directed towards doublet 1). Arrows indicate directions of the respective strokes. Modified from (Linck et al., 2016).

It was observed a pattern within ciliary beating, where cilia were consistently directed towards doublets 5 and 6 in the effective stroke and toward doublet 1 in the recovery stroke (Afzelius, 1988). Doublet 5 and 6 are permanently linked in most cilia, and any sliding between these doublets is prevented (Lindemann and Lesich, 2010). Later, in experiments by Satir and Matsuoka, it was found that only a subset of dynein arms were active in each part of the stroke. They reported that doublets 6-8 were active in the effective stroke and doublets 1-4 were active

in the recovery stroke (Fig. 1.6)(Satir and Matsuoka, 1989). Followingly, they proposed that beating then occurs from activating the two opposing dynein-bridge sets alternately, in which the activity is switched between the opposing sets during a ciliary beat. This is now known as the 'switch-point hypothesis' and is generally accepted as a valid summary of what is known today (Lindemann and Lesich, 2010). Thus, this answers how bending waves can be generated by action of dynein motors within the cilia. Conclusively, the natural follow-up to the question is: what controls the switching between dynein-bridge sets?

As of today, there are three major arguing views on how the axoneme may switch between opposing dynein-bridge sets during a beat and allow controlled movement. A mechanistic approach, the 'geometric-clutch-hypothesis', proposes the switching mechanism to rely on the simple mechanical effect brought about by bending itself. An accumulated tension in the bent region of the axoneme can i.e. terminate dynein activity and perhaps even reactive the other set of dynein arms (Lindemann and Lesich, 2010, Linck et al., 2016). Secondly, the 'CP-spoke control mechanism' is a mechano-chemical view which is based on the CP of the axoneme and its connections to the dynein regulatory complex (DRC). A shear force between microtubules and the CP upon bending may activate an enzymatic regulatory cascade and send a signal through the CP-DRC linkage to the dynein arms (Smith and Yang, 2004, Lindemann and Lesich, 2010). The third theory is based on the direct outcome of dynein activity, where the oscillatory properties belong to the dyneins themselves. In the simplest version of this theory, a bend is created by a sequential activation of dynein arms (Sugino and Naitoh, 1982). This has however been challenged by the small step-length of dyneins, which is not able to generate a full stroke as is seen in nature. To overcome this issue, i.e. multiple dynein-bridge cycles have been suggested (Lindemann and Lesich, 2010).

1.6 Cilia-driven fluid flow

In order to drive an effective fluid flow, a given epithelium must control multiple variables. These include the arrangement of cilia in a cell array, the length of the cilia, the metachronal relation between them, and the ciliary beating frequency (CBF). All of this require coordination at both cell- and tissue level (Kim et al., 2011). For an effective fluid flow, all cilia should (1) exert a stroke that is optimal regarding energy expenditure, (2) beat in the same direction, and (3) beat in a coordinated manner and form a metachronal wave (Sleigh, 1989, Kim et al., 2011, Elgeti and Gompper, 2013). Characteristics of an energy-efficient ciliary stroke, directional beating and metachronal relations between beating cilia will be revised below.

1.6.1 Ciliary beating pattern with optimal efficiency

Sleigh characterized cilia as motile organelles whose activity is dominated by viscous effects due to their small size. He proposed that as water adheres to a cilium, a zone of water surrounding each cilium is dragged forward in the direction of the effective stroke as the cilium beats. As water is also restrained by its viscous adhesion to the cell surface, the extent of water propulsion by cilia will vary with the height of the cilium above the cell surface (Sleigh, 1989). Hence, according to Sleigh, the amount of water a cilium can move vary throughout the beat cycle. As the cilium bends and moves backward in the recovery stroke it carries a much smaller volume back than what was propelled forward (Fig. 1.7). Conclusively, the net volume propelled per beat will necessarily depend on the length of the cilium and the frequency of the beat.

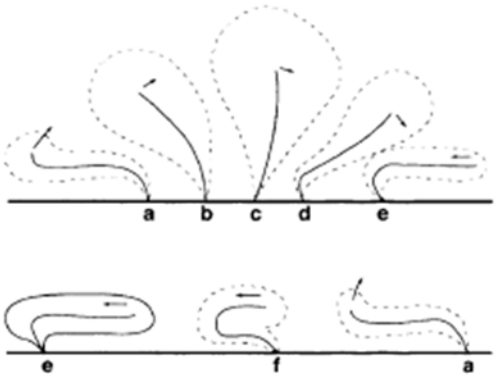

Figure 1.7. Propulsive effect of a cilium throughout the ciliary beat cycle. A zone of water surrounding a cilium is dragged forward in the direction of the effective stroke (top panel). The extent of the zone of entrained water depends on the height of the cilium above cell surface and is therefore seen decreasing towards the recovery stroke (from c-e). Amount of water carried reach a maximum in (c) and is much larger than during the recovery stroke (e,f,a). From (Sleigh, 1989).

1.6.2 Directional beating and planar cell polarity (PCP)

Generation of a directional fluid flow at tissue level requires cilia to beat in a similar direction. The beating direction is defined by the orientation of the basal foot, which is aligned in the direction of the effective stroke (Bayly and Axelrod, 2011, Marshall, 2010). This seems to account for most MCCs, but which stimuli that affect the orientation of basal bodies vary between species. In *Paramecium,* the daughter cell's orientation is inherited from the mother cell. In *Xenopus* larvae the basal bodies first randomly dock at the apical membrane and then reposition in response to fluid flow created by the beating cilia (Guirao et al., 2010). In mammals, cilia orientation is dependent on both hydrodynamic forces and planar cell polarity (PCP) signaling cues (Marshall, 2010).

Planar cell polarity (PCP) refers to a second polarization axis of cells going across the tissue in the rostral-caudal plane. Such a polarization of cells in mammals is controlled by specific PCP signaling molecules, including the Van Gogh-like 2 protein (Vangl2)(Jain et al., 2012). PCP and the alignment of cilia was recently investigated in ependymal cells of mice during early development. About half a day after birth, primary cilia migrated to the rostral end of the cell, leading way for an asymmetric localization of multicilia assembly later in development. A proper orientation of basal bodies depended on both PCP signaling and fluid flow, either generated by cilia themselves or from an external source (Fig. 1.8). Moreover, the ciliary beating axis reoriented upon an induced flow, but realignment was highly dependent on the expression of Vangl2 (Bayly and Axelrod, 2011). Thus, there is a high functional dependence on both PCP signaling and hydrodynamic forces in mammalian cells, as neither is capable to induce proper basal body orientation alone (Guirao et al., 2010). Neither ciliogenesis nor amplitude of ciliary beating is affected in PCP mutant animals, thus suggesting that PCP regulates only the orientation of the cilium and its beating axis (Guirao et al., 2010).

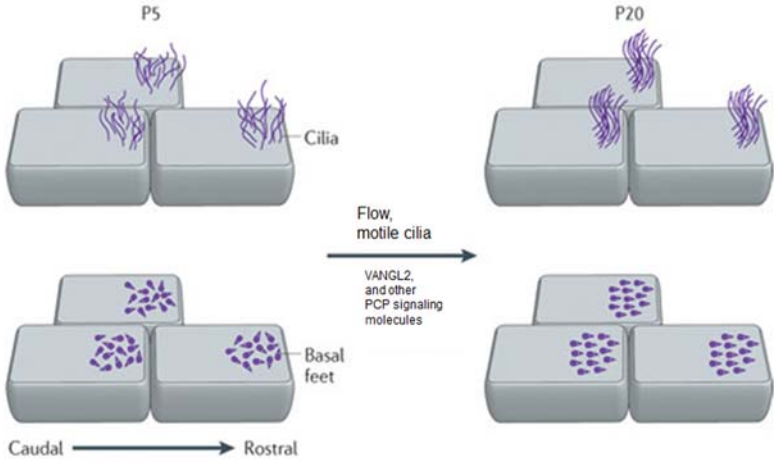

Figure 1.8. Development of PCP in mouse ependymal cells during early development. Illustrations indicate motile cilia (top panel) and basal feet of these cilia (bottom panel). Primary cilia migrate to the rostral end of each cell until 24h after birth, indicating the localization of multicilia assembly (not shown). 5 days after birth (P5) motile cilia are observed as clusters localized to the rostral side of the cells. Cilia are not aligned in any particular direction, determined by the random directions of their basal feet. During 5-20 days after birth (P5-20), motile cilia align in the caudal to rostral direction as response to Vangl2 and other PCP signaling proteins. Modified from (Bayly and Axelrod, 2011).

1.6.3 Metachronal waves in cilia arrays

Cilia sometimes work in pairs, as in *Chlamydomonas*, but usually they are arranged on large arrays, such as in linings of internal organs, where they beat in close coordination. More specifically, cilia beat in metachronal waves, a rhythmic movement where cilia beat with the

same frequency in a sequential order. The result is an out-of-phase wave that appears to move over the cell array (Fig. 1.9). Cilia beating in synchrony would facilitate the beat of their neighbors through hydrodynamic forces, but only a fraction of the force would be converted into forward fluid motion, as a large part of the fluid would just move back and forth. On the contrary, compared with in-phase beating cilia, metachronism is able to increase efficiency of fluid drive by tenfold (Elgeti and Gompper, 2013). The formation of metachronal waves is functionally valuable because it creates a continuous movement of liquid and allows a higher flow rate. Each cilium adds impetus to water already being moved and do not have to accelerate water from rest at the start of each beat (Sleigh, 1989). Modelling work by Guirao et al. shows that a metachronal relation allows cilia to start beating at a lower threshold of ATP and with a higher CBF for each cilium (Guirao and Joanny, 2007).

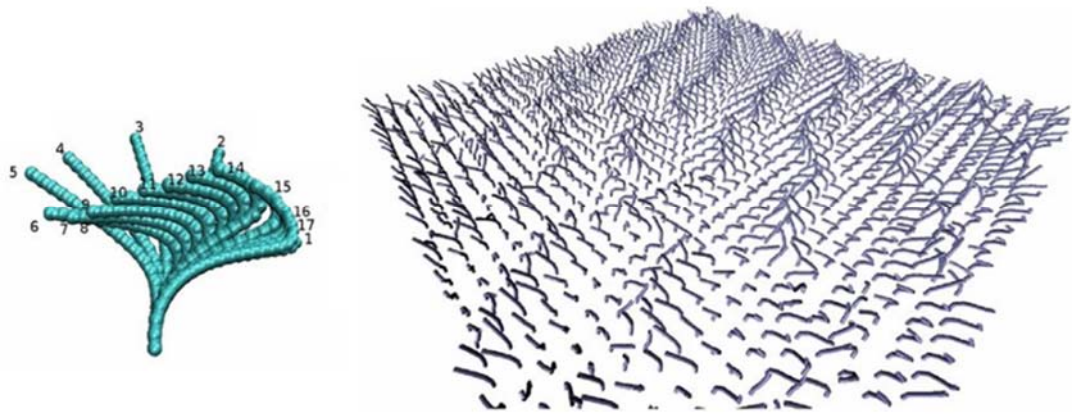

Figure 1.9. Metachronal waves illustrated by a computational cilia model. The simulated ciliary beating is based on the beat pattern of rabbit tracheal cilia in culture medium. The switch between the effective stroke (frames 1-5) and the recovery stroke (frames 6-17) is based on a curvature threshold in the lower part of the cilium. A metachronal wave is demonstrated in a square array of 40x40 beating cilia. Sequential beating of adjacent cilia is recognized by the lines of fully extended cilia during the power stroke. Modified from (Elgeti and Gompper, 2013).

The mechanism by which metachronal waves are coordinated are however not fully understood. Interestingly, cilia seem to self-organize into metachronal beating patterns. It has been hypothesized that a sideway recovery stroke stimulate adjacent cilia to propagate the wave, but indeed, not all tissues which display metachronal waves beat in a three-dimensional manner (O'Callaghan et al., 2012). Sleigh proposed that stimulation of adjacent cilia was not due to direct touch, but by the entrained water zones of each cilium (Sleigh, 1989). Conclusively, modelling work of Guirao and Elgeti propose that hydrodynamic coupling between cilia is the main tool for alignment of a beating cilia array (Guirao and Joanny, 2007, Elgeti and Gompper, 2013).

1.7 Cellular control of ciliary movement

It was observed that cilia have the potential to increase their beating frequency already 25 years ago (Clary-Meinesz et al., 1992, Weiss et al., 1992). The mechanisms underlying active control of CBF are still highly debated. From experiments made in unicellular organisms, increased membrane potential and calcium (Ca^{2+}) ions were the first to show a direct correspondence to regulation of ciliary beating (Weiss et al., 1992). The potential to regulate CBF is essential for proper functioning of many multiciliated tissues and is mediated by various stimuli via second messengers, such as Ca^{2+}, cAMP, cGMP and nitric oxide (NO). Sensory proteins expressed in motile cilia are suggested to provide a continuous feedback to MCCs which respond by regulating CBF (Jain et al., 2012).

1.7.1 Mechanical regulation of CBF

Cilia respond to direct mechanical stimulation. Sanderson and Dirksen (1990) observed that ciliated cells of rabbit trachea grown in culture responded to stimulation by a glass microprobe by increasing their CBF. The increase in CBF was transmitted to neighboring cells within 1-3 seconds, where the lag corresponded to the distance from the stimulated cell. By use of an intracellular Ca^{2+}-indicator (fura-2), the authors observed that cytoplasmic Ca^{2+} concentrations increased at the contact point of the stimulation and spread to as much as 7 neighboring cells by less than a second (Dirksen and Sanderson, 1990). Thus, the wave-like pattern of increased CBF was proposed to depend on a release of Ca^{2+} from intracellular stores, mediated by the passage of IP3 to adjacent cells via gap junctions (Lansley and Sanderson, 1999).

In nature, a mechanical regulation of CBF is of use to maintain the propulsive effort of cilia despite changes in viscosity of the mucus fluid. An increase in cellular Ca^{2+} levels has been implicated in these studies too. Reported findings indicate that all of oviduct, respiratory and ependymal MCCs have a functional reserve which allows them to regulate their mechanical output in response to the properties of the fluid they interact with (Andrade et al., 2005, Johnson et al., 1991, O'Callaghan et al., 2008). In comparison, water-propelling cilia of unicellular organisms exposed to increased viscosity decrease their CBF exponentially upon contact with more viscous fluids (Andrade et al., 2005, Sleigh, 1989).

The response to changes of fluid viscosity is proposed to depend on ion channels permeable to cations, including Ca^{2+}, which are activated upon mechanical stretch. One such example is the TRPV4 channel, localized to cilia of airway and oviduct epithelium (Andrade et al., 2005). Indeed, polymorphisms in the TRPV4 gene are specifically associated with various lung

diseases, such as chronic obstructive pulmonary disease (COPD), characterized by i.e. epithelial damage and mucus hypersecretion (Zhu et al., 2009). Another ion channel is the channel complex made of the polycystins PC-1 and -2, thought to mediate mechanosensation by Ca^{2+} influx upon direct bending or fluid flow (Mangolini et al., 2016). PC-1 and -2 were first acknowledged as renal flow sensors of primary cilia in the kidney, but were recently also localized to motile cilia in the airways, oviduct and ependymal cells of the brain (Wodarczyk et al., 2009, Jain et al., 2012). Mutations in PC1 and 2- encoding genes, PKD1 and 2, are associated with non-optimal mucociliary clearance which lead to airway diseases such as bronchiectasis (Jain et al., 2012), indicating that they are essential contributors to the autoregulation of CBF upon changes in viscosity of the mucus fluid.

Recent studies in primary cilia challenge the common fact that mechanosensation is due to Ca^{2+}-mediated signaling. Delling et al. investigated primary cilia upon exposure to flow in several ciliated organs, such as the kidney, embryonic node and inner ear of a transgenic mouse line. They reported that Ca^{2+} increased at a cellular location distal from the apical membrane, and did in fact not originate in the cellular compartment. Upon flow, Ca^{2+} quickly diffused (< 200ms) from the cell body and in to the cilium compartment. The authors argued this influx could be due to ciliary damage. Further, they propose that previous studies might have misinterpreted (1) image artifacts and change in fluorescence as the cilium bends, or (2) the origin of Ca^{2+}, as imaging speed could be the limiting factor (Delling et al., 2016). These results do not argue against the importance of polycystins in proper cilia functioning, in which mutations repeatedly leads to kidney cysts and lung disease (Jain et al., 2012), but they question the lack of mechanically induced Ca^{2+} signaling as the causative factor of diseases related to loss of polycystins.

1.7.2 Regulation of CBF by bitter substances

An interesting study published in 2009 reported an autonomous protection system in the airways based on ciliary beating. The authors reported that cilia of respiratory epithelia expressed sensory bitter taste receptors and thus could eliminate the noxious compounds by increasing cytoplasmic Ca^{2+} levels and CBF (Shah et al., 2009). Shah et al. studied the substance denatonium, which is the most bitter substance existing and a ligand for the bitter taste receptor T2R4 (Bachmanov and Beauchamp, 2007). Upon application of denatonium, CBF increased by approximately 25% and induced a transient dose-dependent increase of cytoplasmic Ca^{2+}. T2R receptors belong to a family of GPCRs that is broadly tuned to multiple bitter compounds, best known as bitter sensory receptors of the tongue (Bachmanov and Beauchamp, 2007). Four

of these bitter receptors were found in human airway epithelia: T2R4, T2R43, T2R38 and T2R46. All specifically localized to cilia, albeit with different levels and subciliary distribution. For instance, T2R4 was localized closer to the tip of the cilia than the others. Other bitter substances such as thujone, salicin, quinine and nicotine also elicit elevations in Ca^{2+} levels, but only denatonium was reported to increase CBF (Shah et al., 2009). However, if respiratory cells regulate their CBF in a Ca^{2+}-mediated way, it is likely that the other bitter substances have a similar effect on CBF as denatonium. Thus, receptors on the tongue that protect against noxious signals may also act as an airway defense signaling system and play a significant role in airway diseases (Lee et al., 2012).

1.7.3 Regulation of CBF by pH

pH concentration within a cell affects a wide range of cellular functions and is an essential element of regulation of cellular homeostasis. In particular, lowered extracellular pH slows down or inhibits many cellular responses, including enzyme or ion transport activity, DNA and protein synthesis as well as cAMP and Ca^{2+} levels (Lardner, 2001). A study on human respiratory ciliary brushings showed that the MCCs tolerated external pH variations between 3.5 and 10.5. Any pH outside of this range was lethal within minutes (Clary-Meinesz et al., 1998). O'Callaghan found that CBF of ependymal cells in mice could decrease by as much as 14 Hz upon exposure to pH 6.5, and that intracellular pH (pH_i) alone was the crucial factor (O'Callaghan, 1998).

pH can regulate CBF in two different ways, either directly or indirectly. A rapid response to only small changes in pH_i in human airway CBF was reported in the experiments of Sutto et al., indicating that a change in pH_i may act directly on the axonemal machinery by i.e. targeting dynein subcomponents (Sutto et al., 2004). The authors emphasize the outer dynein arms as a potential candidate, as a conformational change of a dynein light chain located on outer dynein arms is previously observed at lower pH (Barbar et al., 2001). pH may also indirectly regulate CBF by kinase/phosphatase systems involving i.e. PKA. The catalytic efficiency of PKA is optimal at near-neutral pH, and acidic pH will inhibit any kinase activity and thus have the ability to slow CBF or even inhibit ciliary beating. In fact, acidic pH not only inhibits PKA but has also shown to activate phosphatases to dephosphorylate PKA targets (Salathe, 2007).

1.7.4 Regulation of CBF by temperature

The effects of temperature on CBF are well documented, where most research is made in mammalian airway epithelial cells. For instance, Svartengren et al. reported CBF ranging from

5.8 to 28.3 Hz in the temperature range 20-43.5°C in ciliated pig tracheal cells (Svartengren et al., 1989). Actually, temperature provides a simple way of generating a change in CBF without exposing cilia to any chemical reagents. *In vivo*, human respiratory cilia are exposed to a wide range of environmental variations in temperature. The temperature effect on human nasal and tracheal brushings has been studied and it was reported that cilia were immotile at very low temperatures and very high temperatures (5°C and 50°C). Otherwise, CBF increased linearly with temperature from 9 to 20°C and plateaued at around 8-11 Hz (Clary-Meinesz et al., 1992). Experiments with ciliated respiratory cells in rabbits showed similar results, where CBF ranged from 6.4 to 11.6 Hz at 20-23°C and 17.2 to 26.7 at 37°C (Lansley and Sanderson, 1999). The correlation of a temperature gradient to CBF levels has also been reported in sperm (Perez-Cerezales et al., 2015) and ependymal cells (O'Callaghan, 1998). In general, the effect of temperature on CBF is much like its effect on most biological processes. Each cell type may respond differently to a temperature gradient, but a similar trend is observed in all MCCs, where cilia beat faster with an increase in temperature.

1.7.5 Intracellular mechanisms regulating CBF

1.7.5.1 Regulation of CBF by the second messengers cAMP and cGMP

The second-messenger cyclic adenosine monophosphate (cAMP) regulates a wide range of cellular functions, including the CBF of cilia in response to modifying stimuli. β-adrenergic agonists known to elevate cAMP levels, such as isoproterenol, increase CBF of respiratory cilia (Verdugo et al., 1980), and activation of the cAMP-dependent protein kinase (PKA) has been associated with an increase of CBF in i.e. *Paramecium* (Hamasaki et al., 1991). In contrast, an elevated level of cAMP in *Chlamydomonas* causes inhibition of flagellar movement (Rubin and Filner, 1973). The "cAMP-signaling pathway" is a signaling cascade which is triggered by the activation of G protein-coupled receptors (GPCRs). Upon binding of specific ligands, GPCRs change their conformation which activates the G-protein complex and adenylyl cyclase (AC), the enzyme that catalyzes the conversion of ATP into cAMP (Fimia and Sassone-Corsi, 2001).

Elevation of intracellular cAMP concentration increase CBF in multiple cells through PKA activation and subsequent phosphorylation of ciliary targets (Tuson et al., 2011). Specific dynein-associated substrates for PKA have been identified in ciliary axonemes in i.e. both *Paramecium* and humans. PKA-phosphorylation of p29, a polypeptide associated with the 22S dynein heavy chain of cilia in *Paramecium*, elevates CBF by increasing the speed of microtubule sliding (Hamasaki et al., 1991). Also, PKA-phosphorylation of a similar A-kinase-

anchoring-protein (AKAP) highly enriched in human airway axonemes efficiently increase CBF (Kultgen et al., 2002). Moreover, an optogenetic tool to study cAMP signalling *in vivo* through control of AC has underlined the essential beat-enhancing effects of cAMP in sperm. Photoactivated AC (bPAC) rapidly elevates cAMP, accelerates flagellar beat of sperm and may even restore fertility (Jansen et al., 2015).

The second-messenger cGMP can also regulate CBF, through activation of the cGMP-dependent protein kinase PKG (Bonini and Nelson, 1988). Regulatory mechanisms by cGMP is less understood compared to cAMP (Wyatt et al., 2003), but indeed, also cGMP phosphorylates the 22S dynein heavy chain in *Paramecium* (Travis and Nelson, 1988). In fact, cAMP and cGMP have similar increasing effects on CBF in *Paramecium*, but different effects on beat direction (Bonini and Nelson, 1988). CBF regulatory effects by cGMP have been reported in other species too, such as human, rabbit and bovine. Nitric oxide (NO) can specifically increase cytosolic cGMP concentrations and application of NO has shown to upregulate CBF in bronchi bovine epithelial cells (BBEC)(Jain et al., 1993). Wyatt et al. (2003) suggested that EtOH-stimulated increases in CBF of BBEC work through NO and require a simultaneous activation of both PKA, via cAMP, and PKG, via NO and cGMP (Wyatt et al., 2003). In a later study, it was found that a combination of cAMP and cGMP was required to generate maximal stimulation of CBF, indicating the existence of a substimulatory pathway where cAMP and cGMP work in combination and not separately (Wyatt et al., 2005).

1.7.5.2 Regulation of CBF by Ca^{2+}

Naitoh and Kaneko showed a correlation between Ca^{2+} and ciliary beating parameters already in the early 70's. They found that cilia of the protozoa *Paramecium* beat in the reverse direction if Ca^{2+} levels were increased above a certain threshold (10^{-6} M)(Naito and Kaneko, 1972). Later, the same Ca^{2+}-dependent regulation of speed and direction of CBF was observed in *Chlamydomonas* and ctenophores (Lansley and Sanderson, 1999, Tamm, 1994). Ca^{2+} has been correlated to regulation of CBF in many studies (Salathe and Bookman, 1999, Lansley et al., 1992, Tamm, 1994), but the effects are not uniform. For instance, elevating cellular Ca^{2+} levels in mammalian MCCs of the respiratory tract increases CBF, but the direction of beating remains similar (Korngreen and Priel, 1994). Furthermore, similar elevations in cellular Ca^{2+} levels induced a rapid ciliary arrest of the gill cilia of Mytilus (Motokawa and Satir, 1975). Thus, a change in Ca^{2+} levels in cells is highly species-dependent and variable. Followingly, many different mechanisms have been proposed for Ca^{2+}-mediated regulation of CBF.

Ca^{2+} ions are ubiquitous second messengers which regulate the activity of various cellular proteins, such as kinases, phosphatases, calmodulin (CaM), AC, cytoskeletal elements, ATPases, membrane channels and more (Zagoory et al., 2001). In general, three different mechanisms could explain how Ca^{2+} influence CBF. Firstly, Ca^{2+} can indirectly affect CBF through Ca^{2+} influx and a following membrane depolarization. For instance, stimulation of frog palate MCCs by ATP was suggested to activate a membrane receptor and increase cellular Ca^{2+} levels opening Ca^{2+}-activated K+ channels which led to a change in membrane potential ultimately enhancing CBF (Weiss et al., 1992). Secondly, Ca^{2+} can directly bind to an axonemal protein which regulate beating characteristics. Such a protein could be calaxin, a Ca^{2+}-binding sensory protein localized to the outer dynein arms in metazoan cilia and sperm flagella. The protein undergoes a conformational change upon binding of Ca^{2+} and may in this way directly influence CBF (Mizuno et al., 2012a). Thirdly, Ca^{2+} can regulate a protein or a second-messenger that controls an axonemal component through a whole-cell cascade of phosphatases and kinases (Lansley et al., 1992). Following experiments with CaM-inhibitors it was proposed that CaM might mediate a change in CBF upon increased cytosolic Ca^{2+} levels (Di Benedetto et al., 1991). For instance, CaM has been found to stimulate CBF through activation of CaM kinase in Tetrahymena (Hirano-Ohnishi and Watanabe, 1989) and through a phosphatase which dephosphorylate a ciliary target in sperm cells (Tash et al., 1988).

1.7.5.3 Crosstalk between cAMP and Ca^{2+} as a regulatory mechanism

Crosstalk between cAMP and Ca^{2+} has been suggested as a potential CBF regulatory mechanism. Forskolin is a compound known to increase cAMP levels through activation of AC and has been implicated in many ciliary studies (i.e. (Sutto et al., 2004)). In a study by Braiman et al. (1998), stimulation of frog mucociliary epithelium with forskolin induced a powerful rise in both intracellular Ca^{2+} levels and CBF. This was proposed to result from higher levels of cAMP and an increased activation of PKA which could induce a rapid and strong release of $Ca^{2+}$from intracellular stores. This Ca^{2+}-dependent stimulation of forskolin induced a relatively short but powerful enhancement of CBF. The authors showed that CBF could also be regulated independently from Ca^{2+}, as forskolin still moderately enhanced CBF upon rem*oval* of extra- and intracellular Ca^{2+}sources. The Ca^{2+}-independent pathway was rather characterized by a moderate but prolonged enhancement of CBF without the initial strong rise in CBF and intracellular Ca^{2+}levels, indicating Ca^{2+} is responsible for the quick elevation of frequency. All effects were abolished with H-89, a selective PKA inhibitor, implying that all effects were induced by cAMP through PKA activity (Braiman et al., 1998).

The interplay between cAMP and Ca^{2+} activity was recently investigated in mouse sperm cells by a FRET-based cAMP biosensor. The biosensor bind cAMP at nanomolar concentrations and reveal the dynamics of total and free cAMP levels in the cells it is expressed. Sperm physiology is regulated by cAMP produced by a 'single atypical adenylyl cyclase' (sAC), an enzyme distinct from the transmembrane ACs. sAC is not activated by forskolin, but by bicarbonate ions (HCO_3^-)(Buffone et al., 2014). The authors observed that a HCO_3^--induced cAMP increase was dependent on Ca^{2+}. cAMP levels in sperm were not altered by stimulation of HCO_3^- in buffers of low Ca^{2+} concentration, while it significantly increased in buffers of high Ca^{2+} concentrations. Moreover, they found that in the absence of HCO_3^-, Ca^{2+} in fact inhibited sAC activity and cAMP production, underlining the various and specific effects of Ca^{2+} (Mukherjee et al., 2016).

1.7.5.4 Ependymal cells are presumably not regulated by Ca^{2+}

Altogether a strong relationship between Ca^{2+} and CBF has been established. Recently, Doerner et al. reported different results in multiciliated ependymal cells of mice. The authors did not observe significant changes in CBF upon Ca^{2+}influx in ependymal cells, indicating that these cells are not tightly regulated by Ca^{2+}levels. First, they found that the ciliary compartment is not independently regulated, but passively coupled to channel activity events in the cell body. Regardless, activation of cellular voltage-gated Ca^{2+}channels by membrane depolarization, in which increased Ca^{2+} levels readily diffused to the motile cilium compartment, did not alter either CBF or fluid flow. These are very interesting results which concludes motile cilia of mouse ependymal cells regulate their CBF in ways distinct from those of respiratory cilia and flagella that power motile cells (Doerner et al., 2015).

1.7.6 Conclusive remarks: motile cilia as sensory organelles

The dual function of motile cilia, being able to both exert a beating stroke and sense the surrounding environment, has been observed in unicellular organisms for a long time. This is illustrated by i.e. *Paramecium*, which changes direction of beating as it reaches an obstacle in its way. Only the last two decades, however, sensory-associated proteins have been associated with MCCs in mammalian respiratory tract, oviduct and brain. The only known response of sensory protein activation of MCCs so far is a change in CBF, but most likely this may change in the coming years (Jain et al., 2012). The ability to regulate CBF is of high importance for proper and adaptable functioning of MCCs and naturally, stimuli will regulate MCCs differently in various tissues and species. The effects on CBF of chemical and mechanical

stimuli as well as temperature and pH are well documented, but how these stimuli specifically interact with the ciliary beating machinery is less understood. The second-messenger systems including Ca^{2+}, cAMP and cGMP are at the core of the CBF regulative mechanisms so far investigated. The effect of Ca^{2+} on CBF was acknowledged already in the 1970s and has been implicated in CBF regulation of many MCCs. Recent results just disconfirmed this as a regulatory mechanism for ependymal cells in mice (Doerner et al., 2015). Significant advances in understanding the intracellular mechanisms regulating CBF have been made, especially by structure-function studies and comparative data in unicellular animals, but many issues remain unsolved.

1.8 Measuring CBF

In order to understand how MCCs control their beating frequency it is important to have a quantitative and reliable method to measure CBF. This is difficult to accomplish for multiple reasons. Firstly, motile cilia are densely packed. A camera recording of multiciliated cell arrays is often not able to separate one cilium from the other. Hence, each recorded image will be a combination of overlapping cilia, which may beat at slightly different frequencies (Sisson et al., 2003). Secondly, both external flow and flow induced by cilia will make recordings vulnerable to drift. A spatial shift of active ciliated cells, as well as acquisition noise, can make analysis of recordings difficult (Smith et al., 2012). Thirdly, because of the high beating frequencies, only high-speed imaging, with sufficiently high sampling rates, is capable of measuring CBF in its full range (Lechtreck et al., 2009, O'Callaghan et al., 2012). Finally, it may be necessary to measure CBF over long time periods to monitor changes upon application of potential stimulants. This requires methods to be automated (Sisson et al., 2003).

1.8.1 Detection methods: past and present

The rate of ciliary beating is defined in Hertz (Hz), which implies the number of beat cycles per second. For many years traditional photodetector systems have been severely limited by their cost, complexity or slow acquisition rate. Early attempts on automated measurements of CBF are i.e. laser light-scattering spectroscopy, photodiode and photomultiplier methods which measure CBF on basis of light intensity changes from ciliary beating under the scope (Svartengren et al., 1989, O'Callaghan et al., 2012). There have been several drawbacks associated with the use of these methods. First, long experiments could not be saved because of very large data size, which puts constrictions on the experimental design. Second, according to the Nyquist–Shannon sampling theorem, the maximum CBF that can be measured is half of

the sampling frequency (Kim et al., 2011). Thus, low sampling rates such as analog video procedures recording at 30 frames per second (fps), restricts accurate CBF measurements to frequencies less than 15 Hz. This is lower than normal CBF of various cell types at physiological temperatures, i.e. ependymal cells.

Today, high-speed digital imaging system accompanied with computerized analysis has revolutionized this field. The sequence of digital images can be captured by a camera and recorded directly to a computer, where rates up to 500 images/s have been used in cilia analysis (Ryser et al., 2007). The images can be analyzed one by one (equivalent to frame by frame) or combined to create a digital video. There are several advantages for high-speed digital imaging, such as revelation of rapid changes in CBF, much faster data analysis and the possibility of whole-field analysis of numerous motile cilia simultaneously (Lansley and Sanderson, 1999). Earlier, the standard procedure to measure CBF was slow-motion replay of high-speed digital recordings of ciliated cells in which beat cycles could be counted manually. This was prone to human bias and surely a highly time-consuming task (O'Callaghan et al., 2012). Today a number of image analysis software programs have been developed to compute CBF from digital recordings (Smith et al., 2012).

1.8.2 Frequency estimation

Two classic ways to estimate CBF from digital recordings are ‘confocal linescan’ and the computation of the Fast Fourier Transform (FFT) of pixels. In the linescan method, a line perpendicular to the axis of the cilia is drawn and confocal microscopy scanning computes a kymograph, a synthetic image of the periodic behavior of cilia. A kymograph gives a graphical representation of the spatial position of cilia over time, where time is represented on the x-axis. Each line in the kymograph represents an individual stroke and CBF can be calculated (Werner and Mitchell, 2013). This method requires input from the researcher and has a very low-throughput. Contrarily, the computation of CBF by the FFT algorithm is automated and characterized by a higher throughput. FFT is a widely used tool for computation of the frequency of signals in image and signal processing (Kim et al., 2011). It converts any signal from its original domain, often time or space, into a representation in the frequency domain. The FFT can be obtained from either a whole image (pixel intensities in the entire image are averaged) or individual pixels of the image, reported as the magnitude vs frequency. The frequency with the highest magnitude is reported as the average CBF (Meste et al., 2015).

1.9 Monitoring Ca^{2+} activity

1.9.1 Ca^{2+} as an intracellular signaling molecule

Ca^{2+} was known to be critical for cellular function already in 1883, when Sydney Ringer and co-workers discovered that tap water containing Ca^{2+} supported contraction of isolated frog heart which Ca^{2+}-free water could not (Miller, 2004). Since then Ca^{2+} has been found to regulate a broad range of vital cellular processes, such as cell motility, gene transcription, muscle contraction, exocytosis, neural activity and ciliary beating, thus having an impact on i.e. fertilization, proliferation, development, learning and memory (Berridge et al., 2000). Cytoplasmic Ca^{2+} is low at resting level but may increase tenfold as a cell becomes active. Several different stimuli can initiate elevations in Ca^{2+} concentration in mammalian cells, such as mechanical and electrical stimulation as well as chemicals such as ATP, muscarinic agonists and bradykinin (Lansley and Sanderson, 1999). Cellular processes can be activated either by an influx of Ca^{2+} into the cell, from external and internal sources, or by an efflux of Ca^{2+} from cytoplasm by pumps or exchangers to restore resting state.

1.9.2 Calcium imaging

The first calcium imaging techniques involved Ca^{2+}-sensitive dyes, which produce light upon increase of Ca^{2+}. The use of fluorescent Ca^{2+} indicators were a successful way to study Ca^{2+}in cellular processes, but their method of delivery was cumbersome. Indeed, chemical dyes need to be loaded onto cells, either directly injected via i.e. a micropipette or incorporated by i.e. hyposmotic shock treatment or chemical-induced permeabilization (Takahashi et al., 1999). It was a breakthrough in the field in 1997, when Tsien and coworkers introduced genetically encoded indicators (GECIs). Opposed to chemically engineered fluorophores, GECIs do not need to be injected prior to experiments. Genes encoding GECI proteins can be integrated in the genome to create transgenic animal models (Akerboom et al., 2012). As protein-based indicators, GECIs have the advantage of being precisely expressed in targeted compartments and the expression of the protein is stable for a long period of time. Thus, since Ca^{2+}-dependent fluorescent response is reversible, GECIs are suitable for *in vivo* analysis where several repetitions over time are needed, such as collecting data from the same cell or a population of cells over several months (Looger and Griesbeck, 2012).

GECIs were at first lagging behind chemical indicators in terms of low signal-to-noise ratio and action potential threshold (Looger and Griesbeck, 2012, Tsien, 1980). Following many years of optimization, the performance of the current generation of GECIs can now be

compared to chemical dyes. GCamp6, which is currently the most sensitive and widely used GECI, is a high-affinity GFP-based Ca^{2+}probe. Green Fluorescent Protein (GFP) is a photosensitive protein which is activated when exposed to blue light and emits green fluorescence (Takahashi et al., 1999). GCaMP contains a single enhanced GFP coupled with Calmodulin (CaM), a Ca^{2+}-binding protein, and a CaM-interacting peptide, M13. As Ca^{2+}binds to CaM, the Ca^{2+}-CaM-M13 interaction induce a conformational change in the engineered GFP-protein, which emit quantitatively measurable fluorescence (Nakai et al., 2001). GCaMP has constantly been improved since the first report of a GCaMP-transgenic mouse line in 2004 (Ji et al., 2004). Starting out with GCaMP3, able to detect three or more action potentials in short bursts, GCaMP5 and GCaMP6 were subsequently developed with improvements in brightness and stability (Akerboom et al., 2012). Also slow variants exist, such as GCaMP6s, suited to detect low firing frequencies with better signal to noise ratio (Badura et al., 2014).

1.10 Zebrafish in research

George Streisinger is the father of zebrafish research. After his early work with microbes, he sought for a more complex and genetically tractable vertebrate system. He chose to work with the zebrafish because of the potential he saw in unraveling the genetics of neurodevelopment. He developed methods for mutation and genetic analysis of the zebrafish and established it as a tractable model organism (Streisinger et al., 1981). Research in zebrafish is however not limited to genetics. Foremost, the rapid, external development of the egg is ideally suited for investigation of developmental biology, as embryogenesis and morphogenesis can be studied *in vivo* (Spence et al., 2008). In fact, all chemosensory modalities are established by the end of the first week (Lindsay and Vogt, 2004). Zebrafish are also advantageous for electrophysiological studies. For instance, early studies investigated the large and easily identifiable Mauthner cells in the brainstem which induce a highly characteristic escape response (Eaton et al., 2001).

Zebrafish have a total of 25.759 protein-coding genes, which is the largest gene set of any vertebrate. In 2001, the Sanger institute in Cambridge started the project of mapping the whole zebrafish genome, and the tenth zebrafish reference assembly was just released in 2014[2]. The full genome sequence of a zebrafish reference strain, Tübingen, is now available (Howe et al., 2013, Spence et al., 2008). 69% of these genes have at least one human orthologue, 71.4% of

[2] All information about the zebrafish genome is found at: *http://www.ensembl.org/Danio_rerio/Info/Annotation*

human genes have at least one zebrafish orthologue and 47% of these have a one-to-one relationship (Howe et al., 2013). Altogether, genetic and developmental similarities between humans and zebrafish establish the zebrafish as a unique opportunity to study human diseases and vertebrate development.

1.10.1 Advantages of zebrafish as an animal model

Zebrafish are members of the teleostei infraclass, which comprise 96% of all fish (Volff, 2005). They offer many experimental advantages and can provide a substitute to other vertebrate models for biological studies. Being 'lower vertebrates' they contribute to the 3Rs (replacement, refinement and reduction) by replacing mammalian experiments (Wyatt et al., 2015). The small freshwater teleost, originally from the Indian subcontinent, is robust and easy to breed and maintain. Females can lay eggs every 3rd day and produce large clutches, up to 200 eggs per spawn. They breed all year round, embryos develop very quickly and fish are able to reproduce already at about 2-3 months of age (Spence et al., 2008). The eggs are transparent and developed externally, which enables direct viewing of vertebrate development. Fluorescent reporter strains makes way for a simple morphological inspection and live imaging of peculiar processes such as cell division, migration and neural circuit formation (Yoshihara, 2009). Conveniently the eggs are relatively large compared to other fish (0.7mm in diameter at fertilization) and the yolk is contained in a separate cell, not interfering with monitoring of developing tissue (Spence et al., 2008). The advantage of transparency is lost after hatching as pigments start to develop. However, mutant zebrafish lacking pigments, such as nacre, can overcome this shortcoming. Fish hatch at around 3 days post fertilization (dpf) and start feeding at approximately 5-6 dpf, as the yolk rapidly depletes during the first week (Yoshihara, 2009).

1.10.2 Genetic engineering techniques in zebrafish

1.10.2.1 Forward and reverse genetics: knock-out of genes

Zebrafish is especially valued today because of their amenability to various genetic engineering techniques. This has led to an existence of a vast collection of mutant and transgenic zebrafish lines as of today. The bias towards mutations that affect development arose because developmental effects are easily identified in mutagenesis screens and many mutations are lethal in post-embryonic stages (Wyatt et al., 2015). Zebrafish mutants were first popularly generated by ENU (N-ethyl-N-nitrosourea)-mutagenesis, a chemical mutagen able to induce large-scale random point mutations. Most of the ENU-induced mutations are small, usually 1bp, affecting only one or a few genes (Wyatt et al., 2015). Large scale ENU genetic screens

of embryos, with the Tubingen and Boston screens standing as the two leading ones (Patton and Zon, 2001), have revealed thousands of genetic mutations essential for embryonic development and behavior. The identification of the genetic mutations generated by ENU-mutagenesis was a very difficult and a highly time-consuming task, particularly because of technological shortcomings and extreme cost for genome sequencing (Wessely and Obara, 2008). With the sequenced zebrafish genome (Howe et al., 2013), genetic forward approaches can more easily be controlled and identified. Few laboratories now mutate genes using insertional mutagenesis with transposons (discussed in the following section) or viral-based methods instead of ENU. Using such methods the location of insert can be readily identified and sequenced by PCR.

Reverse genetic approaches are also readily available for zebrafish. Morpholino antisense oligonucleotides (MOs) are both rapid and economic in use to test the function of genes of interest (Wessely and Obara, 2008). MOs are nucleic acid analogs which contain a backbone of six-membered morpholino rings linked by non-ionic phosphorodiamidate instead of the ribose-phosphate backbone of nucleic acids (Eisen and Smith, 2008). MOs can be microinjected into fertilized zebrafish eggs to decrease the expression of the gene or block gene expression.

However, antisense approaches have shown to induce non-specific effects and therefore require careful controls. Following the improvements in genetic engineering and ease to create new mutant lines, the zebrafish community is now disregarding MOs and emphasize the use of genetic mutations. Targeted genome editing using engineered nucleases has recently gained much attention with the emergence of the CRISPR/Cas9 system. Cas 9 is a nuclease that can be directed to any part of the genome by a specifically customized guide RNA. This is a simple and efficient method, which can be applied to virtually any organism or cell type of interest. Only the last couple of years, this system has transformed biological and biomedical research and brought genetic engineering into the mainstream (Sander and Joung, 2014). By a combination of ENU mutagenesis and targeted CRISPR/Cas9 together with genome sequencing methods, the Zebrafish Mutation Project aims to create a knockout allele in every protein-coding gene and has until now been successful in about 45% (12000 genes)[3] (Wyatt et al., 2015).

[3] Updated info on the project can be found at: *http://www.sanger.ac.uk/science/collaboration/zebrafish-mutation-project*

1.10.2.2 Transgenic technology and transient expression

Generating transgenic animals in zebrafish became very straightforward and efficient following the initial work of Kawakami on Tol2 transposable element (Kawakami, 2007). Transposons are DNA sequences that can jump in or out of a genome by catalysis of transposase enzymes. Several transposon systems, characterized by specific transposon sites flanking the target DNA sequence, exist as of today, whereas the Tol2 transposon system is most widely used (Wyatt et al., 2015). Target DNA, preceded by a promoter of choice, is co-injected with transposase mRNA into a single cell embryo. This results in expression of target DNA in all cells with the promoter active. Thus, by germline transgenesis of the injected DNA construct, transgenic zebrafish lines can be created. Transgenic fluorescent reporters, such as GFP expressed in i.e. the heart, can be incorporated in this system and make screening of transgenic animals even easier. By using a specific promoter, both spatial and temporal expression patterns of the gene of interest can be achieved, thus allowing *in vivo* monitoring of developmental processes (Kawakami, 2007). It is important to note here that transgenic expression under a given promoter does not necessarily recapitulate the endogenous gene expression pattern. Random and sometimes multiple transgenic insertions in the genome can cause expression in non-specific tissues. Moreover, the genes may be unintentionally silenced over time. Therefore, gene trapping methods, where the endogenous gene is coupled with both its endogenous enhancer and promoter is more favored (Wyatt et al., 2015).

Besides transgenic technology, mRNA and DNA injections are standard techniques to overexpress a construct of interest during development. mRNA is synthesized in vitro from cDNA which codes for the target gene sequence. Injection of mRNA at the one-cell stage enables ubiquitous transient expression of target genes. However, mRNA is quickly degraded or diluted as cells divide, and expression will be lost by 2 dpf. DNA may also be injected and will be stable for a longer time than mRNA. Without co-injection of transposase, the DNA will not permanently integrate in the genome, but transient expression can still be observed until 6 days post fertilization or even later. DNA expression is often more intense and sparse, which can be of advantage when studying i.e. activity of individual cells (Wyatt et al., 2015).

1.10.3 Zebrafish as a tool for *in vivo* drug discovery

Comparative genomics and the rapid identification of potential human orthologues, as well as the ability to create disease models through reverse and forward genetics, have established the zebrafish as a tool for studying basic biological processes by *in vivo* screening (Zon and Peterson, 2005). In fact, the zebrafish model system is not only valuable to study metabolism

but also metabolic disease states (Ridges et al., 2012). They are particularly well suited for small-molecule screens because large numbers of embryos can be arrayed in multi-well plates simultaneously and a screen to detect the physiological influence of specific drugs can thus be conducted in a highly efficient manner. By aliquoting test-reagents from a chemical library to the multi-well plates with zebrafish embryos, and allowing a certain period of incubation time, the phenotypic effect of the compound on the zebrafish can be determined either by visual inspection or through an automated read-out. Drug-induced phenotypes in zebrafish larvae can be compared with databases containing thousands of distinct phenotypic effects associated with the activity of specific molecular targets (MacRae and Peterson, 2015). This has in particular been used to target drugs in cancer research, and phenotype-driven chemical screens in zebrafish have successfully identified both compounds and new pathways for targeting cancer metastasis (Stern and Zon, 2003). Also, by taking advantage of genetic and developmental similarities between humans and zebrafish, a zebrafish drug screening of the adult zebrafish model of leukemia identified novel compounds with selective toxicity against the disease (Ridges et al., 2012).

1.10.4 Zebrafish as a model for studying human ciliopathies

Zebrafish has provided significant proofs that cilia play an essential role in human diseases. Thus, it is extensively used as disease model of human ciliopathies. ENU mutagenesis screens first identified several disease-causing mutations in genes encoding ciliary proteins (Drummond et al., 1998, Zhao and Malicki, 2007). When homozygous, these mutations can produce defects in organ systems with pathologies resembling human diseases (Howe et al., 2013). The most prominent feature of cilia defects in zebrafish is a curved body axis, which makes any ciliary mutant easy to characterize in genetic screens. Mutants may also develop pronephric cysts, a randomized left-right asymmetry, retinal degeneration and hydrocephalus, depending on the gene affected. The consistency within ciliary mutant phenotypes has established zebrafish as a diagnostic toolkit, which can test whether novel human mutations are important in cilia biology.

Cilia are abundant in a number of organs early in embryogenesis and both sensory and motile cilia are present in multiple cell types. Motile cilia are found in Kupffer's vesicle between 8-14 somite stages (Essner et al., 2005) and in the inner ear before 24 hpf (Riley et al., 1997), as well as in the spinal canal, olfactory placode and the pronephros (Drummond, 2009). Primary cilia are present in the olfactory placode, inner ear, the pronephros, the lateral line organs and the retina (Drummond, 2009). The most studied ciliated tissues in zebrafish larvae are outlined in

Fig. 1.10. Conclusively, all of the above has established zebrafish as an ideal genetic system for studies of vertebrate cilia.

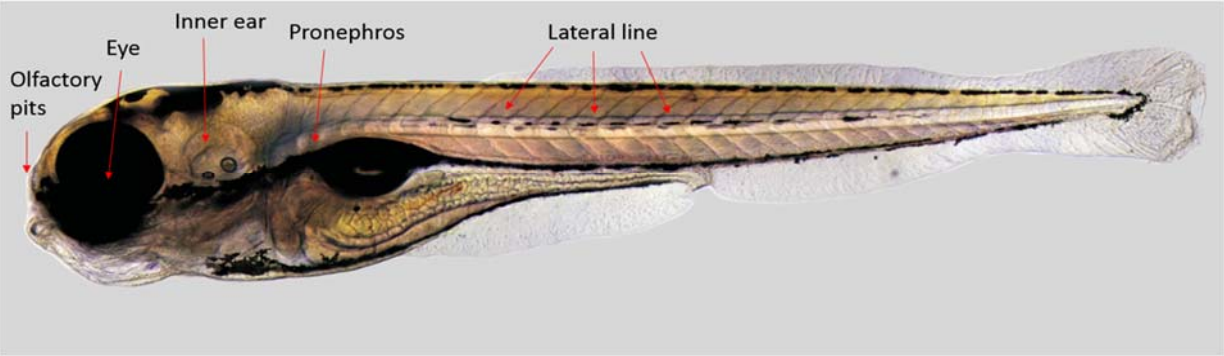

Figure 1.10. The most studied ciliated tissues in wild-type zebrafish larvae at 4 dpf. Cilia are located in the olfactory pits, the eye, inner ear, pronephros and the lateral line. Wild-type larvae have a straight body axis and pigments. Picture is taken by Adam Parslow, Heath Lab[4].

1.10.4.1 Zebrafish ciliopathy mutants

Genetic analysis of 146 families suffering from PCD led forth to the identification of a common mutation in CCDC103, the coiled-coil domain-containing protein 103. CCDC103 is a dynein arm attachment factor, essential for dynein arm assembly and ciliary motility (Panizzi et al., 2012). The gene is regulated by the transcription factor *foxj1a*, a promoter essential for ciliary motility (Hellman et al., 2010). Zebrafish mutants carrying this mutation are named *schmalhans* (*smh*) and completely lack both inner and outer dynein arms. Thus, all cilia are completely paralyzed, also in the pronephros, olfactory pit and in the spinal canal. Morphology and length is however not altered compared to wild-type. Conclusively, the *smh* mutant phenotype is similar to the other ciliary zebrafish mutants that are generated, and shows left-right asymmetry defects, kidney cysts, hydrocephalus and a curved body axis (Panizzi et al., 2012).

Mutations affecting the IFT complexes and the related proteins within the IFT machinery affect ciliary structure and are often the underlying cause for ciliopathies (Lunt et al., 2009). IFT protein homologues are found in many different animal model systems and their implication in ciliogenesis has been demonstrated in i.e. *C. elegans*, *Chlamydomonas* and zebrafish (Pazour et al., 2000, Lunt et al., 2009). For example, a mutation in the IFT88, a complex B core protein, is identified as a causative factor of autosomal recessive PKD (Pazour et al., 2000). Zebrafish with mutation in *ift88*, called *oval*, suffer from cilia degeneration, kidney cysts and a curved

[4] Picture from Heath lab. Can be found at: *http://theconversation.com/animals-in-research-zebrafish-13804*

body axis. Seemingly, IFT-proteins are necessary for maintenance of cilia, but not for the initial assembly (Tsujikawa and Malicki, 2004). Zebrafish with mutation in *elipsa* (*traf3ipi*) lack the binding factor connecting the IFT particle to rab8, which is necessary for proper functioning (Omori et al., 2008). *Elipsa* is characterized by eye defects and an earlier defect in ciliogenesis compared to other mutant strains (Wessely and Obara, 2008, Omori et al., 2008). Also by mutation in other IFT genes, such as IFT52 and IFT57, cilia collapse within the first days and induce similar, but weaker phenotypes in zebrafish embryos (Zhao and Malicki, 2007, Wessely and Obara, 2008).

1.11 The olfactory organ of the zebrafish

The olfactory system is crucial for initiation of many basic behaviors in fish, such as social interactions, feeding, breeding or avoiding predation (Kermen et al., 2013). Distinct odors are associated with distinct behaviors. For instance, amino acids and nucleotides indicate the presence of food and induce a more excited, appetitive swimming pattern (Lindsay and Vogt, 2004); gonadal hormones released in urine trigger sex specific reproductive behavior (Stacey and Kyle, 1983); and compounds from injured fish elicit an alarm response such as darting followed by freezing (Speedie and Gerlai, 2008). Indeed, it has been shown that fish can be olfactory conditioned to learn complex behavioral tasks and respond to unnatural odors. Interestingly, the fish fail to respond to odorants if both nostrils are occluded, thus suggesting that these behaviors are entirely mediated by the sensory responses of the olfactory epithelium (Braubach et al., 2009). The olfactory system is of particular interest in neuroscience because a large variety of stimuli can evoke specific behavioral patterns associated with simple, but interesting neural computations (Kermen et al., 2013).

The olfactory epithelium (OE) is composed of several cell types. There are three morphologically distinct types of sensory neurons in the epithelium. The most prominent ones are the ciliated cells, which have long and slender dendrites that end in a knob bearing few cilia. The other type is microvillus cells, which are characterized by shorter and thicker dendrites bearing microvilli. The third is a more recently discovered cell type specific to fish, the crypt cells, which bears both microvilli and cilia, although few of the latter(Hansen and Zeiske, 1998, Kermen et al., 2013). Cilia and microvilli are decorated with olfactory receptors, which enable detection of odorants. Olfactory receptor neurons (ORNs) expressing the same receptor are dispersed throughout the epithelium but project their axons to the same glomerulus in the

olfactory bulb via the olfactory nerve. The projection pattern of the three distinct sensory cells show a coarse spatial organization in the olfactory bulb (Kermen et al., 2013). Additionally, other cell types surround the sensory neurons. MCCs have longer cilia than ORNs and help move the mucus covering the olfactory epithelium with their beating cilia. Also non-sensory goblet- and rodlet cells are also present, but their functionality is uncertain (Hansen and Zeiske, 1998).

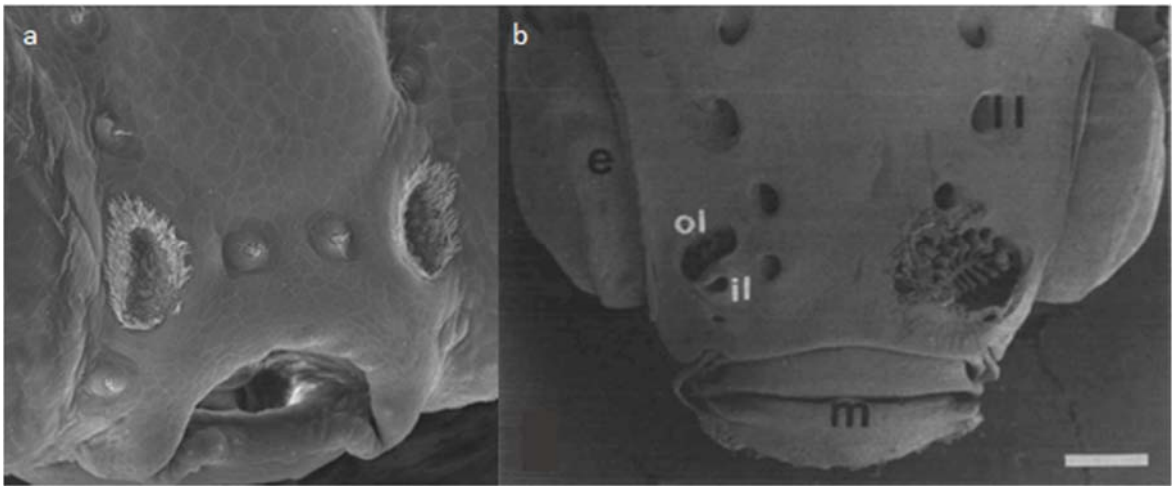

Figure 1.11. Olfactory organ of 5 dpf larvae and adult zebrafish. (a) Head of a 5 dpf zebrafish larvae. Olfactory pits are shaped as hollow cups with a thick fringe of cilia lining the rim of the round opening. They consist of one opening letting water both in and out, positioned by the eyes in the rostral part of the head. SEM. From Max-Planck-Institut[5]. (b) Head of an adult zebrafish, showing the nostril (ol,il), eye (e) and the mouth (m). Skin is removed to demonstrate the olfactory organ proper (left side). It is located in the nasal cavity, positioned between the inlet (il) and outlet nostril (ol) (right side). Lamellae insert into the midline raphe, where MCCs line the rim of lamellae and sensory cells are continuously arranged in the valleys between and on the sides. SEM. Scale bar: 500µm. From (Hansen and Zeiske, 1998).

The OE develops very early and undergoes a massive reorganization at around 2-4 weeks. The earliest signs of differentiated olfactory placodal cells are found at about 14-16 hpf in the rostral area of the head by the eyes. In the following hours, the placode increases and starts to fill the space between the eyes and the forebrain (Hansen and Zeiske, 1993). A transient population of pioneer neurons first grow toward the placode at about 24 hpf, leading the way for the ORNs that form synaptic connections soon after (Whitlock and Westerfield, 1998). Olfactory receptor mRNA are expressed in the ORNs already by 30-35 hpf. The olfactory pits open as small slits around 34-36 hpf and about 15 hours later, the pit has increased into an oval-shaped structure. At this time, MCCs with long cilia, ORNs with knobs bearing fewer cilia, microvillus receptor cells and supporting cells can be distinguished. By 4 dpf the olfactory pit is a round opening,

[5] Picture from Max-Planck-Institut für Entwicklungsbiologie. Can be found at: *https://www.mpg.de/482098/pressRelease20030613*

lined by a thick fringe of cilia around the rim (Fig. 1.11). After 2 weeks the OE starts folding into the characteristic adult morphology, the olfactory rosette (Hansen and Zeiske, 1993). Eventually, the nasal opening will close and only leave one anterior inlet and one posterior outlet, where the water enters and exits the nose (Fig. 1.11)(Hansen and Zeiske, 1998). The multilamellar and rosette-shaped adult OE is positioned between these openings and regains full access to the incoming water (Kermen et al., 2013). The surface of the midline raphe and the rim of each lamella is covered by MCCs cells and are strictly separated from the sensory neurons. ORNs are continuously arranged, located on the sides and in the valleys between the lamellae (Hansen and Zeiske, 1998).

1.12 Aims

Significant advances have been made the last twenty years in understanding the importance of cilia, but much is still unknown about the physiological role these organelles play in most tissues. More research into ciliary biology and function is needed to bring about better ways to cure and treat ciliopathy patients. Thus, the aim of this work is to provide new insights in ciliary biology and in the long term to provide new tools to identify genetic mutations and small molecules affecting or restoring ciliary beating. As cilia are conserved structures throughout evolution, direct links between phenotypic effects resulting from dysfunctional cilia can be drawn from model organisms to humans. Zebrafish provide an unique opportunity to study human diseases and vertebrate development, thus, I will use zebrafish larvae as a gateway to study motile cilia characteristics. My work focuses on the motile cilia of the olfactory epithelium. At 4 dpf, the olfactory epithelium is shaped as a hollow cup (the olfactory pit), which contains olfactory receptor neurons and a thick fringe of motile cilia. In my project, I will combine various molecular, cellular and microscopy approaches in order to

1. characterize the beating patterns and frequencies of MCC cilia in the olfactory pit. To do this, we will develop a high-throughput method to analyze CBF.
2. identify stimuli affecting the beating frequency of cilia and the underlying mechanisms regulating the control of beating frequency.
3. investigate a potential interaction between ORNs and MCCs and characterize mutants with ablated or immobilized cilia for future experiments to further address the physiological relevance of motile cilia in the olfactory pit. In particular, we envision these mutants to shed light on the contribution of motile cilia in olfactory responses.

Chapter 2.

Materials and methods

2.1 Fish maintenance

The animal facilities and maintenance of the zebrafish, *Danio rerio*, were approved by the NFSA (Norwegian Food Safety Authority). Fish received from other labs are kept separated from the main colony in two different rooms, respectively in a quarantine - and a main room. In both rooms fish are kept in 3 liter tanks in a Techniplast Zebtech Multilinking system at constant conditions: 28°C, pH 7 and 600µSiemens. The fish were kept at a 14:10 hour light/dark cycle to simulate optimal natural breeding conditions and they received a normal diet of dry food (SDS 100-400, dependent of age) two times/day and Artemia nauplii once a day (Grade0, platinum Label, Argent Laboratories, Redmond, USA). For experiments, the following fish lines were used: *smh* (received from I. Drummond, MGH Boston)(Panizzi et al., 2012), *elipsa* (received from J. Malicki, University of Sheffield, UK)(Omori et al., 2008), *oval* (received from I. Drummond, MGH Boston)(Tsujikawa and Malicki, 2004), *ift172* (received from J. Malicki, University of Sheffield, UK)(Drummond et al., 1998), *foxj1a-del5* (yaksi lab) as well as wild-type.

2.1.1 Embryo treatment

Eggs were collected after natural spawning and kept in petri dishes in an incubator (28°C) until 3-5 dpf. Embryos were kept in egg water, and after hatching (3 dpf), the medium was exchanged to artificial fish water (AFW, table 2.1). 50% of the water in the petri dishes was exchanged daily. At 5 dpf, embryos had either been used for the experiment, sacrificed or transferred to the main facility to be raised.

Eggs collected from the quarantine to be raised in the main facility were bleached at 1 dpf. Eggs were transferred to bleach solution (table 2.1) for 2 min and washed with AFW, repeated 3

times. Bleached eggs were dechorionated by use of forceps between 48-72 hpf as bleaching toughens the chorion and prevents the natural hatching.

Table 2.1. Solutions used

Solutions	Content
Egg water	1.2 g marine salt 20L reverse osmosis water 20 mL 0.1% methylene blue
Fishwater	1.2g marine salt 20L reverse osmosis water
Bleach solution	0,1ml 5,25% sodium hypochlorite (Fisher, Cat # Fisher:SS290-1, kept at 4°C) 170ml egg water

2.2 Fixation and immunostaining of zebrafish larvae

2.2.1 Fixation of larvae

Larvae were anesthetized on ice. Medium was exchanged to PFA/PBS (4% PFA, 4°C) and incubated overnight at 4°C or at room temperature for 3 hours. The next day samples were washed (3x1min) in PBS (phosphate buffered saline) on a horizontal shaker. The samples were stored in PBS at 4°C until further use.

2.2.2 Immunostaining

The complete protocol with a list of solutions is found in table 2.2. Fixed larvae were washed with 0.1%PBS-Tween (0.1%PBST, 3x10min) and treated with acetone in order to permeabilize the sample (100% acetone, 1h incubation at 20°C). After acetone treatment samples were washed with PBS (3x10min) and unspecific bindings were prevented by incubation in blocking buffer containing Bovine serum albumine (1% BSA/PBS, 1h). Larvae were incubated with primary antibody (acetyl tubulin, table 2.2) overnight at room temperature. On the second day samples were washed (0.1%PBST, 4x20min) and subsequently incubated with the secondary antibody (Alexa-labelled GAM568, table 2.2) overnight at 4°C. The third day samples were incubated with DAPI nucleic acid stain solution (0.1% DAPI/0.1%PBST, 1hr), washed

(0.1%PBST, 4x20min) and transferred to a series of increasing glycerol concentrations (25%, 50% and 75%). Stained embryos were stored in 75% glycerol at 4°C.

Table 2.2. Immunostaining protocol

Treatments	Solution	Duration	Temperature
Wash	0,1% PBS-Tween	3 x10 min	Room temperature
Permeabilization	100% acetone	1 hour	-20 °C
Wash	PBS	3 x10 min	Room temperature
Blocking	1%BSA/PBS	1 hour	Room temperature
Incubation of primary antibody	Acetylated tubulin (1/1000 mouse IGG2b, Sigma) in 1% BSA/PBS	Over night	Room temperature
Wash	PBS-Tween	4 x 20 min	Room temperature
Incubation of secondary antibody	Goat anti-mouse 568 (1/1000, life technology) in 1% BSA/PBS	Over night	4°C
Staining of nuclei	0,1% DAPI in 0.1% PBS-Tween	1 hour	Room temperature
Wash	PBS-Tween	4 x 20 min	Room temperature
Preparation for storage	25% Glycerol 50% Glycerol 75% Glycerol	Until sunken to bottom of tube	Room temperature
Storage	75% Glycerol	∞	4°C

2.3 Confocal imaging

2.3.1 Preparation of samples

The head of larvae immunostained with acetylated tubulin (AcTubulin) and stained with DAPI were positioned vertically in glycerol in a custom-made chamber so that olfactory pits were facing directly upwards. Fish lines used for confocal imaging was *oval*, *elipsa*, *ift172*, *foxj1a-del5* and *smh* as well as wild-type. Straight-tailed larvae from the same clutch were used as controls.

2.3.2 Imaging and digital image analysis

Images were obtained with a Zeiss confocal microscope and a 10x objective (Zeiss, NA 0.3, plan). Wavelength of monochrome laser was 405 for DAPI and 561 for acetylated tubulin. Images were analyzed with ZEN LSM-software (Zeiss) and the java-based image processing program ImageJ.

2.4 Image capture and analysis of ciliary beating frequency (CBF)

2.4.1 Preparation of samples

High-speed microscopy recordings of motile cilia were conducted with live embryos paralyzed with α-bungarotoxin (Invitrogen BI601, 1 mg/mL) and then embedded in 2% low melting point (LMP) agarose prepared in AFW. Agarose is porous and allows the fish to breathe properly during the whole course of the experiment. Agarose covering the nostrils was removed to allow free ciliary beating. Larvae were mounted as shown in Fig. 11, at an angle of about 60 degrees, to enable the best visualization of olfactory pits.

2.4.2 Image acquisition by video microscope

Olfactory pits of zebrafish larvae were visualized by a Bresser transmitted light microscope using a 63x water immersion objective lens (Zeiss, NA 0.9, plan). High-speed digital recordings were captured with an Allied Vision Manta camera. Frames were acquired and stored by custom made software written in C++ (by Robbrecht Pelgrims), and further analysis was conducted in MATLAB. Videos were acquired at approx. 100 frames per second (fps). The size of images varied among experiments. After recording, larvae were sacrificed following approved procedures.

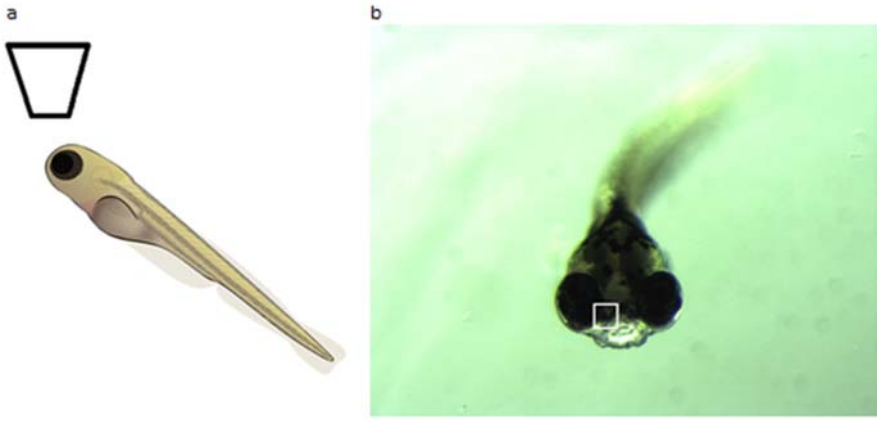

Figure 2.1. Positioning of mounted fish for microscopy imaging. (a) Schematic presentation of larva embedded in agarose, tilted upwards for direct viewing of olfactory pits. (b) Field of view through the light microscope. Right olfactory pit is indicated by white box.

2.4.3 Delivery of stimulants to larvae

Several approaches were used to apply the stimulants listed in table 2.3. Delivery methods are further described below.

Table 2.3. Stimulants delivered to larvae

Stimulant	Concentration	Delivery method
Flow	3 mL/min	Pinch-valve
Temperature	24±2°C to 32±2°	Pinch-valve
Denatonium	20mM	Pipette
KCl	40mM	Pipette
Forskolin	25µM	Pipette
LED	488nM	LED-lamp

To accurately control the delivery of flow, a home-made delivery system was used. The set-up is illustrated in Figure 2.2, consisting of 2 sets of tubes and a pinch-valve controlled by an Arduino. The system was used to accurately control the timing of flow-delivery. A flow of 3 mL/min was used in the experiments.

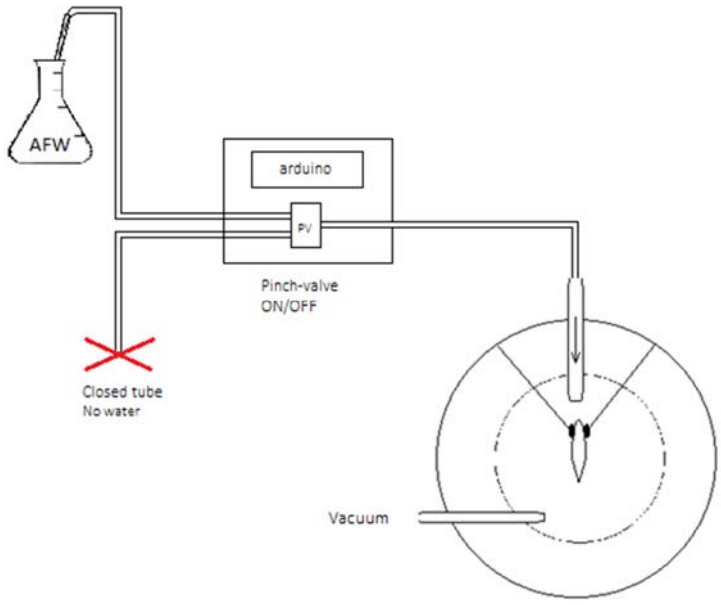

Figure 2.2. Illustration of flow-delivery setup. Zebrafish larvae were embedded in agarose in the middle of a round fluordish. Water-delivery was provided through a tubing controlled by a pinch valve (PV) and an arduino. PV alternated between ON (AFW delivery) and OFF (No flow, closed tube). Water flow was maintained by acceleration of gravity. A vacuum pump positioned behind larvae provided suction to prevent water overflow.

Temperature was controlled by an 'automatic temperature controller' (Warner). It contained a heating device placed on the outlet tube of the flow-delivery system and a thermometer positioned in contact with the incoming water to monitor the current temperature. There was constant flow throughout the experiment. By limitations of the device, fine regulation of temperature was impossible and it was set to either increase or decrease between 24±2°C to 32±2°. Regulation of temperature was nonlinear.

As flow significantly increased ciliary beating frequency (CBF), chemicals were delivered to the fish manually to ensure that potential effects were not masked by elevated CBF resulting from flow. Concentration of each chemical is listed in table 2.3. A control recording of olfactory pit MCCs was made before application of each drug (30 sec, approx. 100 fps). After delivery of drug by pipette (approx. 1 mL), larvae were bathed in the solution for 2 min before a second recording (30sec, approx. 100 fps) was made to establish post-treatment CBF. A different larva was used for each treatment.

Larvae were exposed to LED by a XLamp XP-E LED lamp (Cree) controlled by an arduino. Lamp was positioned directly above the mounted larvae. An 850 mW radiant flux at approx. 560nm wavelength was delivered to larvae for 1 min.

2.5 Genotyping *smh* mutants

2.5.1 Isolation of gDNA

For genotyping potential mutant embryos of the fish line *smh*, fins of adult fish were clipped and the gDNA was isolated. Isolation was done by lysing the fin segment in PCR lysis buffer supplemented with Proteinase K (0.1mg/ml) at 50°C overnight (recipe 1). The reaction was ended by heat (95°C, 10 min) and debris were spun down.

2.5.2 PCR amplification of gene fragment and verification of mutants

A 436-bp fragment spanning the mutation point was PCR amplified with *smh* genotyping primers. A PCR reaction mix was made (recipe 2) and PCR was run according to protocol (table 2.4). After PCR amplification, samples (6µl) were mixed with loading dye (2µl, LD 6x orange, Life Technology) and separated by electrophoresis (130V, app. 20 min) on a 2% agarose gel containing SYBR safe (Life Technology). As single bands were observed and the negative H2O control was blank, the amplified fragment was digested with BfaI (Life Technology), a restriction site introduced by the *smh* mutation. By incubation (1hr, 37°C), mutant DNA was cut into fragments of 351 bp and 85 bp. Dye (6µl, LD 6x orange) was added to the samples.

The DNA fragments were separated by agarose gel electrophoresis (130V, 1h) and visualized using a gel documentation system (Bio-Rad).

Recipe 1. PCR lysis buffer recipe

Ingredient	Concentration	Volume (mL)
Tris, pH 7-9	1M	0.5
EDTA	0.5M	0.2
Triton X-100		0.1
Proteinase K	5mg/ml	1
Millipore water	-	48.2
		Total: 50

Table 2.4. PCR protocol

Step	Temperature
Step 1	98°C
Step 2	98°C
Step 3	55,5-66,0°C
Step 4	72°C
Step 5	
Step 6	72°C
Step 7	4°C

Recipe 2. PCR reaction mix

Ingredient	Final concentration	Amount (µl)
gDNA	-	1
5XPhusion HF Buffer	1x	5
25mM dNTP	2.5mM	0,2
10µM Forward primer (GCAGGAATGGAGAACTCTGA)	0.25µM	0,5
10µM Reverse primer (GGTGATTTGCTTTATAAAATGTCTC)	0.25µM	0,5
100% DMSO	8.3µM	0,6
2U/ul Phusion Hot start II High fidelity DNA polymerase	0.5 U	0.25
Millipore water	-	11.95
		Total: 20µl

2.6 Microinjections

2.6.1 Preparation of the injection mix

On the morning of the injection a plasmid DNA encoding GCaMP6s under the *foxj1a* promoter and flanked by tol2 integration sites (pT2K *foxj1a:gcamp6*, 1µl, 25ng/µl final) was mixed with an aliquot of transposase mRNA (tol2, 1µl, 25ng/µl final), KCl (10µl, 0.4M final) and phenol red (2µl) in nuclease-free water (table 2.4). The injection mix was handled with gloves and kept on ice throughout the injection session.

Table 2.5 DNA:RNA injection mix for microinjections

Ingredients	Concentration	Amount	Purpose
Plasmid	500ng/µL	1µl	Plasmid, to express Ca^{2+} indicators in MCCs
Tol2	500ng/µL	1µl	Transposase mRNA, to integrate plasmid into genome of fish
KCl	0.2M	10µl	to make the osmolarity of the cell cytoplasm
Phenol Red	2µl/20µl	2µl	for better visualization
RNase-free water	-	6µl	RNase-free reagents are essential during preparation of injection mix to avoid degradation of transposase mRNA

2.6.2 Injections

1. Injection needles were made from glass capillaries using a laser-based micropipette puller (Sutter). The needle was filled with the injection mixture and connected to a microinjector (Femtojet, Eppendorf). The tip was cut with forceps to open the needle and allow outflux of solution.
2. The injection volume was calibrated to inject 1nL of prepared injection mix by using a micrometer slide (pyser-sgi) upon adjustment of different settings on the injector (pressure, time of injection and back pressure-settings).
3. One male and 2-3 females of wild-type zebrafish larvae were transferred to breeding tanks the day before the injections. A divider was used to separate males from females and allow timed mating. Eggs were collected within 15 min after rem*oval* of divider. Embryos were injected at the one-cell stage.
4. Fertilized eggs were transferred to a prewarmed injection mold of agarose (1% agarose in egg water), enabling a stable positioning of the eggs during injection.

5. Injection material (plasmid vector of *foxj1a:gcamp6* and transposon mRNA) was injected directly into the cell.
6. Injected embryos were transferred to petri dishes and stored at 28°C. At the end of the day the medium was changed and dead and unhealthy embryos were removed.

Uninjected embryos from the same clutch were left as controls to compare development and survival. Injected larvae with gene insert were verified with fluorescent microscopy. In GFP-positive larvae the insertion of the transposon is stable whilst the mRNA will follow natural mRNA degradation and hence only be transiently available.

2.7 Light sheet microscopy imaging

Light sheet microscopy imaging of *hspGGFF19b:gfp* larvae was used to investigate beating patterns of individual cilia. Olfactory pits of larvae were recorded for 2-3 sec at 900 fps. To investigate spontaneous Ca^{2+} activity, transgenic larvae were recorded for 5 min at 100 fps.

2.7.1 Preparation of samples

Larvae were paralyzed with α-bungarotoxin (Invitrogen BI601, 1 mg/mL) and mounted in agarose in a homemade chamber. Larvae were positioned so that they were directly facing the sheet of light from the light sheet microscope. The agarose in front of the olfactory pits was removed. The chamber was filled with AFW so that larvae was completely covered.

2.7.2 Imaging and digital image analysis

Microscopy recordings were obtained by a custom-made light-sheet microscope (built in our laboratory by Maximillian Hoffmann) with a 20x water immersion objective (Olympus, NA 1.00, plan) and a laser of 488 nm wavelength (Cobalt). Images were acquired by the provided software and analyzed in ImageJ and matlab.

2.8 Two-photon microscopy imaging

Two-photon microscopy imaging of *foxj1a:gcamp6* larvae allowed to characterize spontaneous Ca^{2+} activity and the change in Ca^{2+} activity in response to flow. Admission of flow was controlled by a pinch-valve flow-delivery system, such as previously described (section 2.6.3). Recordings were of 6 min in total, at 35 fps. Ca^{2+} activity is presented as the change in fluorescence (F) over time by dff, $F\text{-}F_{baseline}/F_{baseline}$. Baseline is the average value of the first 100 frames (no Ca^{2+} activity).

2.8.1 Preparation of samples

To measure spontaneous Ca^{2+} activity, *foxj1a:gcamp6* larvae were paralyzed and up-right positioned in agarose to allow recording of a higher number of cells. To measure Ca^{2+} activity in relation to flow, paralyzed larvae were positioned in agarose as explained for light microscopy experiments (section 2.4.1).

2.8.2 Imaging and digital image analysis

Microscopy recordings were acquired by a two photon microscope (Scientifica) with a 16x water immersion objective (Nikon, NA 0.8, LWD 3.0, plan) and laser of 920 nm wavelength. Acquired images were processed with Matlab.

Chapter 3.

Results

3.1 Morphology of olfactory pit in 4 dpf zebrafish larvae

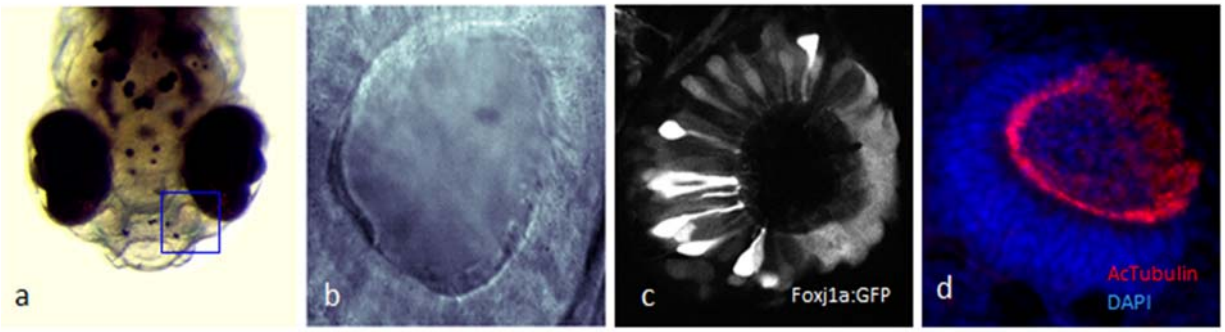

Figure 3.1. Representation of the olfactory pit of a 4 dpf zebrafish larvae. (a-b) Light microscopy image of wild-type larva. Olfactory pit is indicated by the blue square. (b) Motile cilia are situated around the whole rim of the nostril, building a thick fringe of cilia. The lateral region closest to the eye (upper right corner) presents cilia on the top of the rim. (c) Olfactory pit of a *foxj1a:GFP* larva acquired by two-photon microscopy. The acquisition plane is tilted so the lateral side (right) shows the cuboidal multiciliated cells (MCCs), while the medial side (left) shows the pear-shaped ciliated olfactory receptor neurons (ORNs) that are situated in the bottom of the cup. (d) Confocal image of the olfactory pit of a wild-type larva. Acetylated tubulin (AcTubulin) immunostaining shows that cilia are enriched at the outer rim of the olfactory pit. Staining also reveals cilia in the medial part of the cup, most likely including cilia of ORNs. The olfactory pit has a less steep wall on the lateral side (seen in orthogonal view) where also cilia are located on the outside of the rim. Right is lateral and left is medial for all images (b,c,d).

The olfactory pits develop from placodal cells located between the developing forebrain and the eyes. They are at first indicated by small slits (34-36 hours) and widen into *oval*-shaped openings at 2 days post fertilization (dpf). The ciliated and microvillus sensory neurons, multiciliated cells (MCCs) with longer cilia and support cells can be distinguished in the epithelium by electron microscopy at that time (Hansen and Zeiske, 1993). Beating cilia can be seen by light microscopy at 3 dpf, but the olfactory pits are quite small (data not shown). Finally, the olfactory pit openings of larvae at 4 dpf are bigger, structures are well-defined and ciliary

beating is more easily characterized. Hence, I decided to continue my experiments with 4 dpf zebrafish larvae.

In order to characterize the morphology of the olfactory pit in zebrafish larvae, I used several microscopy techniques. The olfactory pit, marked with a blue square in Fig. 3.1a, is located on the medial side of the eyes above the mouth. At 4 dpf the olfactory pit is a hollow structure with a round opening and MCCs densely arranged around the rim (Fig. 3.1b). A transgenic zebrafish line expressing GFP under the *foxj1a* promoter (*foxj1a:gfp*) labels multiple cell types in the olfactory pit, which can be differentiated on the basis of their morphology (Fig. 3.1c). MCCs are cuboidal cells, which have a large bundle of motile cilia extending from the cell body into the cavity of the olfactory pit. Ciliated olfactory receptor neurons (ORNs) are characterized by pear-shaped, slender cell bodies and are located below the MCCs. They extend into the bottom of the cup and end in dendritic knobs bearing fewer, non-motile cilia (Fig. 3.1c)(Hansen and Zeiske, 1993).

In order to further map the distribution of cilia in the olfactory pit, larvae were fixed and immunostained for the cilia marker acetylated tubulin (AcTubulin) and stained for DAPI (Fig. 3.1d). As AcTubulin is enriched in both primary and motile cilia, no distinction could be made between the two. Confocal images verify that cilia line the outer rim as well as the interior of the pit to some extent. Ciliary distribution is clearly of a lower density in the middle of the pit. Furthermore, as seen with orthogonal views of confocal images, the pit is not a uniform hollow structure. The lateral wall is less steep and cilia extend up on the surface of the rim in this area (Fig. 3.1d). This can also be seen by light microscopy (Fig. 3.1b), where cilia are beating at the surface of the olfactory epithelium (supplementary video S1). Altogether, these findings show that MCCs are cuboidal cells, located principally at the outer rim of the olfactory epithelium that can be labeled using *foxj1a* promoter.

3.2 Analysis of ciliary beating frequency (CBF)

3.2.1 Analysis of CBF using the Fast Fourier Transform (FFT) algorithm

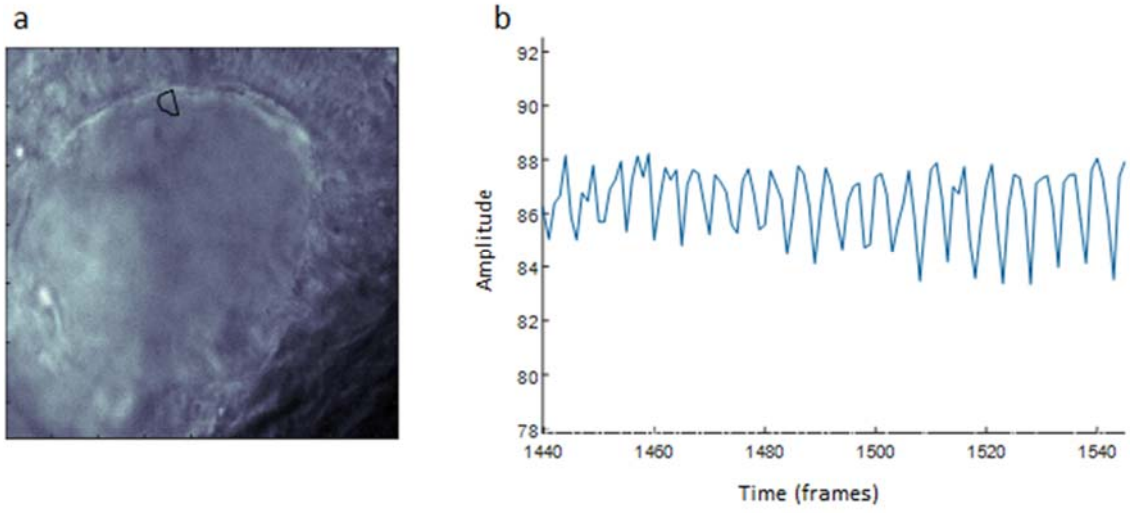

Figure 3.2. Pixel intensity change over time indicates the ciliary beat frequency (CBF). CBF is reported as the number of beating cycles per sec, or Hz. (a) First image of high-speed light microscopy recording (30 sec, 107 fps) of the olfactory pit of a wild-type larva. A region of interest (black circle) is selected at the border of the epithelium where freely beating cilia are observed. (b) Oscillatory activity in the region of interest from (a). The graph shows the pixel intensity change as a function of time. 1 sec, equivalent to 107 frames, is represented here. There are 21 cycles within frames 1440-1547, equivalent to 1 sec, indicating a CBF of 21 Hz for the region of interest.

To measure the ciliary beating frequency (CBF) in olfactory pits of 4 dpf wild-type larvae, high-speed recordings were made at approx. 100 frames per second (fps). Larvae were paralyzed, embedded in agarose and positioned so that the front of the head was tilted upwards to make the olfactory pits available for light microscopy imaging. Any agarose surrounding the nostrils was removed to allow free beating of cilia. Light microscopy recordings were focused at the rim of the olfactory pit where beating cilia could be observed. The recordings were subsequently analyzed by specific functions written in Matlab software. Fig. 3.2a shows a descriptive image of a high-speed light microscopy recording. Beating cilia interfere with the transmission of light and result in an oscillatory change of light intensity over time, as indicated in Fig. 3.2b. For the region of interest indicated in Fig. 3.2a, 21 oscillations occurred during 1 sec (107 frames), thus indicating a CBF of 21 Hz.

In order to identify the CBF throughout the olfactory pit, we automated our CBF analysis. To this end, we analyzed the frequency of oscillations, as described above, for every pixel of the recording using the Fast Fourier Transform (FFT) algorithm of Matlab. The pixel intensity change throughout the recording is converted to a function of its frequency components by FFT.

The FFT of a pixel is represented in a graph, similar as in Fig. 3.3c, with frequency plotted against its power. The frequency with highest power (corresponding to 24.5 in Fig. 3.3c) is the most abundant frequency found in the pixel and corresponds to the CBF. Thus, the peak frequency of each pixel is automatically detected and can be presented in a heat map, as in Fig. 3.3b. Regions of the heat map with distinct beating frequencies correlate to the areas where motile cilia extend into the cavity of the olfactory pit, as seen in Fig. 3.3a. No specific frequency was detected in the middle or outside the pit, where also no beating cilia were observed. The FFT components of all pixels are averaged and represented in a graph as in Fig. 3.3c. The frequency with the highest power is reported as the average CBF of all cilia in the olfactory pit.

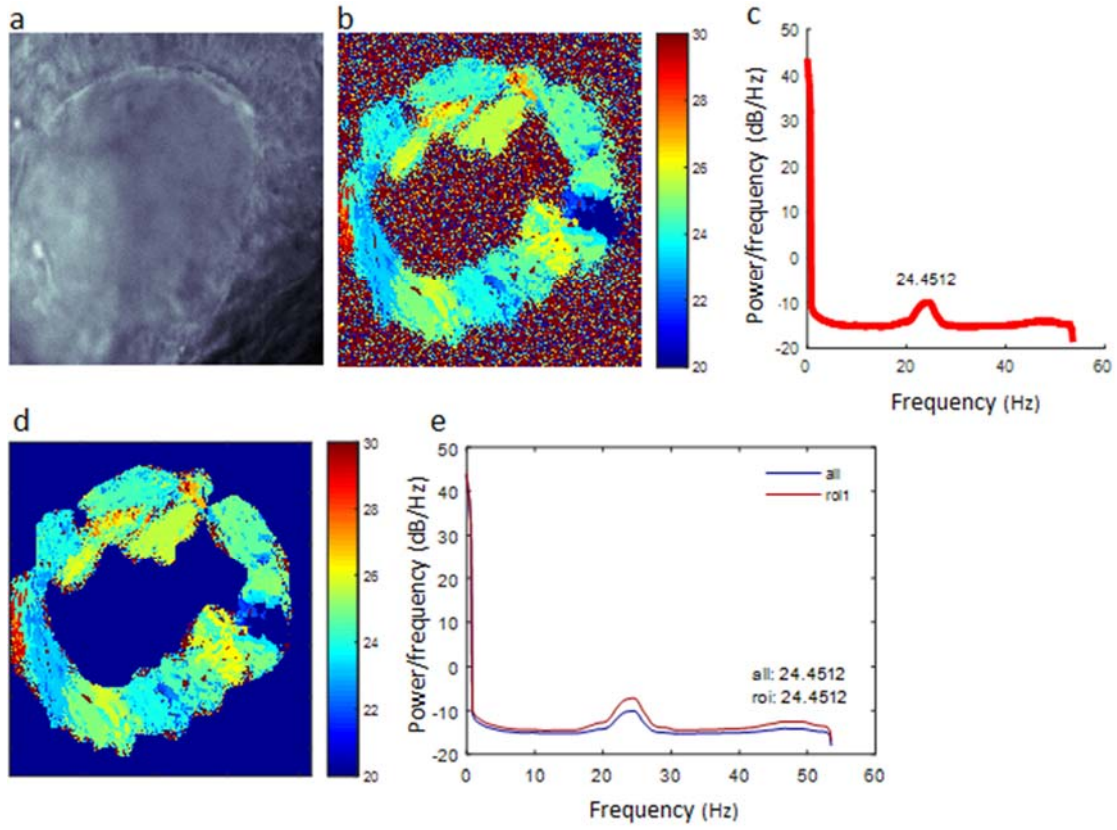

Figure 3.3. Analysis of CBF of olfactory pit in 4 dpf zebrafish larvae by FFT algorithm. (a) Light microscopy recording of the olfactory pit of zebrafish larva, same example as in Fig. 3.2. (b) Pixel intensity change throughout the whole recording is converted to a function of its frequency components by FFT. The most abundant frequency for each pixel is represented in a heat map. The activity in the heat map corresponds to the localization of beating cilia in the pit. (c) Average of the FFT frequency obtained for all pixels of the recording, where power (dB) is presented as a function of frequency (Hz). The most abundant peak frequency indicates the average CBF of the MCCs in the olfactory pit, 24.5 Hz. (d) Exclusion of background noise by selection of a region of interest (ROI). (e) Exclusion of background noise does not interfere with output of CBF analysis, but increase the power of the signal. The average peak frequency is similar for both the whole-field analysis and the ROI, 24.5 Hz. Color scale: 20-30 Hz.

To compute the average frequency in Fig. 3.3c, all pixels were taken into account whether oscillatory activity was detected or not. To investigate whether background noise from regions

devoid of beating interfered with the results of our CBF analysis, a region of interest (ROI) was drawn to exclude the area without ciliary beating activity (Fig. 3.3d) and the FFT algorithm was rerun. The peak frequency values obtained for the whole image and the ROI did not differ, except for a higher power of the signal as noise was excluded (Fig. 3.3f). This indicated that background noise did not interfere significantly with our estimation of CBF by FFT. Hence, to increase the throughput of our method, I did not exclude the background unless the detected signal was too weak to be estimated.

3.2.2 FFT analysis of wild-type and cilia mutant larvae

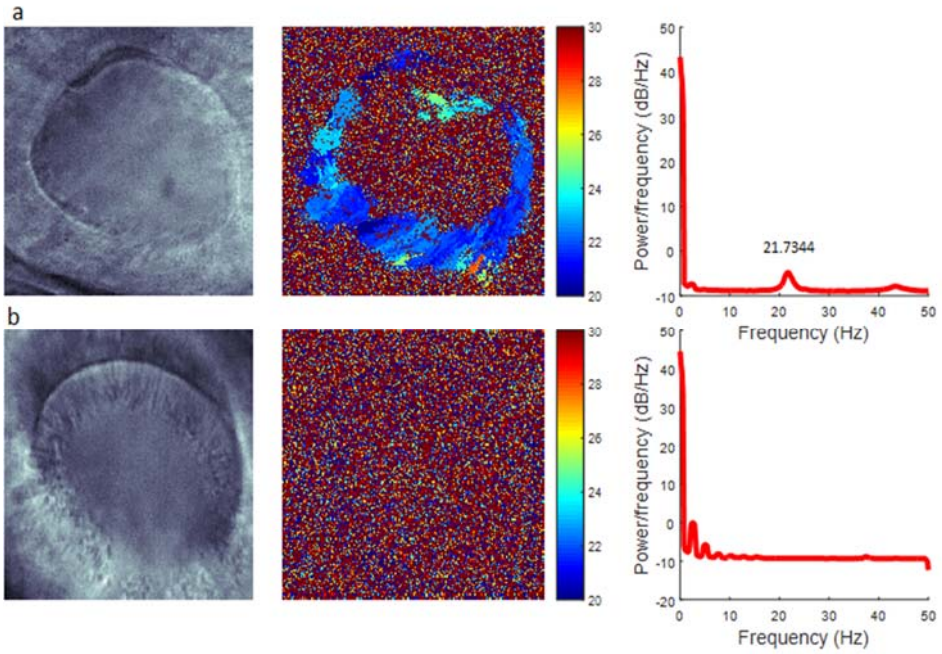

Figure 3.4. Comparison of ciliary beating analysis of wild-type and mutant *smh* larvae. (a) High-speed light microscopy recording (10 sec, 107 fps) of the olfactory pit of a wild-type larva is analyzed pixel by pixel by the FFT algorithm. Peak frequency of each pixel is represented in a heat map, which displays the distribution of beating cilia in the olfactory pit. Cilia beat at an average frequency of 21.7 Hz. (b) Analysis of ciliary activity in olfactory pit of *smh* mutant larva. Cilia of olfactory pit were easily seen in the light microscopy recording (10 sec, 107 fps, supplementary video S2), but no ciliary beating was detected. Only noise is displayed in the heat map and no average peak frequency is generated. The irregularities of the average FFT outputs below 10 Hz are of unknown origin and may be due to signal processing artifacts of the FFT algorithm. Color scale: 20-30 Hz.

The zebrafish *schmalhans* (*smh*) mutant is devoid of both inner and outer dynein arms and cilia are immotile (see section 3.7.1). *Smh* larvae were used here to validate the FFT method described above. Larvae were paralyzed and positioned in agarose, as previously explained in section 3.2.1, and ciliary beating was investigated by high-speed light microscopy and FFT analysis. Cilia of *smh* were easily seen in light microscopy recordings, but they did not move (supplementary video S2). Furthermore, no beating was detected in olfactory pits of *smh*

mutants by FFT analysis (Fig. 3.4b). In contrast, analysis of CBF in olfactory pit of the control larva showed a characteristic heat map with indication of activity in the area of cilia localization and a clear peak average frequency of 21.7 Hz (Fig. 3.4a). These results prove that this procedure only detects cilia that beat actively, and thus prove the validity and accuracy of our method.

3.2.3 Characterization of ciliary beating pattern and direction

In order to identify the beating pattern and direction of olfactory MCCs, I tracked motile cilia of individual MCCs over time by the use of an enhancer trap line (*hspGGFF19b;UAS:GFP*) that sparsely labels MCCs in the olfactory epithelium. The cilia beating pattern could be investigated by combination of *hspGGFF19b;UAS:GFP* with light sheet microscopy, which allows recordings of as much as 900 Hz of a single optical plane.

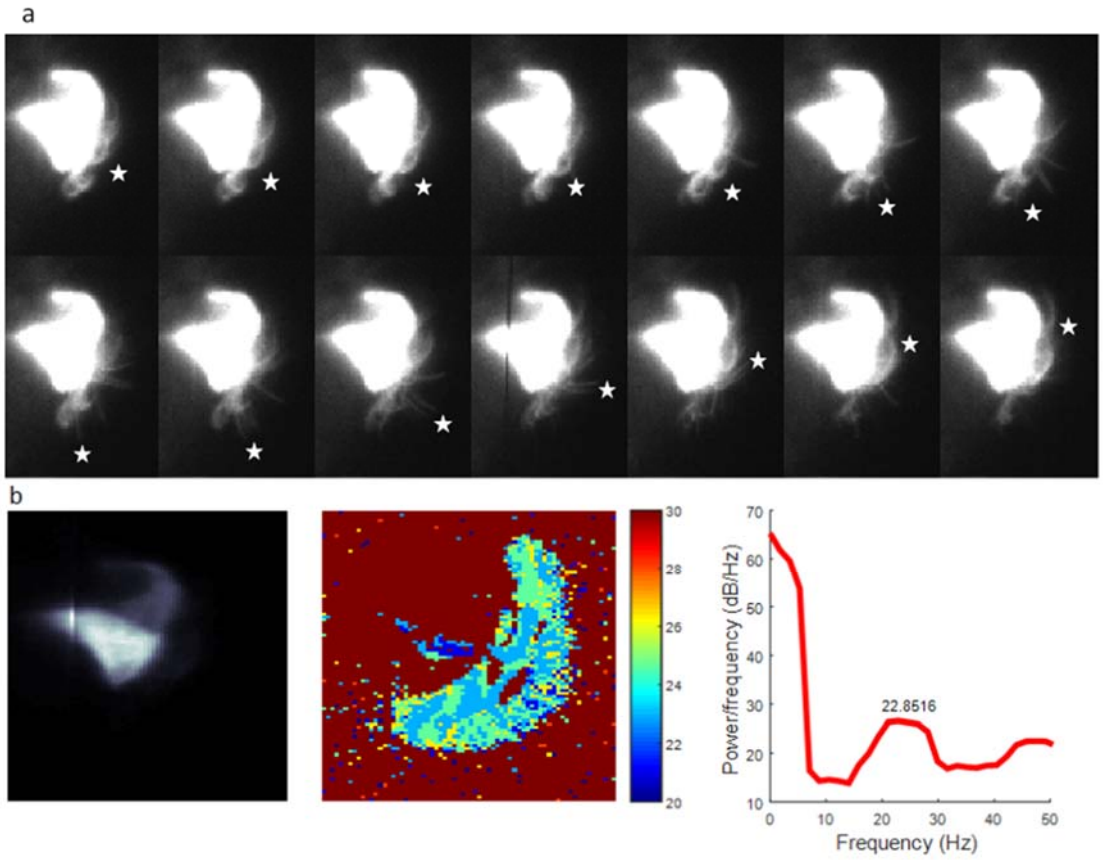

Figure 3.5. Light sheet microscopy recording of individual MCCs reveal the ciliary beating pattern. (a) Snapshots of a light sheet microscopy recording (900 fps) of two individual MCCs in the olfactory pit of *hspGGFF19b;UAS:GFP* (supplementary video S3). Montage consists of 14 images, each separated by 1.1 ms. Stars indicate a subset of cilia beating through the last part of the recovery stroke (top panel) and completing the effective stroke (bottom panel). The outside of the olfactory pit is to the right. (b) The CBF of the same recording analyzed by the FFT algorithm. A heat map is generated which display the active area of cilia. Average CBF is 22.9 Hz. Color scale: 20-30 Hz.

Cilia are fully extended during the effective stroke and beat toward the outside of the olfactory pit (Fig. 3.5a, bottom panel). As the effective stroke is completed the cilia retreats by almost 180° and stay close to the cell membrane in such a way that it creates a retracting whip-like motion (supplementary video S3). Fig. 3.5a (top panel) shows two MCCs in which a subset of its cilia is half way through the recovery stroke, in the middle of its returning path (indicated by stars). Estimated by FFT analysis of the light sheet recording, cilia of *hspGGFF19b;UAS:GFP* beat at an average frequency of 22.9 Hz (Fig. 3.5b).

In order to fully characterize the duration of one beat I manually counted the number of frames necessary to perform the effective and recovery strokes. 7 countings were made at different time points of the recording. Based on a frequency of acquisition of 900 fps, the effective stroke lasted 15.4±1.4ms and the recovery stroke 28.6±2.1ms. Thus, the complete ciliary stroke lasted for about 44ms, which equals 22.7 Hz (events/s). The effective stroke was estimated to be almost twice the speed of the recovery stroke, as shown in Fig. 3.5a. The CBF values obtained upon manual count and the automated FFT analysis only differed by 0.2 Hz, thus validating our FFT analysis.

Taken together, these findings describe the bi-phasic beating pattern of MCCs in the olfactory pit of zebrafish larvae and identify that ciliary beating propels fluid out of the olfactory pit. The results obtained from high-speed light sheet microscopy recordings corresponded to values previously achieved with simple light microscopy. Besides, recordings of approx. 100 fps are sufficient to detect CBF, as twice the original frequency is the limit to detect the original bandwidth of a signal according to the Nyquist–Shannon sampling theorem. Altogether, since light microscopy provides accurate results with higher throughput, easier specimen preparation and lower data size, the estimation of CBF was done by light microscopy in subsequent experiments.

3.3 Physiology of olfactory pit in 4 dpf zebrafish larvae

3.3.1 Individual variability

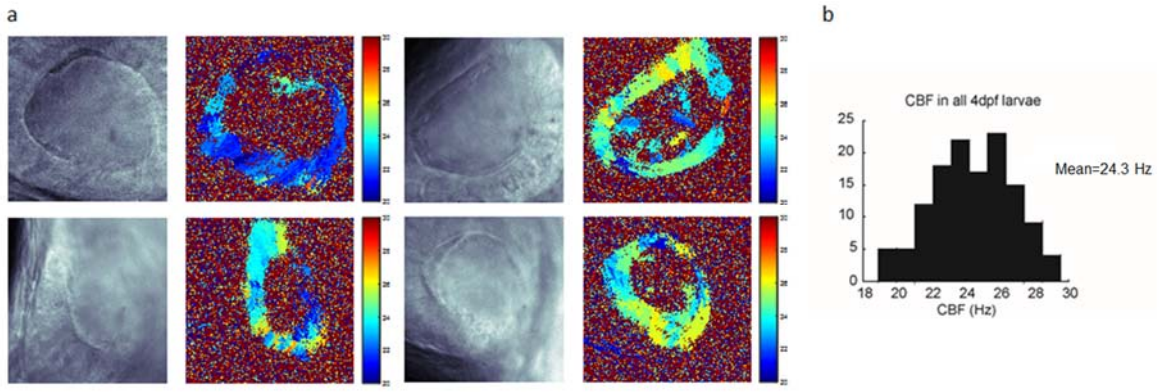

Figure 3.6. CBF of MCCs in olfactory pit of wild-type larvae at 4 dpf. (a) Examples of light microscopy recordings of 4 wild-type larvae showing individual differences of the olfactory epithelium. (b) The CBF of all wild-type larvae analyzed (n=130) is normally distributed with a mean CBF value of 24.3 ± 2.35 Hz, ranging from 18,9-29,5 Hz. Patches of distinct beating frequencies can be seen.

Larvae show individual differences in the shape of their olfactory pits, shown by 4 examples in Fig. 3.6. The variability observed is due to developmental differences, and positioning of larvae may itself induce small differences in how the olfactory pit looks upon microscopy. Regardless, the CBF is relatively stable between individuals. A histogram of in total 130 wild-type larvae at 4 dpf (ciliary beating was analyzed as explained in section 3.2) shows a normal distribution of CBF with a mean value of 24.3 ± 2.35 Hz, ranging from 18.9 to 29.5 Hz. Altogether, this suggests that CBF is stable across individuals, even though small morphological differences between olfactory pits can be observed.

3.3.2 Patches with distinct beating frequencies

Patches with local beating frequencies can be distinguished in the ciliary lining of olfactory pits in most recordings (i.e. Fig. 3.3, 3.6, 3.7). The FFT analysis of CBF can be shown in a spectrogram to visualize changes of CBF over time. In a spectrogram, such as in Fig. 3.7a, the FFT is color-coded and plotted as a function of time (right panel) for a given ROI (indicated by a red outline in the left panel). In the example of Fig. 3.7a, CBF is medium-high (approx. 27 Hz) and consistent throughout the recording. CBF stability is shown by a straight line of peak averages in the spectrogram presenting the full length of the recording (5 min, plotted on the y-axis).

Not limited by ROIs, ciliary beating stability and frequency for several subregions can be visualized by FFT analysis heat maps (explained in section 3.2.1) at subsequent time points of a recording. Heat maps in Fig. 3.7b are estimated from 10 sec time bins, separated by a gap of 20 sec. The CBF within patches remained stable throughout the recording, as seen by the consistency in colors of all heat maps (Fig. 3.7b). Cilia in the right area (green) beat at approx. 25 Hz. In comparison, cilia in the middle bottom region (yellow) beat at a higher frequency, approx. 27 Hz (represented in Fig. 3.7a), and cilia in the top left corner (dark blue) beat at approx. 20 Hz. Within the full recording of 5 min, the average CBF of the ventral olfactory pit (whole field of view) ranged from 22.4 Hz to 24.4 Hz (data not shown). All together, this shows that distinct beating frequencies remain stable and the relationship between surrounding patches is consistent.

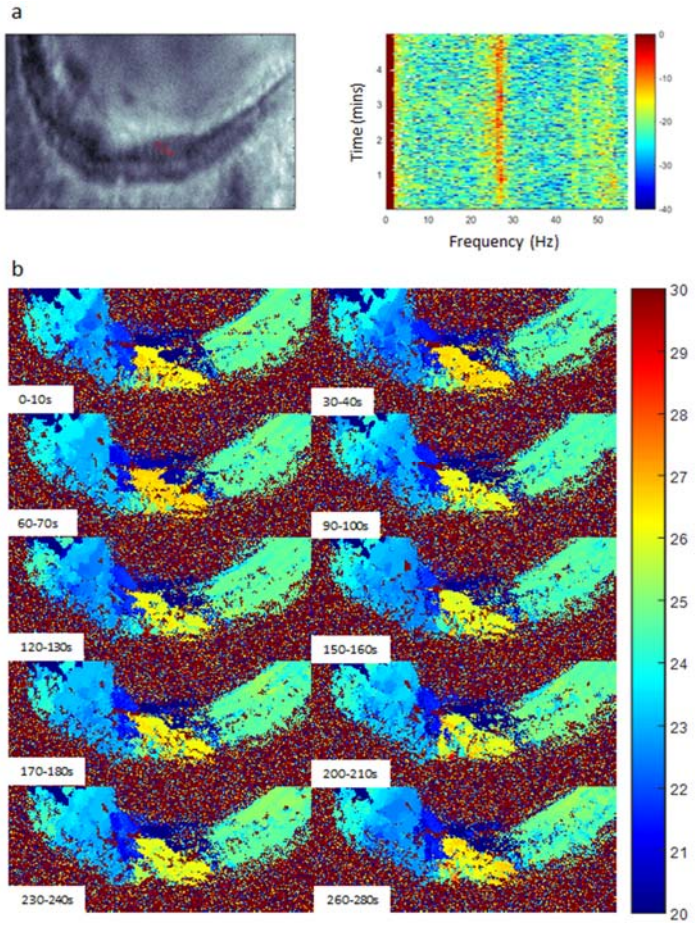

Figure 3.7. Subregions of the ciliary lining of the olfactory pit beat with distinct frequencies. (a) Light microscopy recording (5 min, 107 fps) of the ventral part of the olfactory pit of a wild-type larva. FFT analysis of a ROI (red circle) is represented in a spectrogram showing the frequency of beating (Hz) as a function of time (min). The red color in the plot indicates the most abundant frequency for each time point. The straight line (red) indicates a medium-high frequency (～27Hz), which remains stable throughout the recording. (b) FFT analysis of the same recording represented as heat maps of 10 sec time bins separated by 20 sec (time is indicated in each heat map). Distinct subregions maintain their CBF and the relationship to surrounding subregions throughout the recording (280 sec shown). CBF varied between 22.4-24.4 Hz (not indicated in figure).

3.4 Regulation of CBF

3.4.1 Water flow increases CBF of MCCs

Cilia have previously shown to respond to mechanical forces by adaptation of their beating properties. In order to test whether olfactory MCCs respond to such stimuli, I applied different flows and measured the change of CBF. To this end, larvae were paralyzed and embedded in agarose as previously described. A custom-made setup, maneuvered by an Arduino, controlled the admission of flow to larvae, which were positioned to directly face the incoming flow. The CBF of motile cilia in the olfactory pit was characterized with and without flow by high-speed light microscopy and FFT analysis, as described in section 3.2.1. All experiments showed that MCCs in the olfactory pit of 4 dpf zebrafish larvae respond to an induced flow of water (3 mL/min) by increasing their CBF. Lower flow induced an increased CBF as well, but more moderate (data not shown).

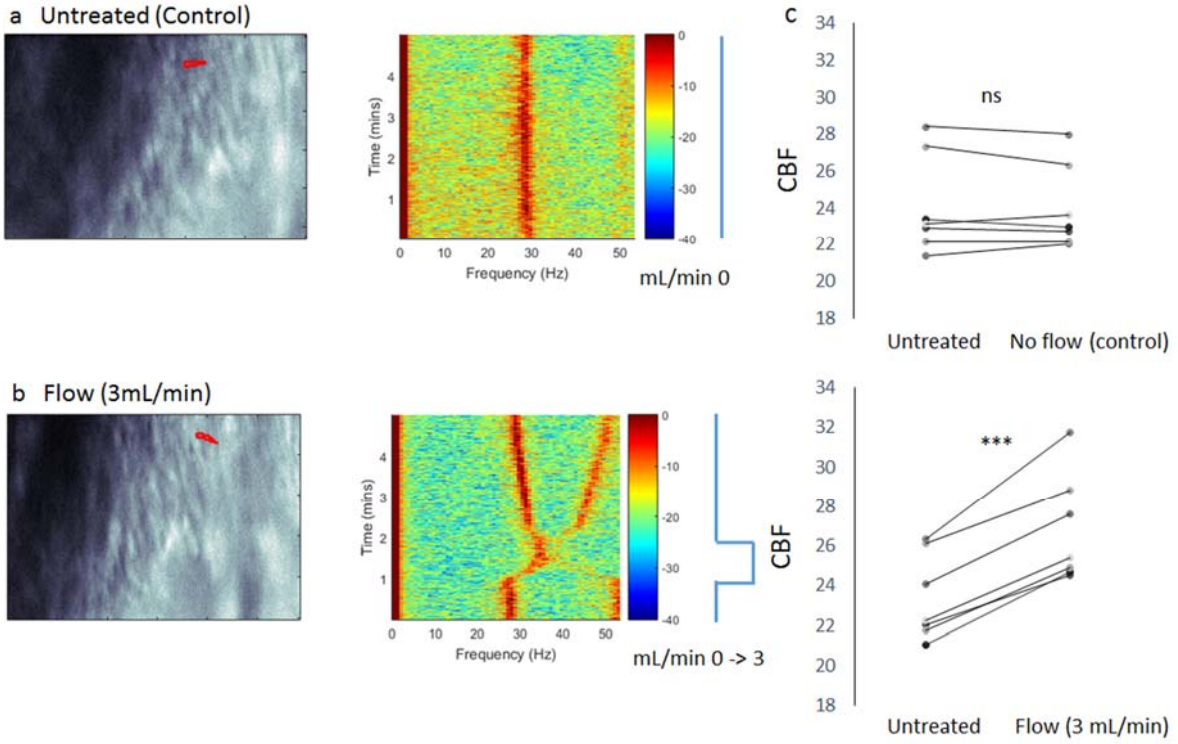

Figure 3.8. Flow increases CBF of MCCs in olfactory pits of 4 dpf wild-type larvae. (a) The CBF of wild-type olfactory pit was analyzed by FFT and shown in a spectrogram (5 min, 107 fps). The frequency was stable throughout the recording, indicated by a straight line of peak average frequencies. (b) The same larva was subsequently exposed to high flow (3 mL/min). CBF increased rapidly at the onset of flow (at 1 min) and reached a maximum value after 30 sec (at 1.5 min). After the flow was shut off (at 2 min), CBF decreased slowly. Cilia did not reach the initial CBF 3 min after the flow was stopped. (c) Induced flow (3 mL/min) increased average CBF of larvae (n=7) from 23.4±2.2 Hz (measured for the 0-10th sec) to 26.8±2.7 Hz (measured for the 90-100th sec), which is a statistically significant increase (paired-samples t-test, ***p<0.0001). In contrast, average CBF of controls (n=7), measured at 0-10th and 90-100th sec, did not change significantly over time (paired-samples t-test, ns p=0,674). Blue bars to the right of the spectrograms indicate the level of flow (mL/min) at certain time points of recording.

CBF of olfactory pits of wild-type larvae was first analyzed without application of flow, as controls (Fig. 3.8a). Subsequently a second recording was made where flow was applied (Fig. 3.8b). CBF was estimated by FFT analysis and shown in a spectrogram. The spectrogram of a control larva not exposed to flow, Fig. 3.8a, generated a straight line of the FFT peak frequencies, which indicate a relatively stable CBF through the full recording (here at approx. 28 Hz). This was observed for all larvae not exposed to flow. These results are consistent with previous s of CBF of the olfactory pit of untreated wild-type larvae. FFT analysis of the 0-10th sec and 90-100th sec in recordings of control larvae (n=7) showed there was no significant difference between the CBF in the two time periods (paired-samples t-test, Fig. 3.8c).

In subsequent sessions, flow was applied after 60 sec of recording for a duration of 60 sec. The 3 min following the stimulus were also recorded. Larvae stimulated with flow (3 mL/min) showed a distinct increase in CBF upon application. As shown in the spectrogram analysis (Fig. 3.8b), the CBF increased quickly as the flow was applied and reached a maximum value 30 sec after the onset of the stimuli. CBF slowly decayed as the flow stopped. By the end of recording, 3 min after the offset of flow, the average CBF was higher than at the beginning of the recording, indicating that 3 min post-flow is not sufficient for MCCs of the olfactory pit to recover initial CBF. FFT analysis of the 0-10th and 90-100th sec (where CBF was at its maximum level) of recordings show that the MCCs of the olfactory pit of wild-type larvae (n=7) increased their average CBF by 12.7% upon exposure to flow. Average CBF significantly increased from 23.4±2.2 Hz to 26.8±2.7 Hz (paired-samples t-test, Fig. 3.8c).

To investigate whether flow increased the CBF in the whole olfactory pit or just in subregions, whole-field FFT analysis of ciliary beating was conducted. CBF is shown in FFT analysis heat maps estimated from bins of 10 sec (Fig. 3.9). Each interval in the recording is shown and duration of applied flow is marked with a black box. The relationship between subregions with distinct beating frequencies was preserved throughout the flow-treatment, strengthening the findings in section 3.3.2. CBF increased to a maximal level already 30 sec after the onset of flow and did not increase further (estimated from the colors in heat maps). Beating frequency slowly decreased after the flow was turned off. The initial CBF was not regained at the end of the recording (estimated by the differences of color between the first (blue) and last (green) heat map, Fig. 3.9). Thus, CBF increased in the whole area of the olfactory pit that was investigated by similar kinetics.

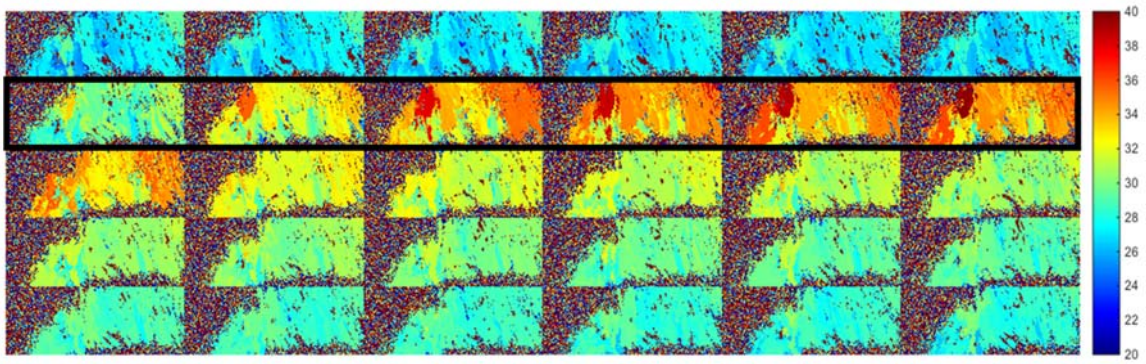

Figure 3.9. Flow increases CBF in the entire olfactory pit of wild-type larvae at 4 dpf. (a) The same recording as used earlier (Fig. 8) was analyzed for the whole field of view. FFT pixel analysis of the full recording (5 min) is shown as heat maps of 10 sec time bins. Flow duration is indicated by the black box. All cilia of the olfactory pit increased their CBF upon application of flow. Cilia beat relatively stably at ~25 Hz the first min (top panel). After 30 sec of applied flow (black box), cilia were beating at their maximal value and CBF plateaued at ~36 Hz. After the flow was turned off, the frequency slowly started to decay. Initial CBF was not regained at the end of recording. Color scale: 20-40 Hz.

To identify whether CBF increased by a regulatory mechanism or merely because of hydrodynamic forces on the cilia, mutant *smh* larvae with immotile cilia (see section 3.7.1 for characterization of *smh*) underwent the same treatment as wild-type larvae. Olfactory pit ciliary beating in *smh* larvae was analyzed by FFT analysis and shown in a spectrogram (Fig. 3.10). No beating was detected in either untreated *smh* (Fig. 3.10a) or *smh* subjected to flow (Fig. 3.10b). This indicates that the observed increase in CBF is not the result of hydrodynamic forces generated by the flow. Rather, my findings suggest that MCC actively regulate their CBF upon a mechanosensory stimulus.

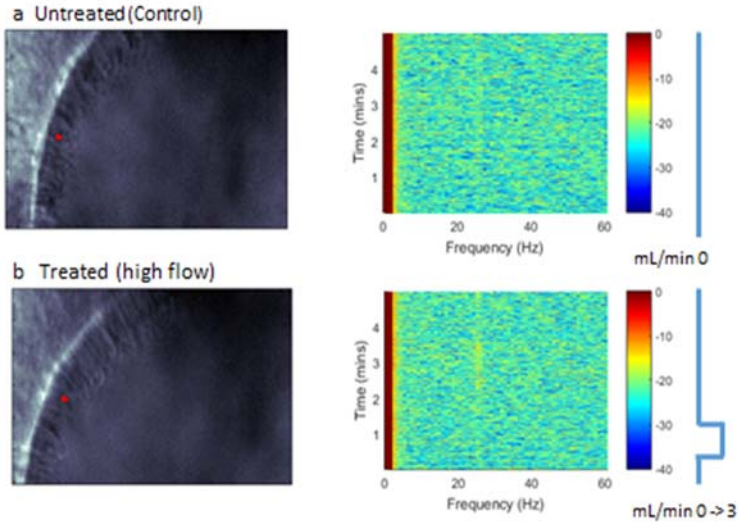

Figure 3.10. Flow does not generate ciliary beating in olfactory pits of *smh* mutants whose cilia are immotile. (a) Light microscopy recording (5 min, ~100 fps) of cilia in the olfactory pit of *smh* mutants. No movement was detected, as shown by the absence of signal in the spectrogram. (b) CBF analysis of the same olfactory pit as flow was applied in the 2nd min of recording. No signal was detected in the spectrogram analysis either before, during or after the onset of flow. Blue bars to the right of the spectrograms indicate the level of flow at certain time points of recording.

3.4.2 Temperature increases CBF of MCCs

Previous studies indicate that ciliary beating is sensitive to temperature (i.e. (Sisson et al., 2003)). In order to test whether MCCs in the olfactory pit of zebrafish larvae were also temperature sensitive, wild-type larvae were prepared for light microscopy recordings, as previously described, and exposed to water flow of different temperatures. CBF was first measured as larvae were exposed to increasing temperatures and subsequently measured as the temperature was decreased to initial level.

Temperature was monitored with an automatic temperature controller (Warner I.C). This instrument has a heating apparatus coupled to the outlet of the flow which is able to control the temperature from 24±2°C to 32±2°C. The water flow was continuously heated/cooled from the starting time point of recording, but due to limitations of the utilized device the increase in temperature was non-linear. By contrast, the decrease of temperature appeared more linear as it depended mostly on the flow. Larvae were continuously exposed to flow throughout the whole recording, and average CBF of cilia in olfactory pits was therefore higher than usual (compare Fig. 3.8c with Fig. 3.11c).I characterized the CBF of motile cilia in the olfactory pit exposed to increasing and decreasing temperatures by high-speed light microscopy and FFT analysis, as described in section 3.2.1.

Cilia of MCCs in olfactory pits of wild-type larvae increased their CBF in response to temperature increments. In the example of Fig. 3.11a, olfactory pit MCCs started responding to the temperature changes at about 1 min of treatment and CBF increased abruptly from the initial level of 30.3 Hz to a maximum value of 42.2 Hz within 2 min (exact values not indicated in figure). CBF plateaued at ±42 Hz and did not increase further. Due to limitations of the device, the exact temperatures at a given time point were impossible to obtain. This makes the interpretation of the resulting spectrograms, as Fig. 3.11a, difficult. FFT analysis of the 0-10th sec and 170-180th sec (when max CBF was reached) of recordings show that average CBF increased by 39% upon exposure to higher temperatures. CBF significantly increased in average from 28.0±1.8 Hz at 24°C to 39.2±2.8 Hz at 32°C (paired-samples t-test, Fig. 3.11c).

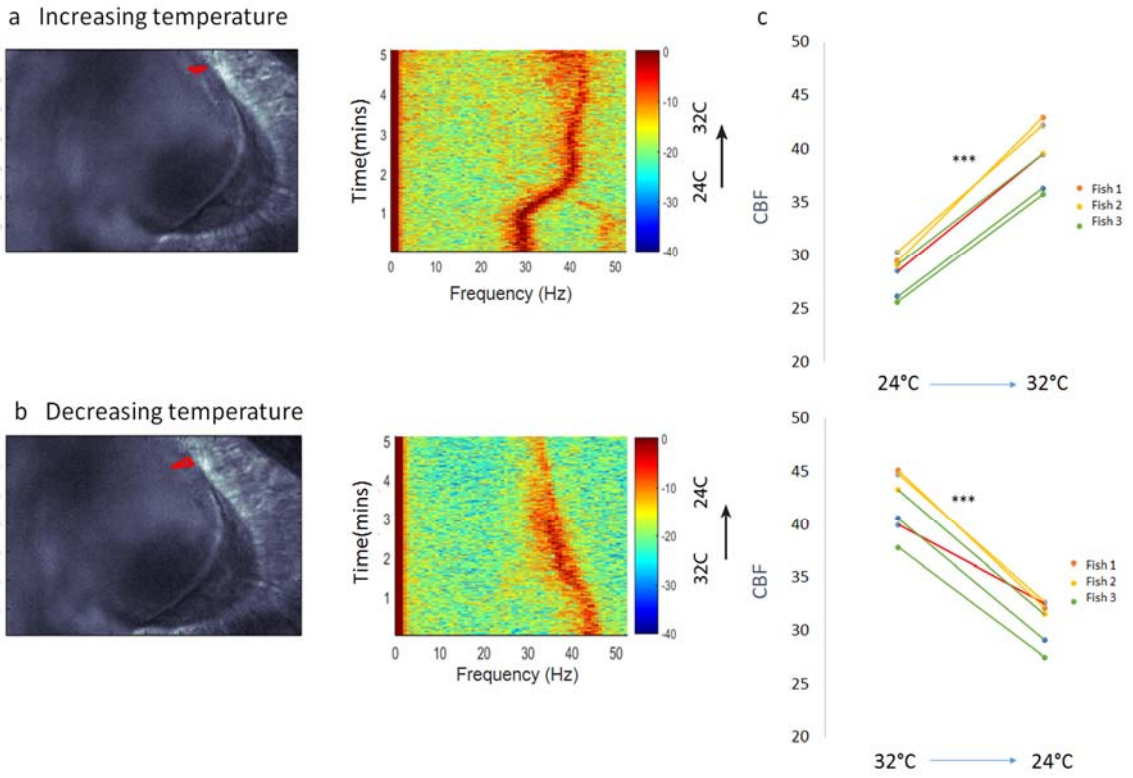

Figure 3.11. Temperature regulates CBF of MCCs in olfactory pits of 4 dpf wild-type larvae. CBF was measured from light microscopy recordings (5 min, ~100 fps) of the olfactory pit of wild-type larvae subjected to a temperature increase (a) or decrease (b). (a) Upregulation of temperature from 24±2°C to 32±2° elevated CBF. CBF increased abruptly after 1 min and plateaued around 40 Hz after 2 min. Some drift observed at the end of the recording interfered partially with the frequency analysis and resulted in a wider CBF on the spectrogram. (b) Downregulating temperature from 32±2°C to 24±2°C decreased CBF. Decrease in temperature was characterized by a slow, but stable, decay of CBF towards initial level. (c) For increasing temperatures, CBF was estimated from the 0-10th sec and 170-180th sec (when max CBF was reached) of the recording. Average CBF increased from 28.2±1.9 Hz to 39.4±2.9 Hz (paired-samples t-test, *** $p<0.001$). For decreasing temperatures, CBF was estimated from the 0-10th sec and 290-300th sec of recording. Average CBF decreased from 41.9±2.9 Hz to 30.9±2.1 Hz (paired-samples t-test, ***$p< 0.001$). Larvae (n=3) are color-coded, and the color correspond to the same larvae in both graphs.

Larvae which were stimulated by high temperatures decreased their CBF close to initial frequency when the temperature was brought back down to 24±2°C. In the example of Fig. 3.11b, a decay in CBF started within 60 sec and was slower and more linear compared to the abrupt increase observed in Fig 3.11a. FFT analysis of the first and last 10 sec of recording show that CBF decreased in average by 17% upon exposure to lower temperatures. Average CBF significantly decreased from 41.6+2.8 Hz at 32°C to 34.7+2.0 Hz at 24°C (paired-samples t-test, Fig. 3.11c). Altogether, my findings suggest that olfactory MCCs can regulate their CBF according to the temperature of the environment, as previously shown for other ciliated cell types.

3.4.3 Testing the effect of chemicals on CBF

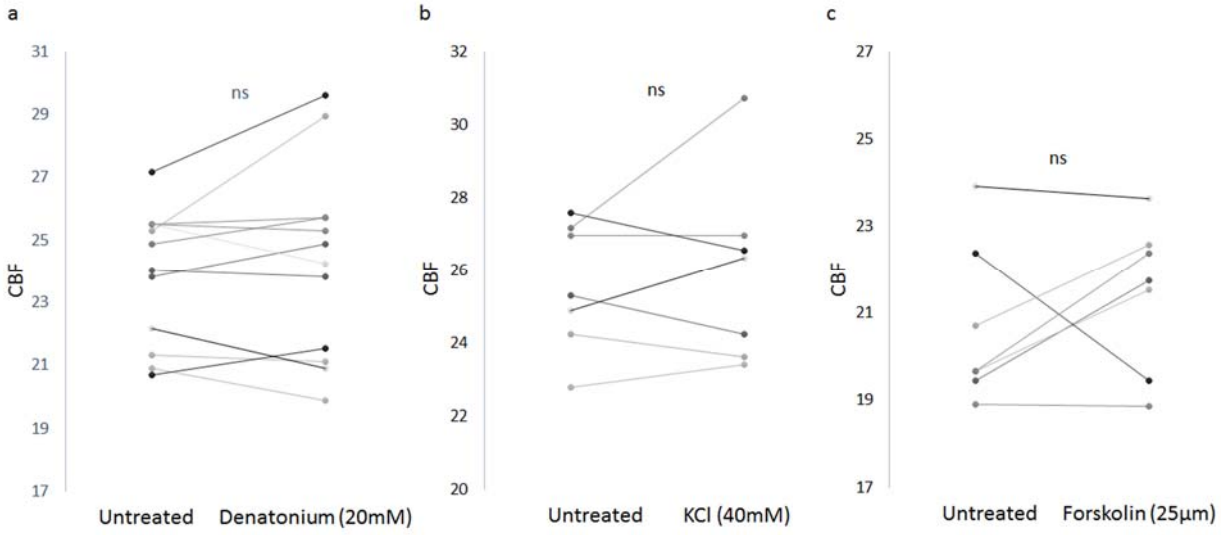

Figure 3.12. CBF of wild-type larvae before and after 2 min treatment with the indicated drug. Each line corresponds to one larvae. (a) Denatonium (20mM) and (b) KCl (40mM) were suspended in AFW, and (c) forskolin (25µM) in DMSO. CBF was characterized before (untreated) and after treatment by FFT analysis of light microscopy recordings (30 sec, ~100 fps). 4 dpf wild-type larvae were bathed in solution for 2 min before CBF post-treatment was analyzed. Neither of the indicated drugs significantly changed CBF (paired-samples t-test, ns $p>0.5$).

Many MCCs increase their CBF upon stimulation with various chemicals. Bitter compounds increase CBF and cellular calcium (Ca^{2+}) levels in respiratory MCCs via bitter receptors expressed in the cilium (Shah et al., 2009). KCl depolarizes cells, increases Ca^{2+}levels, and is thus a potential candidate to regulate CBF, either cell-autonomously or via other cells (Conductier et al., 2013, Mueller et al., 2013). Also, forskolin enhances CBF by acting through the second messenger cAMP (Braiman et al., 1998). In order to test whether these molecules affected CBF of olfactory MCCs in zebrafish larvae, I measured CBF before and after application of drugs at concentrations reported in the literature. Larvae were paralyzed and embedded in agarose as previously described. For each drug I characterized the CBF in the olfactory pit before and after treatment by light microscopy and FFT analysis, as described in section 3.2.1. A waiting period of 2 min between application and recording was provided to allow time for the compound to diffuse to the cell. Control larvae were treated with artificial fish water (AFW) or DMSO as the drug vehicle. All controls showed normal ciliary beating (data not shown).

Treatment of wild-type larvae (n=12) with denatonium (20 mM) did not significantly increase CBF, as average CBF only changed from 23.9±2 Hz to 24.3±3.Hz after treatment (paired-samples t-test, Fig. 3.12a). CBF was neither significantly affected in wild-type larvae (n=7) upon treatment with KCl (40mM), in average only increasing from 25.6±1.8 Hz to 26.0±2.6 Hz (paired-samples t-test, Fig. 3.12b). Also, average CBF of wild-type larvae (n=7) did not significantly differ before and after treatment of forskolin (25µM), measured as 20.7±1.8Hz and 21.4±1.7Hz, respectively (paired-samples t-test, Fig. 3.12c). Altogether, my findings suggest that the MCCs of the olfactory pit do not regulate their CBF in response to bitter substances, the depolarizing agent KCl or increased cAMP levels by forskolin, contradicting findings in other MCC types.

3.5 Ca^{2+} activity in MCCs of the olfactory pit

Ca^{2+} has shown to regulate CBF in various ciliated cells. In order to assess whether Ca^{2+} may also regulate CBF in olfactory MCCs, I characterized Ca^{2+} activity in MCCs of the olfactory pits of zebrafish larvae using two different fish lines. First, the enhancer-trap line *hspGGFF19b:gal4;uas:gcamp6s* and second, a transient line generated by microinjection of *foxj1a:gcamp6*-plasmid with transposase mRNA in embryos. Both express the genetically encoded Ca^{2+} indicator GCaMP6s in MCCs of the olfactory pit and thus emit green fluorescence. Combined with two-photon imaging, I could measure spontaneous Ca^{2+} activity as well as Ca^{2+} activity following the delivery of flow, reported as the change of fluorescence over time (dff).

3.5.1 Spontaneous Ca^{2+} activity in MCCs of olfactory pit of transgenic larvae

In order to first identify the spontaneous Ca^{2+} activity in olfactory MCCs, two-photon microscopy recordings (10 min, 26 fps) were made of *foxj1a:gcamp6* larvae. Paralyzed larvae were up-right positioned in agarose, and agarose surrounding the olfactory pits were removed to allow free ciliary beating. Diagram in Fig. 3.13 shows the Ca^{2+} activity (dff) in the MCCs in the olfactory pit of 5 individual larvae. Only cells of good health were chosen for the analysis. Further characterization of spontaneous Ca^{2+} activity is outlined in Fig. 3.14. There was in average 0.4 Ca^{2+} peak events per minute with a duration of 25 sec and an average peak amplitude of 43,7% (dff). Fig. 3.14d shows the trace of an average Ca^{2+} peak (dff/time) in the MCCs of the olfactory pit of *foxj1a:gcamp6* larvae. Visualization of how oscillatory Ca^{2+} waves are displayed in the olfactory pit can be seen in supplementary video S4.

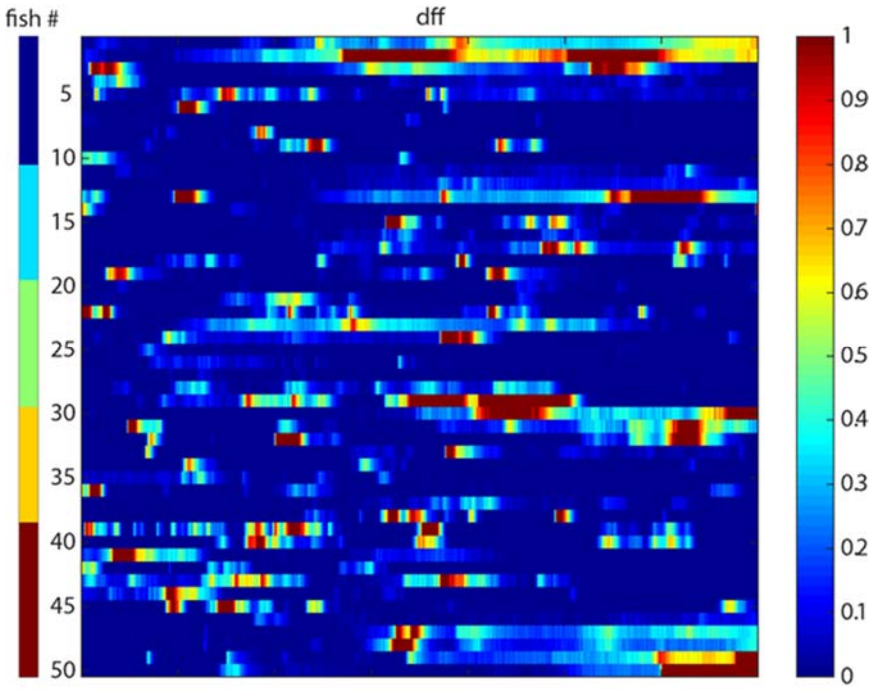

Figure 3.13. Spontaneous Ca^{2+} activity in MCCs of the olfactory pit of 4 dpf *foxj1a:gcamp6 larvae*. (a) two-photon microscopy recording (10 min, 26.3 fps) of paralyzed transgenic larvae showed a wide distribution of random Ca^{2+} events, presented as dff. Number of fish is indicated in the left axis (n=5). Each line of the dff-diagram represents one cell. Color scale (right) indicates range of dff, from 0-1.

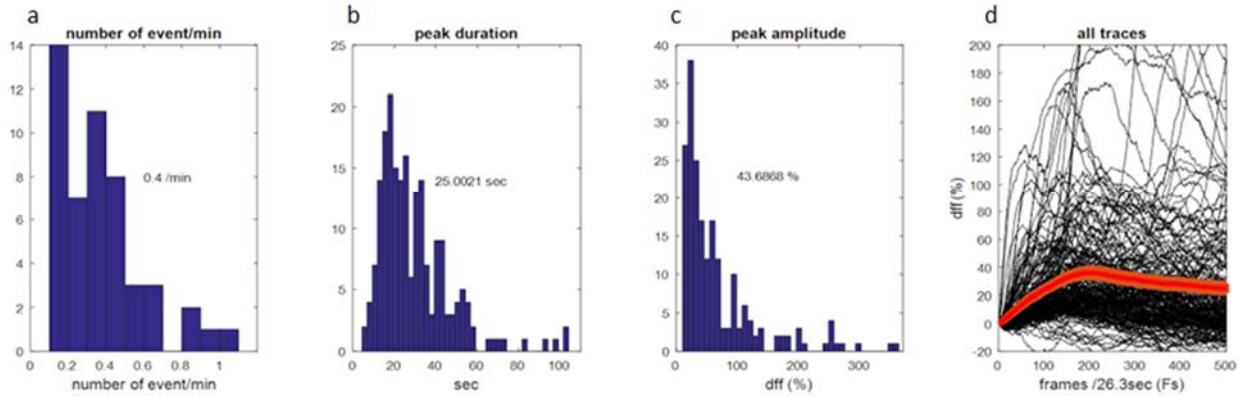

Figure 3.14. Further characterization of spontaneous Ca^{2+} peaks in MCCs of olfactory pit of 4 dpf *foxj1a:gcamp6* larvae. Analysis are based on all Ca^{2+} peaks detected in Fig 3.14., shown in histograms. (a) Most cells presented few Ca^{2+} events/min (<0.5). Median value of frequency of events is 0.4/min. (b) Most peaks lasted about 25.0 sec with (c) an amplitude of 43.7% dff. All values indicated on the graphs are the median value. (d) The trace of the average Ca^{2+} peak in a MCC of the olfactory pit, represented as dff per time (in frames, 26.3 frames/sec).

My findings suggest that MCCs of the olfactory pit of 4 dpf zebrafish larvae display dynamic Ca^{2+} events which can be measured with the genetically encoded Ca^{2+} indicator GCaMP6s.

3.5.2 Investigating correlation between CBF and Ca^{2+} activity

Since CBF of olfactory pit MCCs increases in response to flow (see section 3.4.1), I wanted to test whether an application of flow to larvae would correlate to Ca^{2+} activity. In these experiments we used larvae injected with *foxj1a:gcamp6s* and two-photon microscopy imaging combined with a similar Arduino-controlled flow-delivery system as used in previous experiments.

Paralyzed *foxj1a:gcamp6s* larvae were embedded in agarose as previously described for experiments with flow by light microscopy (see section 3.4.1). The diagram in Fig. 3.15 shows the Ca^{2+} activity (dff) in the MCCs of the olfactory pits of 6 individual larvae within a two-photon microscopy recording of 6 min. Only cells of good health were chosen for the analysis. Flow (3 mL/min) was applied to larvae after 2 min and left on for 1 min in total (green box). There was no particular correlation between the onset of flow and Ca^{2+} activity in the MCCs of the olfactory pit (Fig. 3.15). The activity was slightly decreasing after the flow turned off, which may result from phototoxic effects of the laser combined with flow (data not shown).

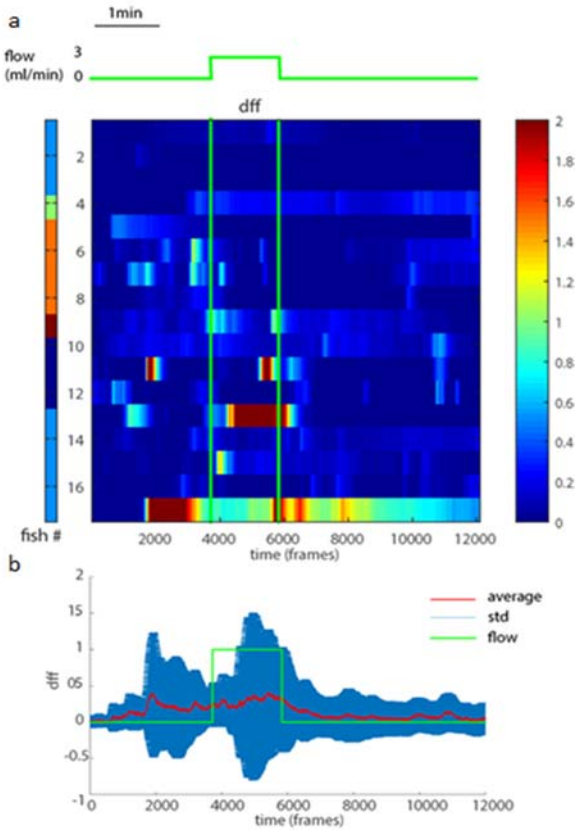

Figure 3.15. MCCs of olfactory pit of 4 dpf *foxj1a:gcamp6s* larvae do not induce Ca^{2+} peaks upon application of flow. (a) Ca^{2+} activity (dff) of transgenic larvae characterized by two-photon microscopy recordings (6 min, 35 fps). Number of fish is indicated in the left axis and corresponding lines in the dff-diagram are individual cells. Flow was applied after two min (green lines). Green bars (top) indicate the level of flow at certain time points of recording. Color scale (right) shows the range of dff, from 0-2. (b) Graph indicating the average and standard deviation for all cells analyzed over time (in frames, 35 frames/sec). Period of flow duration is marked in green.

To further investigate the relationship between Ca^{2+} activity and ciliary beating I wanted to investigate a potential correlation between spontaneous Ca^{2+} events and CBF. In these experiments, olfactory pits of *hspGGFFf19b:gal4;uas:gcamp6s* larvae were imaged by light sheet microscopy. Recordings were made at 100 fps, allowing simultaneous recording of Ca^{2+} levels and CBF. Beating frequency was characterized by FFT analysis, as described in section 3.2.1.

A 5 min light sheet microscopy recording of MCCs in olfactory pit was sufficient to detect 1-2 Ca^{2+} fluctuations per cell, represented in Fig. 3.16. Cells with characteristic Ca^{2+} peaks were analyzed by the FFT algorithm at time points before, during and after the peak to see whether the rise in Ca^{2+} concentration was correlated to a change in CBF (n=20). The two representative MCCs that displayed a clear Ca^{2+} peak in Fig. 3.16 did not change their CBF during or after the peak, shown by the spectrograms of two ROIs within the beating range of the cilia (Fig. 3.16a'',b'').

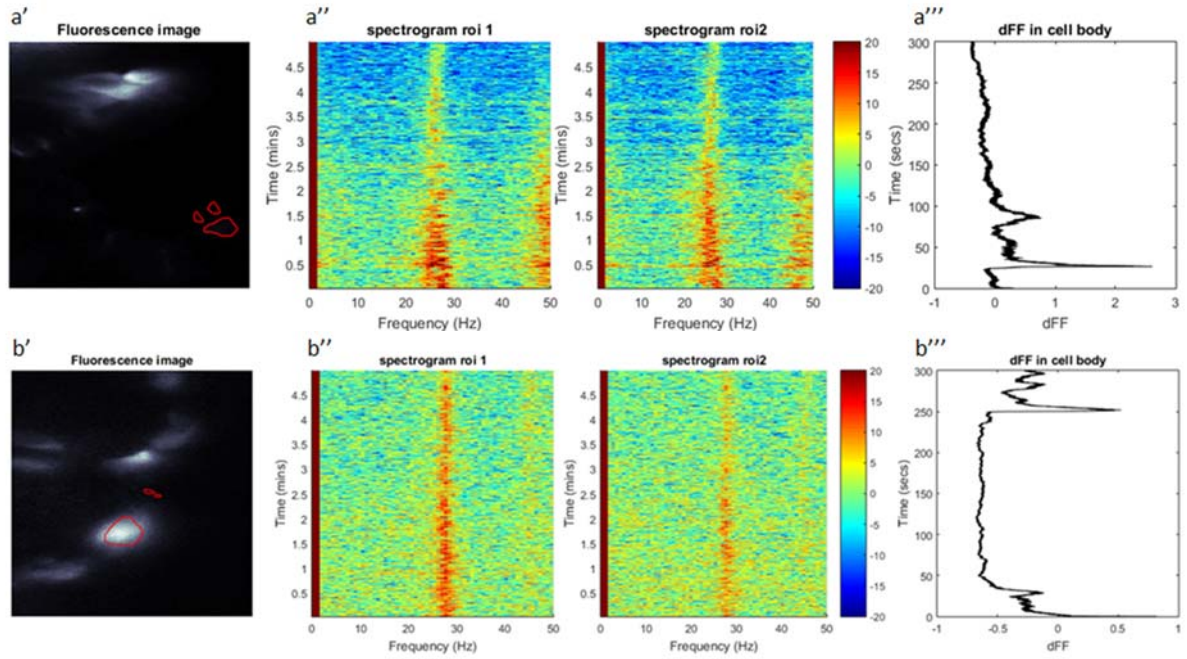

Figure 3.16. Increase in spontaneous Ca^{2+} levels in olfactory pit of *hspGGFF19b:gal4;uas:gcamp6s* larvae does not correlate with increasing CBF. (a,b) Spontaneous Ca^{2+} activity in single MCCs was investigated by light sheet microscopy recordings (5 min, 100 fps). 2 different representative cells are presented. (a'',b'') two regions of interest within the range of active ciliary beating (the smallest ROIs in a',b') are represented in spectrograms. No particular deviations from the initial CBF can be seen. (a''',b''') Ca^{2+} activity of the indicated MCC (the largest ROI in a',b') shown as a function of dff over time. (a''') A distinct Ca^{2+} peak is detected in the first min of recording. (b''') A distinct peak of lower amplitude is detected in the last min of recording.

Taken together, these results show that the investigated MCCs display dynamic Ca^{2+} activity, but that they are not related to CBF, contradicting findings in many other MCCs.

3.6 Testing interactions between ORNs and MCCs

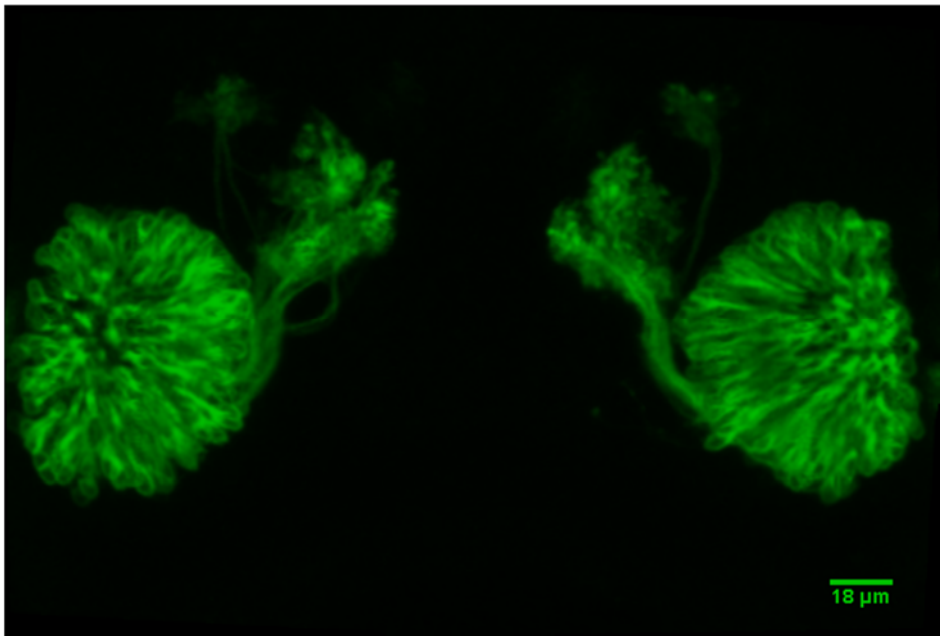

Figure 3.17. Confocal microscopy of *OMP:ChR2-YFP* larvae at 4 dpf. YFP-tagged ChR2 is expressed in ciliated ORNs of the olfactory pits, characterized by pear-shaped slender cell bodies and axonal projections into glomeruli of the olfactory bulb. Scale bar: 18 µm.

Because of the proximity between MCCs and ORNs I hypothesized that the two cell types could interact. To investigate whether the activity of neighboring ORNs influenced MCC ciliary beating, I utilized a transgenic zebrafish line in which ciliated ORNs could be activated by optogenetics. The transgenic line *OMP:ChR2-YFP* expresses the light-sensitive cation channel channelrhodopsin-2 (ChR2) coupled with the marker protein YFP under the endogenous OMP (olfactory marker protein) promoter. OMP is expressed strongly and specifically in ciliated ORNs during the whole developmental period (Celik et al., 2002). Thus, expression of ChR2 under this promoter enables light to specifically and temporally regulate ciliated ORN activity (Bellmann et al., 2010). The ciliated ORNs of YFP-expressing larvae (*OMP:Chr2-YFP*), shown by confocal imaging in Fig. 3.17, can be activated by direct exposure of 488 nm LED light.

The CBF of *OMP:ChR2-YFP* larvae was measured upon stimulation with blue LED light. Larvae were paralyzed and embedded in agarose as previously described. The same custom-made setup as described in section 3.4.1 controlled admission of LED light to larvae. I then characterized the beating frequency of motile cilia in the olfactory pit with and without LED light exposure by high-speed microscopy recordings and FFT analysis, as described in section 3.2.

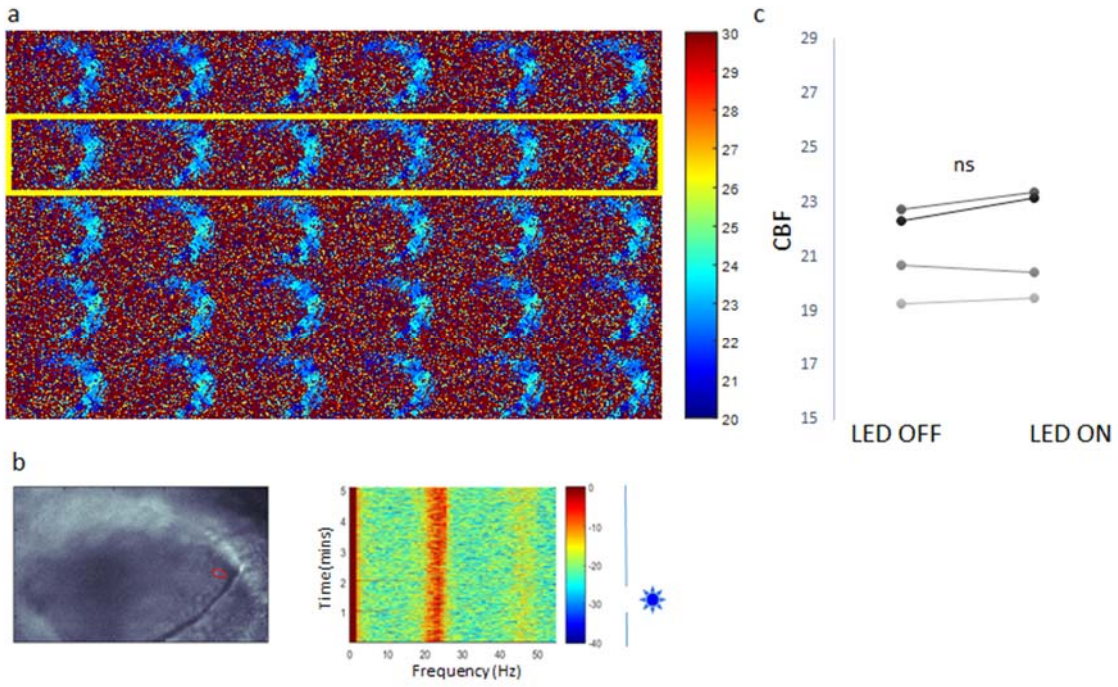

Figure 3.18. Activation of ciliated ORNs does not induce a change in CBF of MCCs in olfactory pit of *OMP:Chr2-YFP* larvae. (a) FFT analysis of light microscopy recording (5 min, 107 fps) of olfactory pit of *OMP:Chr2-YFP* with inducible ORNs. Analysis is shown in heat maps estimated of 10 sec time bins. The average CBF of cilia in the olfactory pit is around 20-23 Hz (indicated by blue color). LED exposure (yellow box) does not induce a change in ciliary activity as heat maps are similar for all time bins. Color scale: 20-30 Hz. (b) Same recording shown in a spectrogram. Blue bars to the right indicate time of LED exposure. No LED was used except for 1 min (indicated by sun, 60-120 sec). No change in CBF is seen in the spectrogram, at the onset of LED. (c) FFT analysis of CBF was run on the 0-10th sec (LED OFF) and on the 110-120th sec (last 10 sec of LED exposure, LED ON) of all recordings (n=4). The relationship between pre- and post-treatment CBF is not significant (paired-samples t-test, ns: $p>0.5$).

Fig. 3.18a shows the FFT frequency heat map for a 5 min light microscopy recording (approx. 100 fps), estimated from 10 sec time bins. All intervals of the recording are shown and time of LED exposure is indicated by the yellow box. No difference in CBF can be seen in the heat maps. This is verified by visualization of the same recording in a spectrogram (Fig. 3.18b). No deviations from the initial frequency is observed either in the period with LED exposure (LED ON, 60-120 sec) or in the period without LED exposure (LED OFF, Fig. 3.18b). FFT analysis of the 0-10th sec of recording (LED OFF) and the 110-120th sec (LED ON) confirm that there is no significant difference in the average CBF for the treated and untreated periods (Fig. 3.18c). My findings suggest that there are no communicative mechanisms between ciliated ORNs and MCCs in the olfactory pit of zebrafish larvae at 4 dpf that regulate CBF.

3.7 Mutants

In order to understand the function of beating cilia in the olfactory pit it is of advantage to analyze the olfactory phenotypes of mutant larvae with ciliary defects in the olfactory epithelium. Zebrafish mutants with genetic mutations in ciliary genes are the most straightforward approach to perform these experiments. For this purpose I characterized 5 mutant lines that were available in our laboratory. 4 were originally identified in ENU mutagenesis screen and acquired through collaboration: *elipsa*, *smh* and the intraflagellar transport (IFT) mutants *oval* (*ift88*) and *ift172*. Moreover, one mutant line targeting the *foxj1a* gene was generated in our laboratory by the CRISPR/Cas9 method. All mutations resulted in the loss of function of the affected gene.

Cilia defects in zebrafish are associated with typical phenotypes and can therefore easily be identified. The hallmark is a curved body axis. For the following experiments, 4 dpf larvae were obtained from an incross of genotyped heterozygous adults. Homozygous mutants were identified based on their curved body phenotype. Straight-tailed larvae from the same clutch were selected as controls, and thus included both heterozygous mutants and wild-type. For each mutant line I first characterized the morphology and the ciliary distribution of the olfactory pit by confocal imaging. Larvae were immunostained with AcTubulin, a cilia marker, and DAPI. All controls showed a normal distribution of cilia with densely labeled MCC cilia at the outer rim of the pit and ORN cilia in the middle and bottom of the pit (i.e. Fig. 3.19a'). Later, I characterized the CBF of motile cilia in the olfactory pits of controls and mutants by high-speed light microscopy and FFT analysis, as described in section 3.2.1.

3.7.1 Zebrafish *smh* mutant

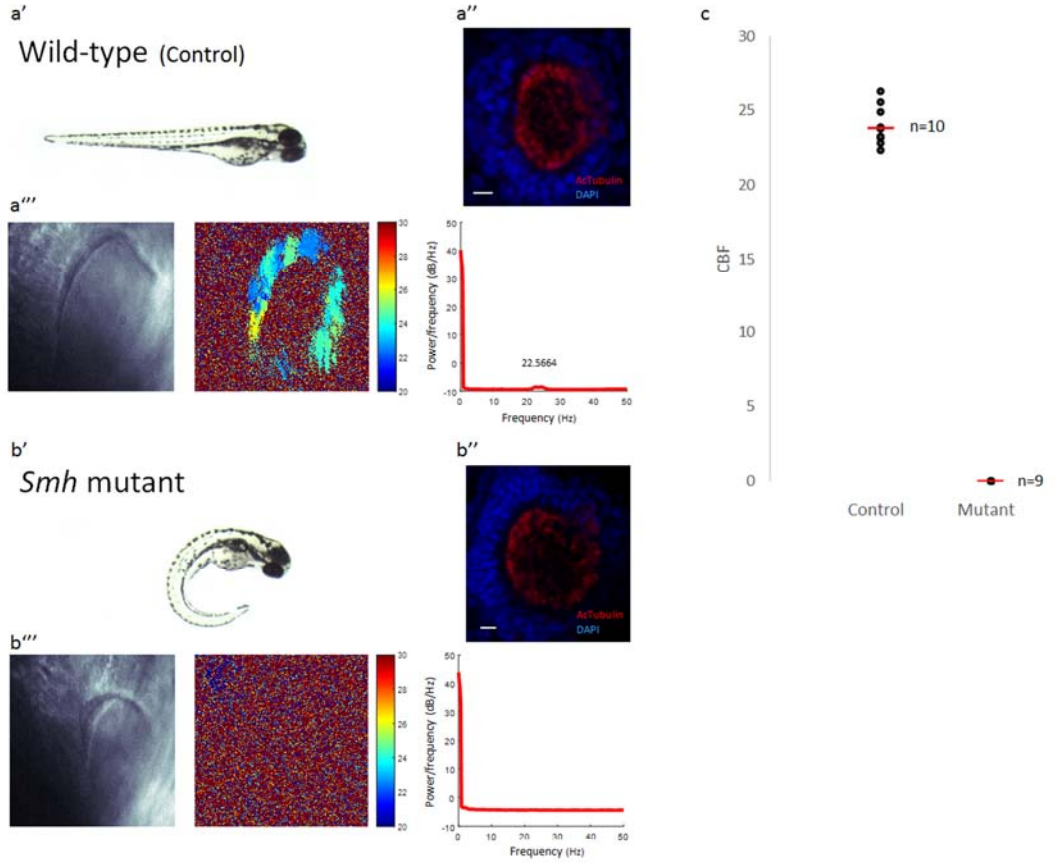

Figure 3.19. Characterization of the cilia mutant *smh* at 4 dpf. (a) Representative example of control larvae with (a') straight body-axis, (a'') labeled cilia in the olfactory pit (AcTubulin immunostaining by confocal microscopy) and (a''') normal ciliary beating (here: average CBF of 22.6 Hz). (b) Representative example of *smh* larvae with (b') curved body axis and (b'') labeled cilia in the olfactory pit (AcTubulin immunostaining), similar to control larvae. (b''') No ciliary beating in the olfactory pit was detected by FFT analysis. (c) Scatter plot representing the CBF of all the characterized control larvae (n=10) and *smh* mutants (n=9). Average CBF (red bar) of the control larvae equals 23.9±1.2Hz. No ciliary activity was detected in *smh* mutants. Scale bar: 10µm.

The zebrafish *schmalhans* (*smh*) mutants have a mutation in *ccdc103* which affect both inner and outer dynein arm assembly, making cilia immotile (Panizzi et al., 2012). *Smh* mutants have a curved body axis (Fig. 3.19a'). The preserved cilia morphology of *smh* mutants at 4 dpf is shown by confocal microscopy imaging (compare Fig. 3.19a'' to b''). No ciliary beating was detected in *smh* mutants by FFT analysis of light microscopy recordings (Fig. 3.19b'''). In contrast, motile cilia located at the periphery of the olfactory pit of the control larvae showed normal ciliary beating (Fig. 3.19a'''). The scatter plot in Fig. 3.19c shows the distribution of the CBF measured for all the characterized *smh* mutants (n=9) and control larvae (n=10). The average CBF of the control larvae is equal to 23.9±1.2 Hz .

3.7.2 Zebrafish *elipsa* mutant

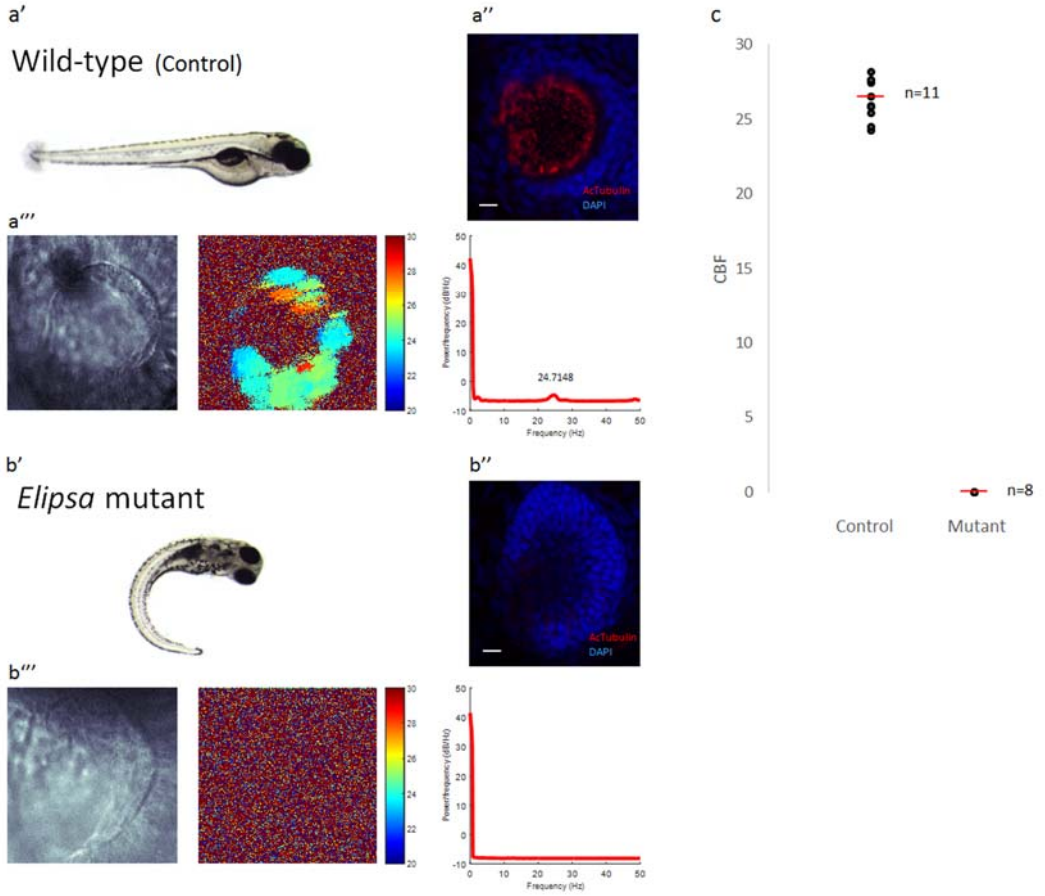

Figure 3.20. Characterization of the cilia mutant *elipsa* at 4 dpf. (a) Representative example of control larvae with (a') straight body-axis, (a'') labeled cilia in the olfactory pit (AcTubulin immunostaining by confocal microscopy) and (a''') normal ciliary beating (here: average CBF of 24.7 Hz). (b) Representative example of *elipsa* larvae with (b') curved body axis and (b'') no labeled cilia in the olfactory pit (AcTubulin immunostaining). (b''') No ciliary beating in the olfactory pit was detected by FFT analysis. (c) Scatter plot representing the CBF of all the characterized control larvae (n=11) and *elipsa* mutants (n=8). Average CBF (red bar) for the control larvae is 26.3±1.3 Hz. No ciliary beating was detected in *elipsa* mutants. Scale bar: 10µm.

The protein encoded by *elipsa (traf3ip1)* is important for linkage of the IFT particle to the membrane-associated GTPase Rab8 (Omori et al., 2008). The zebrafish mutant *elipsa* has a curved body axis (Fig. 3.20a'). The complete absence of cilia in the olfactory pit of *elipsa* mutants is shown by immunostaining with AcTubulin and confocal imaging (Fig. 3.20b''). In comparison, control larvae have AcTubulin-labeled cilia, densely located at the periphery of the olfactory pit and also represented in the bottom of the cup (Fig. 3.20a''). Motile cilia in the olfactory pit of the control larvae show normal beating behavior by FFT analysis of light microscopy recordings (Fig. 3.20a'''), while no ciliary beating was detected in *elipsa* mutants (Fig. 3.20b'''). The scatter plot in Fig. 3.20c shows the distribution of the CBF measured for

all the characterized *elipsa* mutants (n=8) and control larvae (n=11). The average CBF of the control larvae is equal to 26.3±1.3 Hz.

3.7.3 Zebrafish *oval* intraflagellar transport mutant

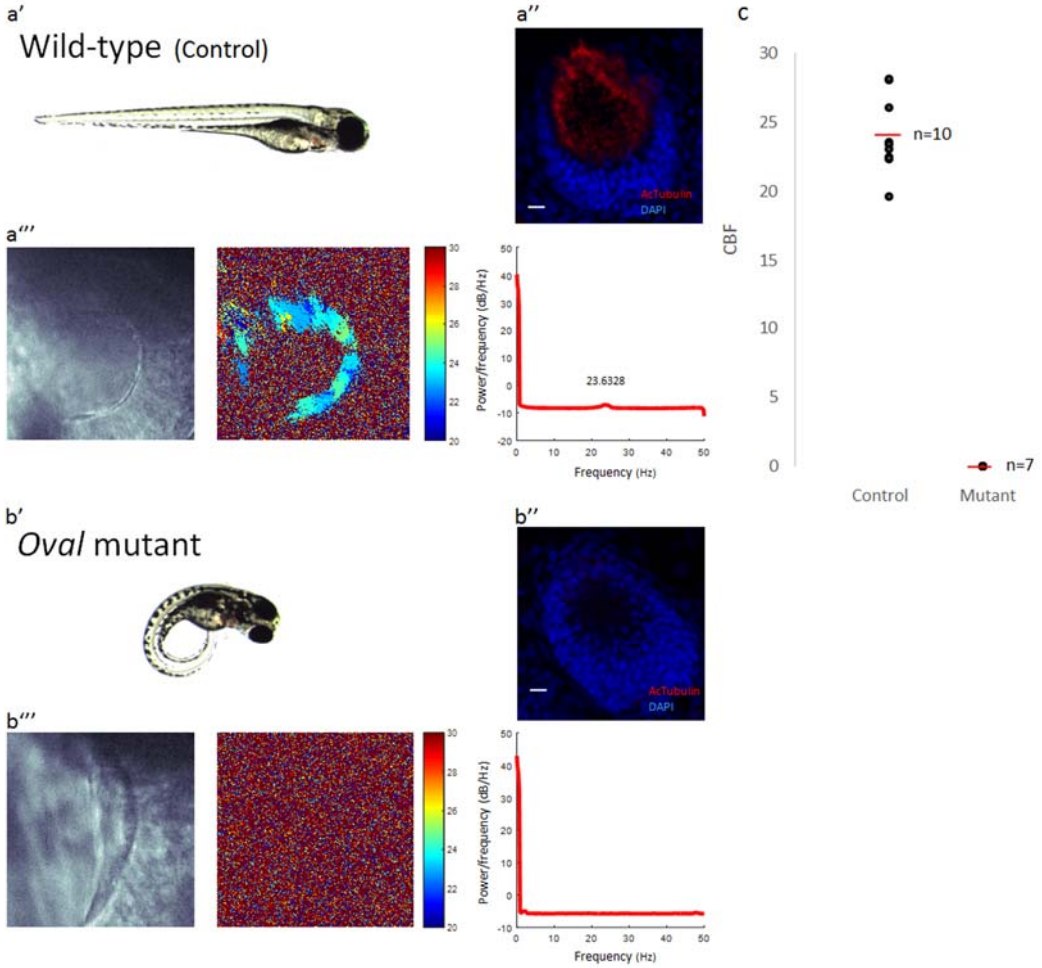

Figure 3.21. Characterization of the cilia mutant *oval* at 4 dpf. (a) Representative example of control larvae with (a') straight body-axis, (a'') labeled cilia in the olfactory pit (AcTubulin immunostaining) and (a''') normal ciliary beating (here: average CBF of 23.6 Hz). (b) Representative example of *oval* larvae with (b') curved body axis and (b'') no labeled cilia in the olfactory pit (AcTubulin immunostaining). (b''') No ciliary beating in the olfactory pit was detected by FFT analysis. (c) Scatter plot representing the CBF of all the characterized control larvae (n=10) and *oval* mutants (n=7). Average CBF (red bar) for the control larvae is 23.9±2.6Hz. No ciliary beating was detected in *oval* mutants. Scale bar: 10µm.

The zebrafish mutant *oval* carries a stop codon in the *ift88* gene encoding an IFT complex B protein. *Oval* mutants show a curved body axis (Fig. 3.21b') and the complete loss of cilia in 4 dpf mutant larvae is shown by confocal imaging (Fig. 3.21b''). Furthermore, no ciliary beating was detected in *oval* mutants (n=7) by FFT analysis of CBF (Fig. 3.21b'''). In comparison, control larvae (n=10) had a regular distribution of cilia in the olfactory pit (Fig. 3.21a'') which

showed normal ciliary beating (Fig. 3.21a'''). The average CBF of the control larvae is equal to 23.9±2.6 Hz (Fig. 3.21c).

3.7.4 Zebrafish *ift172* intraflagellar transport mutant

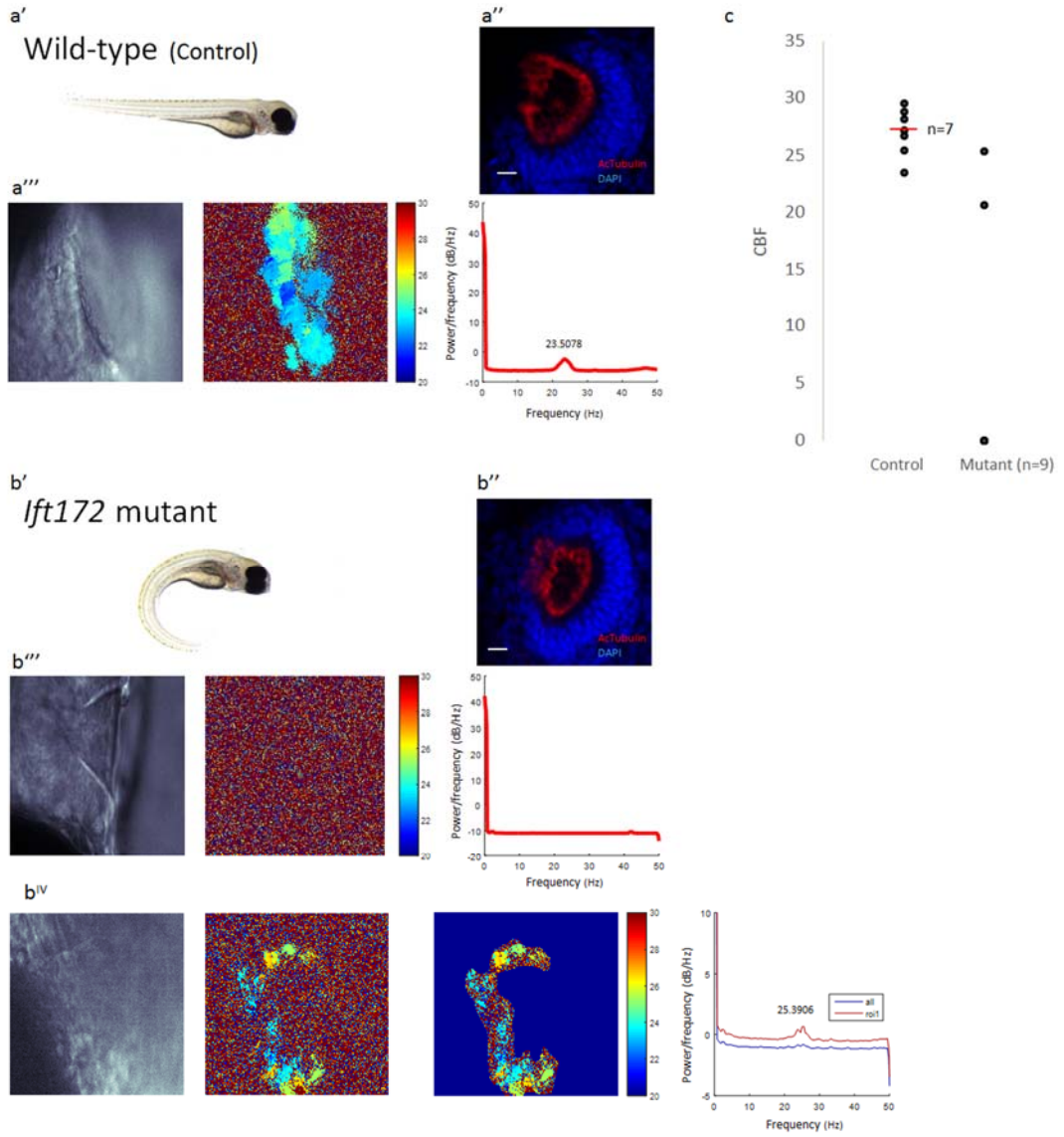

Figure 3.22. Characterization of the cilia mutant *ift172* at 4 dpf. (a) Representative example of control larvae with (a') straight body-axis, (a'') labeled cilia in the olfactory pit (AcTubulin immunostaining) and (a''') normal ciliary beating (here: average CBF of 23.5 Hz). (b) Representative example of *ift172* larvae with (b') curved body axis and (b'') labeled cilia in the olfactory pit (AcTubulin immunostaining), similar to control larvae. Presence of ciliary beating varied between larvae. (b''') No ciliary beating was detected for 7 mutant larvae. (b^{IV}) Ciliary beating was detected in 2 mutant larvae (here: average CBF of 25.4 Hz). (c) Scatter plot representing the CBF of all the characterized control larvae (n=10) and *ift172* mutants (n=9) analyzed by FFT. Average CBF (red bar) for the control larvae is 27.0±2.1 Hz. No ciliary beating was detected for 7 *ift172* mutants, but 2 larvae beat at 20.7 and 25.4 Hz. Scale bar: 10µm.

The intraflagellar gene *ift172* encodes a subunit of the intraflagellar transport subcomplex IFT-B, required for proper cilia formation (Cole, 2003). *Ift172* mutants have a curved body axis

(Fig. 3.22. b'). Furthermore, they have a normal distribution of cilia in the olfactory pits, shown by confocal microscopy imaging (compare Fig. 3.22a'' to b''). Ciliary beating was analyzed by FFT analysis of light microscopy recordings and results were not homogenous. In 7 of the 9 mutants analyzed, no CBF was detected by FFT analysis, as in the example shown in Fig. 3.22b'''. Two mutants showed ciliary beating in the olfactory pit, but with a weaker signal than what was measured for control larvae. No true peak was detected by whole-field FFT analysis and background noise had to be excluded, as in the example shown in Fig. 3.22b^{IV}. The two *ift172* mutants that displayed ciliary beating in the olfactory pit beat at 20.7 Hz and 25.4 Hz. In comparison, motile cilia located at the periphery of the olfactory pit of the control larvae showed normal ciliary beating (Fig. 3.22a'''). The scatter plot in Fig. 3.22c shows the distribution of the CBF measured for all the characterized *ift172* mutants (n=9) and control larvae (n=7). The average CBF of the control larvae is equal to 27.0±2.1 Hz.

3.7.5 Zebrafish *foxj1a-del5* mutant

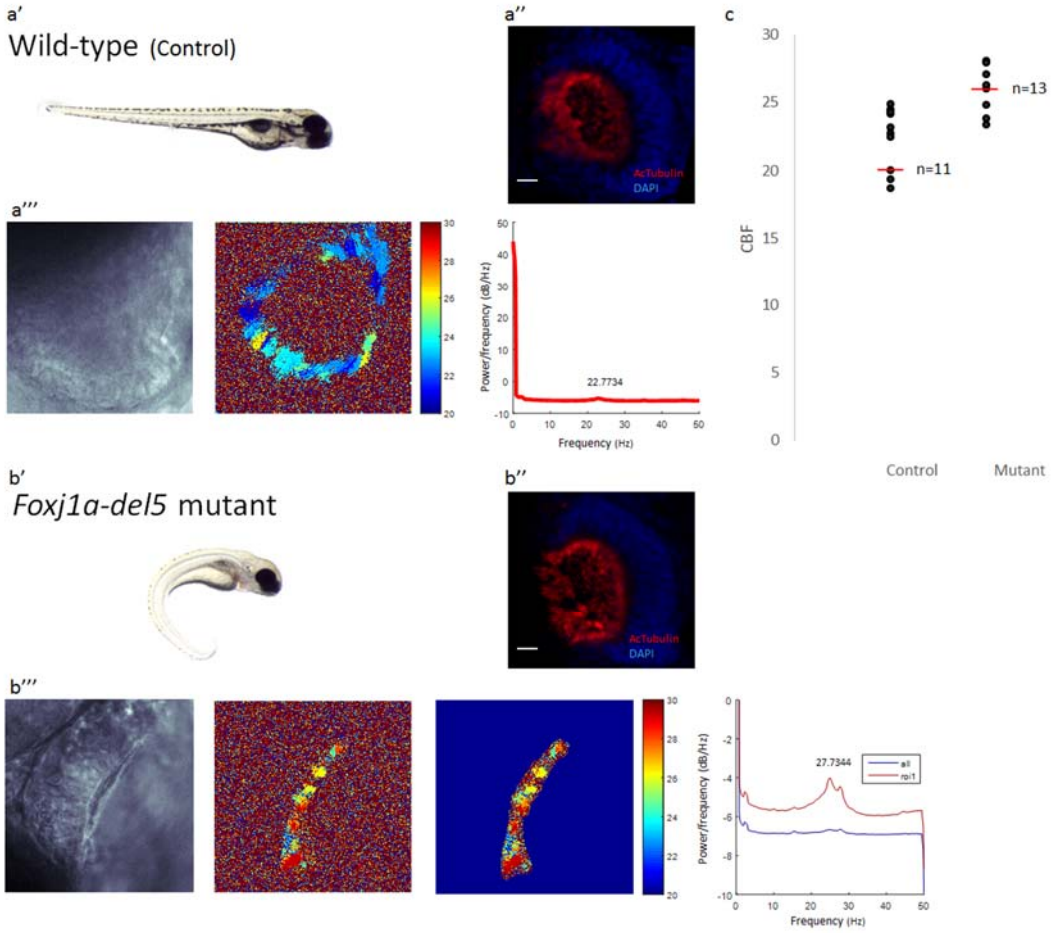

Figure 3.23. Characterization of the cilia mutant *foxj1a-del5* at 4 dpf. (a) Representative example of control larvae with (a') straight body-axis, (a'') labeled cilia in the olfactory pit (AcTubulin immunostaining) and (a''') normal ciliary beating (here: average CBF of 22.8 Hz). (b) Representative example of *foxj1a-del5* larvae with (b') curved body axis and (b'') labeled cilia in the olfactory pit (AcTubulin immunostaining), similar to control larvae. (b''') Ciliary beating in the olfactory pit was detected, but background noise had to be excluded to generate a CBF by FFT analysis (here: average CBF of 27.7 Hz). (c) Scatter plot representing the CBF of all the characterized control larvae (n=11) and *foxj1a-del5* mutants (n=13) analyzed by FFT. Average CBF (red bar) for the control larvae is 22.6±2.2 Hz and, 25.9±2.4 Hz for *foxj1a-del5* mutants. *foxj1a-del5* mutants beat significantly higher than controls (wilcoxon rank sum test, p=0.01). Scale bar: 10µm.

Foxj1a-del5 is a zebrafish CRISPR-mutant line generated in our laboratory with a 5 bp deletion in the *foxj1a* gene, which results in a nonsense mutation. *Foxj1a* encodes a transcription factor which regulates the transcription of motile cilia genes (Hellman et al., 2010). Visual response, heart looping, left-right asymmetry and kidney cysts have not been investigated yet. Homozygous mutants have the characteristic curved body axis, which indicates ciliary defects (Fig. 3.23b'). Confocal images of mutant larvae show a normal distribution of cilia in the olfactory pit (compare Fig. 3.23b'' to a''). Motile cilia located at the periphery of the olfactory pit of the control larvae showed normal ciliary beating (Fig. 3.23a'''). *foxj1a-del5* displayed

ciliary beating, but with a weaker signal than what was observed in control larvae. Light microscopy recordings showed that beating was of a lower amplitude than what was seen for control larvae (data not shown). Background noise had to be excluded to generate peak frequencies by FFT analysis (Fig. 3.23b’’’). The scatter plot in Fig. 3.23c shows the distribution of the CBF measured for all the characterized *foxj1a-del5* mutants (n=13) and control larvae (n=11). The average CBF of the control larvae is equal to 23.8±0.8 Hz. In comparison, the average CBF of *foxj1a-del5* mutants is 25.9±2.3 Hz, which is significantly higher than for controls from the same clutch (wilcoxon rank sum test p=0.01, Fig. 3.23c).

3.7.6 Mutants: conclusive remarks

The availability of ENU mutants and amenability of zebrafish to genetic engineering techniques provide us with a great variety of mutants. Among the 5 mutants analyzed, 4 different phenotypes could be identified. First, *elipsa* and *oval* lack cilia in both MCCs and ORNs. Second, *foxj1a-del5* have a normal distribution of cilia in the olfactory pit, but ciliary beating is affected. Motile cilia in *foxj1a-del5* beat with a higher frequency compared to control larvae and with a lower amplitude. Whether the *foxj1a* mutation interferes with ORNs is still not known. Third, *ift172* mutations affect the motility of the cilia, without affecting the morphology of ORNs. However, *ift172* larvae do not show a complete penetrance of the disrupted beating phenotype. Finally, *smh* mutations affect only the motility of the cilia, without affecting the morphology and physiology of ORNs. Thus, as it presumably does not interfere with the sensory function of ORNs, it is valuable to identify the role of motile cilia in MCCs.

Chapter 4.

Discussion

4.1 The morphology of the olfactory pit of zebrafish larvae at 4 dpf

The olfactory placodal cells start to develop as early as 14 hpf. At 34-36 hpf the epidermis covering the placodal cells separate and the olfactory pits open as small slits where ciliated cells can be seen. By 48-50 hpf, multiciliated cells (MCCs) are distinguished (Hansen and Zeiske, 1993). Finally, at 4 dpf, motile cilia cover the rim of the olfactory pits, which are shaped as hollow cups just between the mouth and the eyes, and consist of one opening letting water both in and out. In this project, I fully characterized the MCCs of the olfactory pits of 4 dpf zebrafish larvae using multiple approaches. I used markers of multiciliated epithelium, identified based on literature and analogy to ciliated epithelial cells of the mammalian respiratory tract, and performed immunohistochemistry on whole mount embryos. I also investigated the localization, shape and ciliary beating patterns of MCCs by transmitted light, confocal, two-photon and light sheet microscopy.

The accessibility of MCCs is remarkable. Studies on olfactory MCCs in zebrafish larvae allow *in vivo* preparation and no fluorescence is needed to detect ciliary beating in the olfactory pits. Furthermore, the close proximity to neurons and support cells make olfactory MCCs suitable for investigation of cell-to-cell communication, in particular between epithelial cells and neurons. MCCs are cuboidal cells that comprise the top cell layer of the olfactory pit, overlying the olfactory receptor neurons (ORNs). In contrast to MCCs, ciliated ORNs have long, slender projections extending into the bottom of the olfactory pit. Motile cilia of MCCs are densely located around the rim of the circularly shaped pit. Acetylated tubulin staining also label cilia

in the bottom of the pit. As no ciliary beating is detected in this area by CBF analysis, the labeled cilia are most likely the immotile cilia protruding from the dendritic knobs of ORNs. Furthermore, the lateral side of the olfactory pit is less steep than the remaining, where also cilia extend to the top of the rim.

4.1.1 Analysis of ciliary beating in the olfactory pit

The estimated beating frequencies within the olfactory pit varies between larvae, but are relatively stable across individuals. Values range within a normal distribution between 19-28 Hz, with a mean CBF of 24.3 Hz. Also, CBF remains stable within individuals, found to vary within a range of ±2 Hz in a time period of 5 minutes. By FFT analysis of ciliary beating in the olfactory pit, patches with distinct beating frequencies can be observed within heat maps representing CBF. These areas are of various sizes and average frequencies, but have defined borders. We still do not understand the mechanisms establishing and maintaining these patches over time. They may be a result of neighboring cells that correlate their CBF. Indeed, it has earlier been proposed that a collective increase in CBF of adjacent cells resulted from the passage of IP_3 via gap junctions, which activated a release of Ca^{2+} from intracellular stores (Lansley and Sanderson, 1999). Thus, perhaps MCCs in the olfactory pit are also connected by gap junctions, or communicate by other means. Alternatively, the water flow created by ciliary beating may create local subareas of fluid mechanic properties, which cilia locally adjust to. Patches may also correspond to individual cells with distinct beating frequencies, although many of the patches seem too big to only comprise one cell.

By light sheet microscopy of a fish line with sparse labelling of MCCs in the olfactory pits, the ciliary beating pattern of MCCs could be characterized. Cilia beat in a two-phase manner, consisting of a fast effective stroke and a slower recovery stroke. The effective stroke was estimated to be about twice the speed of the recovery stroke for the cilia of the MCCs of *hspGGFF19b;UAS:GFP* larvae. Thus, the beat pattern highly resembles the whip-like ciliary stroke described in other organisms, ranging from unicellular organisms to mammalian tissues. Moreover, cilia extend into the opening of the pits and their effective stroke push fluid outwards. Their unidirectional beat resembles respiratory ciliary beating which move mucus out of the lungs. Thus, ciliary beating of MCCs of the olfactory pit may be of similar use and function to increase or decrease the exchange of water in the olfactory pits. The importance of ciliary beating is further discussed in section 4.4.

4.2 Regulation of CBF in the olfactory pit of zebrafish larvae at 4 dpf

An active control of CBF serves different purposes in various animals and tissues. In unicellular organisms it may induce a change in swimming speed or direction, while in higher vertebrates, the MCCs have acquired many different functions. Indeed, an active control of CBF is of high importance in many multiciliated tissues. For instance, in the human airway it allows to keep the mucociliary flow constant despite exposure to higher viscous loads and to protect against toxic compounds. Many factors can actively control CBF, including mechanical forces, temperature, pH, neurotransmitters, chemical compounds and bitter substances. Potential CBF regulators may have very different effects in various tissues, most likely representing the different functions cilia have acquired in each environment. Despite significant advances in understanding the intracellular mechanisms controlling regulation of CBF, many questions still remain elusive. Some of the mechanisms have been explained by the regulation of second messengers. I will specifically discuss the role of Ca^{2+} and cAMP as intracellular regulators. Here I provide an analysis of the MCCs in the olfactory pit of zebrafish larvae, discussed in the coming sections.

4.2.1 Mechanosensation

If beating cilia serve the purpose of either slowing or enhancing the fluid exchange rate of the olfactory pit, an adapting response to the property of the incoming flow would be essential for proper functioning. In agreement with this hypothesis, cilia of olfactory MCCs increase their beating frequency upon an enhanced flow of water. The effect of flow on cilia of MCCs is characterized by a distinct increase in CBF quickly after application. In average, CBF increased by approximately 13%. After the flow is turned off, a slower, steady decay starts immediately. Indeed, a change in CBF upon viscosity changes of the mucus has been observed in all of respiratory, ependymal and oviduct cells. The mechanosensor TRPV4 is suggested to be involved in the coupling of fluid viscosity changes to epithelial ciliary activity cilia (Andrade et al., 2005, Johnson et al., 1991, O'Callaghan et al., 2008). Furthermore, the polycystin-1 and -2 channel complex (PC-1 and -2), primarily known as cation channels in primary cilia, are also localized to ependymal, oviduct and airways MCCs and hypothesised to regulate CBF upon activation (Jain et al., 2012, Wodarczyk et al., 2009). It is therefore possible that mechanosensors, such as TRPV4, PC1 and PC2, are localized to olfactory cilia of zebrafish larvae and contribute to the increase in CBF upon incoming flow.

4.2.2 Temperature

A clear difference between ciliary beating at low and high temperatures has previously been shown for most cell types, including ependymal and respiratory tract cells (O'Callaghan)(Clary-Meinesz et al., 1992), as well as sperm (Perez-Cerezales et al., 2015). I now report a similar effect in MCCs in the olfactory pit of zebrafish. However, molecular mechanisms underlying the increase of CBF by temperature remain unknown. As all biological conditions are known to speed up due to increased temperatures, it is possible that regulation of CBF merely results from an increased metabolism of the cell, where ATP and the rest of the cell machinery function at high-speed. Alternatively, the response to temperature can be mediated by temperature sensitive receptors. Indeed, both TRPV channels 1-4 and PC-1 and -2, which previously have been localized to MCCs, are thermosensitive (DeCaen et al., 2013). An increased Ca^{2+} influx through such channels upon higher temperatures may regulate CBF.

In my experiments, temperature could be set to increase or decrease between 24±2°C and 32±2°C. An increasing water temperature from 24±2°C to 32±2°C elevated CBF levels in average with approximately 40%. The temperature plateaued at 32±2°C after about 2 minutes, and CBF did not increase further. It is not known whether this is due to a reached maximal limit of CBF or if higher temperatures could have further increased CBF. The rapid increase observed in my experiments could be due to a quick and non linear increase in temperature by the temperature controller used in the experiments, or to specifically high kinetics of the regulative mechanism of CBF. Additionally, my experiments show that the control of CBF is reversible. Reducing the temperature of the water flow decreased CBF for all larvae. In 5 minutes, CBF decreased in average 17%. The decrease was more continuous and slower than the abrupt rise in CBF upon upregulation of temperature. This difference may be explained by a slower and more gradual decrease in temperature by the automatic temperature controller. Alternatively, the mechanism for downregulating CBF can be characterized by distinctive slower kinetics than for mechanisms at play in upregulation of CBF.

As the exact temperature and CBF at a set time point could not be accurately monitored, it is difficult to make clear conclusions on the relationship. Follow-up experiments with a tighter temperature control and monitoring must be conducted to make further conclusions. In fact, there is a wide range of temperatures within the natural habitat of zebrafish, extending from 6°C in the winter to more than 38°C in the summer (Spence et al., 2008). Therefore, high temperatures are physiologically relevant and a correlation to CBF is thus worth to study. Only cilia of ependymal cells in mammals are known to beat as fast as 40 Hz, which by directing the

cerebrospinal fluid they bring nutrients and other substances to neurons and play an important role in host defense (O'Callaghan et al., 2008). The use of such a high frequency of ciliary beating in the olfactory pit of zebrafish larvae, however, remains an open question. Future studies should aim to investigate whether a CBF higher than 40 Hz could be of any physiological relevance, or if it is merely a result of higher cell metabolism at increasing temperatures.

4.2.3 Chemicals

Measurement of CBF upon application of chemical components was challenged by the effect of flow on CBF. If the chemical stimuli increase CBF with identical mechanisms as those that are activated upon delivery of flow, use of a constant flow may mask the ability of cilia to beat faster upon chemical stimulation. Therefore, to exclude this possible bias, chemicals were manually applied by a pipette. CBF was first recorded to establish a baseline value. The chemical component was applied followed by an incubation time of 2 minutes, and a new recording was made to establish the CBF after treatment.

4.2.3.1 Denatonium

In a report from 2009, Shah et al. described a mechanism increasing CBF of epithelial respiratory cells upon application of bitter substances. The authors showed that bitter taste receptors are localized to cilia in the respiratory tract. Denatonium, which is a ligand to the bitter taste receptor T2R4, increased CBF of respiratory cilia by as much as 25% (Shah et al., 2009). Conclusively, they proposed that the T2R receptors of the respiratory cilia could be associated with an autonomous protection system in the airways which aid elimination of noxious substances. Possibly, the MCCs in the olfactory pit of zebrafish larvae could serve the same function and eliminate potential noxious substances from the olfactory pit by an increased CBF. My results did not show a change in CBF upon application of 20 mM denatonium, indicating that MCCs of the olfactory pit in zebrafish larvae do not share the CBF enhancing response to bitter substances as seen in cilia of the respiratory tract.

In the report of Shah et al., a maximal increase in both CBF and Ca^{2+} was induced by 1mM denatonium, thus implying that the concentration used in my experiments should be sufficient to induce a response. However, the increase in cellular Ca^{2+} levels was rapid and not lasting more than a minute. In addition, the CBF was estimated by a 1 second confocal microscopy line-scan. Hence, it is a possibility that denatonium did activate olfactory MCCs, as previously reported in respiratory cells, but that the increase in CBF was too brief to be detected by light

microscopy and FFT analysis of CBF after 2 minutes of incubation. Alternatively, MCCs of olfactory pits may not express T2R receptors at 4 dpf and such a defense mechanism against bitter compounds may not be necessary for zebrafish. It is possible that it may develop later in life.

4.2.3.2 Forskolin

Forskolin, an adenylyl cyclase (AC) activator, is commonly used as a tool in biochemistry to raise levels of cAMP. Forskolin has been shown to induce an increase in CBF in i.e. frog mucociliary epithelium, and simultaneously increase Ca^{2+} levels. The increase in CBF is thought to work through activation of the cAMP-dependent kinase PKA, and has shown to regulate CBF via both a Ca^{2+}-dependent and independent pathway (Braiman et al., 1998). It is also established that elevated cAMP levels increase the flagellar beat in sperm cells (Mukherjee et al., 2016). In contrast, a similar increase in cAMP levels, induced by forskolin, decreased CBF of ependymal cells (Nguyen et al., 2001). An effect of forskolin on CBF of olfactory MCCs would indicate a potential regulatory mechanism for these cells, working either through cAMP, PKA or Ca^{2+}.

Interestingly, application of 25 μM forskolin did not induce any detectable changes in CBF of MCCs in the olfactory pit. Based on literature, 25 μM is an average concentration of forskolin applied to specimen to induce AC activity. Thus, the concentration used in my experiments should be sufficient to increase cAMP levels. In the study by Braiman et al. (1998), who applied 1-50 μM forskolin to mucociliary epithelium, 25 μM induced the maximal increase in CBF within 140±84 sec after application. This indicates that an effect induced by forskolin should have been detected through the protocol I used in this experiment, where the 2nd recording included the 120-150th second after application of the drug. These results may therefore indicate that CBF of olfactory pit MCCs is regulated by neither cAMP nor PKA. To verify that in fact AC in MCCs of the olfactory pit is activated by forskolin, we plan to monitor intracellular Ca^{2+} levels of the MCCs upon forskolin treatment. If AC is activated, we expect to observe increased Ca^{2+} activity in the cells. Alternatively, we can test the effect of cAMP in a more controlled manner, by optogenetics using a light-inducible bacterial AC (bPAC)(Jansen et al., 2015).

4.2.3.3 KCl

As KCl is known to induce membrane depolarization in cells, a response to KCl treatment of zebrafish larvae would indicate that depolarization of MCCs or the neighboring ORNs regulate

ciliary motility in olfactory epithelial cells. KCl has previously been shown to increase CBF, but, at least in the literature encountered in this work, all suggest that KCl acts in a non cell-autonomous way. For instance, Conductier et al. stimulated neurons with KCl, which secreted melanin-concentrating hormone, and the CBF of adjacent ependymal cells subsequently increased (Conductier et al., 2013). Furthermore, recently published results showed that CBF of ependymal cells in mice did not increase by membrane depolarization induced by 20-140 mM KCl (Doerner et al., 2015), in fact disregarding membrane depolarization as a way of regulating CBF in some cells. I wanted to test if the MCCs of the olfactory pit of zebrafish larvae responded to KCl, either directly or indirectly via i.e. ORNs.

In my experiments I did not observe any changes in CBF upon treatment with 40mM KCl. In the studies of Doerner et al. (2015), 40mM KCl decreased the membrane potential of ependymal cells from -87±3 mV to -31±1 mV by influx of Ca^{2+}. Whether 40mM KCl is sufficient to depolarize ORNs and/or MCCs in the olfactory pit of zebrafish larvae was not specifically tested in these experiments. This could have been done by the combination of transgenic larvae with Ca^{2+} indicators expressed in ORNs and/or MCCs and two-photon microscopy calcium imaging. An increased Ca^{2+} activity would indicate a membrane depolarization. Alternatively, the effect of KCl may be minor and transient. Indeed, in the studies of Doerner et al., KCl induced membrane depolarization immediately upon application, so it is possible that a potential change in CBF was not detected in my experiments due to the incubation time of 2 minutes before the second recording. Lastly, KCl may simply not modulate CBF of MCCs in the olfactory pit.

4.2.4 The role of Ca^{2+} in regulation of CBF

The link between Ca^{2+} and regulation of CBF is well documented in respiratory epithelial cells (Salathe and Bookman, 1999), sperm (Mizuno et al., 2012b), as well as many other MCCs. A very recent report, published during my master thesis, disconfirmed Ca^{2+} as the regulative mechanism for ependymal cells. Therefore, I wanted to investigate the Ca^{2+}-characteristics of MCCs in the olfactory pit of zebrafish larvae.

Two-photon microscopy of a fish line with GCaMP6s expressed in olfactory pit MCCs revealed a highly active and spontaneous Ca^{2+} activity. In average, most cells fired once per 2.5 minutes with a peak amplitude of almost 44% dff. To our knowledge, this is one of the first reports showing high spontaneous Ca^{2+} signals in MCCs *in vivo*. We still do not understand the molecular mechanisms generating and sustaining these Ca^{2+} events and their functions.

Interestingly, neighboring cells appeared to have correlated Ca^{2+} responses in time. Ca^{2+} activity was sometimes observed to translate across the cell layer as a wave. Such a wave of Ca^{2+} has previously been reported by Dirksen & Sanderson in rabbit tracheal cells, which was explained as the passage of IP_3 to adjacent cells through gap junctions and release of Ca^{2+} from intracellular stores (Dirksen and Sanderson, 1990). An increase in CBF followed the increase in cellular Ca^{2+} levels, emphasizing the role of Ca^{2+} in CBF regulation of respiratory cilia. It is therefore possible that also MCCs of the olfactory pit in zebrafish larvae are connected by gap junctions, which allow i.e. IP_3 diffuse to adjacent cells. This mechanism could as well contribute to the distinct patches within the olfactory epithelium displaying similar CBF, which we observed in most olfactory pits.

To test a potential relationship between Ca^{2+} activity and CBF, flow, which had previously shown to induce an increase in CBF, was applied to MCCs. No difference in Ca^{2+} activity before or during the onset of flow was observed. If anything, it seemed like there was a decrease in activity after the flow was turned off, but these results could not be quantified and need more studies to be concluded. In addition, the spontaneous Ca^{2+} activity observed in MCCs was not correlated with changes in CBF as assessed by light sheet microscopy and FFT analysis. Even though Ca^{2+} events happened every 2 minutes, the CBF was relatively stable over periods of 5 minutes.

Altogether, these findings suggest that intracellular Ca^{2+} activity does not control CBF. Further experiments are needed to understand the functions of Ca^{2+} in olfactory MCCs. We plan to specifically address whether Ca^{2+} is necessary for the cilia to beat by for instance applying Ca^{2+} free medium or Ca^{2+} chelators and measure CBF. By using mutant zebrafish models we will also test whether the presence of cilia or beating cilia is necessary for generating or sustaining Ca^{2+} activity.

4.2.5 pH

pH has previously shown to regulate CBF in many ciliated tissues and cells, such as ependymal (O'Callaghan, 1998), respiratory (Sutto et al., 2004) and sperm cells (Mannowetz et al., 2012). I investigated here the effect of pH on the CBF of the olfactory epithelium in wild-type larvae upon application of AFW with three different pH values (pH 3, 3.5 and 4,3). No effect was seen after delivery of AFW with pH 4.3 for 20 minutes. On the contrary, AFW with pH 3.5 and 3 gave heterogeneous results. In some experiments, acidic pH resulted in the cilia sticking to each other and becoming immotile. In other experiments, the low pH had dramatic effects on the

olfactory pit, where the MCCs died and dissociated from the olfactory pit. Moreover, a recovery of beating upon washing of the olfactory pit with AFW was observed in some larvae. The results were highly various and thus very difficult to quantify. More experiments and an optimization of a better protocol is needed to conclude the effect pH has on motile cilia of MCCs in olfactory pit.

4.2.6 Conclusive remarks: MCCs of the olfactory pit as sensory organelles

CBF of MCCs in the olfactory pit of zebrafish larvae are sensitive to flow, temperature and maybe pH. This implies that MCCs of the olfactory pit are able to respond to mechanical stimulation as well as to other stimuli not related to shear force.

Treatment with KCl did not increase CBF, indicating that the CBF of MCCs is not influenced by membrane depolarization of neither MCCs nor ORNs. A membrane depolarization was however not confirmed (this is further discussed in section 4.4.1). Moreover, they do not respond to bitter substances, which has been shown to increase CBF of respiratory cells, associated with a protective defense system to increase the elimination of harmful substances. This does not argue against the existence of such a protective system in zebrafish larvae whatsoever, but it implies that it is not activated by bitter substances or not present as early as 4 dpf.

The intracellular mechanisms controlling CBF regulation of olfactory pit MCCs are still uncertain. CBF was not affected upon treatment of larvae with forskolin, and the increased CBF induced by flow did not correlate with Ca^{2+} activity in the MCCs. Hence, my findings suggest that regulation of CBF is most likely not dependent on cAMP and Ca^{2+} signaling. By further addressing the roles of cAMP and Ca^{2+} in regulating CBF as explained, as well as including other secondary messengers, we hope to eventually dissect by which mechanism MCCs regulate their beating frequency.

By comparison to other multiciliated tissues studied, the average CBF of MCCs of olfactory pit in zebrafish larvae mostly resembles the CBF observed for ependymal cells, which beat above 20 Hz. As neither ependymal cells seem to be regulated by Ca^{2+}, the MCCs of the olfactory pit resemble ependymal cells both in terms of CBF and the mechanisms regulating CBF (as summarized in table 4.1). Thus, MCCs of the olfactory pit of zebrafish larvae could potentially be a high throughput gateway to study ependymal cilia characteristics.

Table 4.1. Cellular regulation of CBF. The effect on CBF of olfactory pit, ependymal, and respiratory MCCs by molecules and stimuli tested in this thesis is summarized.
Effects on CBF: + (increase), - (decrease), ± (reversible), no effect (NO), not known (?)

Stimuli	Olfactory pit (20-28 Hz)	Ependymal cells (20-40 Hz)	Respiratory cilia (8-10 Hz)
Mechanical forces	+	+	+
Temperature	±	±	±
Bitter (denatonium)	NO	?	+
KCl	NO	NO	?
cAMP	NO	-	+
Ca^{2+}	?	NO	+
pH	±	±	±

4.3 Analysis of CBF by light microscopy and FFT analysis

Various techniques are currently used to measure CBF. For instance, one technique rely on a manual count of CBF by slow motion replay of recordings acquired at a high frame rate (up to 500/sec). Such methods are time consuming, prone to human bias and thus, has a very low throughput. Alternatively, a single line of beating cilia is obtained by confocal microscopy at high frequency of acquisition and CBF can be estimated from a count of peaks in kymographs reflecting ciliary beating. However, this method depends on a straight border of cells for a high quality image, is very sensitive to drift and movement of the sample, and can only measure CBF of limited numbers of cells. In this project, we developed and automated a new method that allows recording of a wide field of the olfactory pit and subsequent CBF analysis. For this purpose, I used light microscopy and digital recordings at a frequency of about 100 fps. Further, data was analyzed with the FFT algorithm of Matlab. I validated this method through several control experiments. First, no CBF was detected in recordings of the mutant line *smh*, whose cilia are immotile, indicating that the described method only detect cilia which are moving. Second, the frequency measured by light sheet microscopy of a single MCC corresponded very well to the frequency output of the FFT analysis obtained by transmitted light microscopy. Moreover, the CBF obtained by light-sheet microscopy agreed to the number of complete strokes per second, including both the effective and recovery stroke, indicating that (1) the CBF

output of the automated FFT analysis corresponds to the frequency of a complete ciliary stroke and (2) microscopy recordings at 100 fps is sufficient to accurately detect CBF.

Altogether, our method has many advantages compared to current methods. First, whole populations of cilia can be investigated at once, thus generating lower amounts of data. Multiple cell analysis and low data generation is particularly beneficial when CBF is measured over a longer period of time. Second, no fluorescence marker of cilia is required for our experiments. Third, detection of CBF and changes of CBF upon various stimulations at a low frequency of acquisition (approx. 100 fps) is beneficial compared to higher frame rate recordings due to low data generation. Last, light microscopy is relatively cheap in comparison to other techniques, as only a simple microscope, a good objective and a camera are necessary to generate quality images over time. However, this method cannot measure the beating pattern, direction and angle of cilia over time. For this purpose, I used light sheet microscopy, which allows recording of single optical planes up to 900 fps. However, acquiring light sheet microscopy recordings is a cumbersome task compared to simple light microscopy. This is mostly due to settings of the light sheet microscope, which must be adjusted separately for every recording. In addition, light sheet microscopy requires a fluorescent labeling of cilia. Hence, I only used light sheet microscopy to obtain a detailed analysis of single cell beating and the direction, speed and angle of ciliary stroke.

4.4 The physiological relevance of MCCs in olfactory processing

Because MCCs are located at the entrance of water both as it enters and as it exits the olfactory pit of zebrafish larvae, it is likely that they are involved in olfactory processing in some way. Indeed, the flow generated by MCCs can be important for clearance of old odorants and to allow entrance of new ones. In analysis of individual beating patterns by light sheet microscopy of fluorescent larvae, we observed that the stroke is always directed out of the olfactory pit, indicating that MCC-induced flow may drive an effective outward flow of the water of the pit. Possibly, this outward flow could create a vortex that speeds up the entrance of new water into the pit. We currently lack any information of the the fluid dynamics in the olfactory pit of zebrafish at 4 dpf. Follow-up experiments in the laboratory will test the biophysics of the induced flow by ciliary beating of MCCs, where i.e. fluorescent beads could be added to the olfactory pits and their velocity could be measured by fluorescence microscopy.

For clarity in this discussion: influx and efflux of water containing odors in larvae at 4 dpf is different from adults. In adult fish, water carrying odorants enter and pass to the olfactory organ

proper through an incurrent nostril and exits through an excurrent nostril. The water current is created in two different ways: water can be driven by the pressure differential between the incurrent and excurrent nostril due to the forward motion of the fish and/or water flow is driven through the nasal cavity by motile cilia of non sensory MCCs (Emde, 2012). In 4 dpf larvae the olfactory pit is shaped as a single hollow cup, lined by a thick fringe of beating cilia, and only one opening let water both in and out .

4.4.1 Interactions between ORNs and MCCs

If MCCs have a role in olfactory processing it is possible that communicative pathways between ORNs and MCCs are established. A previous report showed that neurons located in proximity to the brain ventricles (in the lateral hypothalamic area) regulated the CBF of ependymal cells in mice (Conductier et al., 2013). Thus, I wanted to test whether an activation of neuronal activity could influence ciliary beating of MCCs of the olfactory epithelium. I first tested whether ORNs could affect CBF upon application of KCl, a chemical known to induce action potentials in neurons. As previously discussed, no change in CBF was observed upon application of KCl, but a depolarization of ORNs was neither confirmed. Also, KCl may have multiple effects on the different cell types of the olfactory pit. Thus, I wanted to more specifically control the activation of the ciliated ORNs. For this purpose, I used transgenic larvae expressing ChR2, a light-activated protein channel, in the cilia of ORNs. In such a manner I could control the depolarization of the cell membrane of only ciliated ORNs in a temporal way. Transgenic larvae were screened with a fluorescent microscope to verify the expression of YFP-tagged ChR2 in olfactory pits.

The depolarization of ORNs, induced by exposure of LED light for 1 minute, did not modify CBF of the larvae tested in my experiments. Possibly, if the communication between ciliated ORNs and MCCs is very weak, the variability between individuals may mask the effect of the optogenetic activation. As experiments were only done with 4 transgenic larvae, it is anyways not likely to observe any statistical difference. However, since my preliminary results were not promising enough, I did not pursue these experiments in this thesis. Alternatively, 1 minute of optogenetic activation may not be sufficient to induce a change in MCC ciliary beating, or activation of ciliated ORNs may simply not regulate CBF. It is possible that such communicative interaction develop later in life.

4.5 Characterization of mutant lines for future studies

If the flow generated by MCCs is important to deliver or clear odors in olfactory pit, loss of cilia motility will influence the response of ORNs to odors by influencing either the amplitude or kinetics of odor response. To test this hypothesis, we need to specifically ablate or immobilize cilia of MCCs. Genetic mutants are the most straightforward approach to manipulate cilia. However, ciliated ORNs require their primary cilia to respond to odors. Thus, genetic mutations affecting both primary and motile cilia will have effects on odorant sensation per se by disrupted ciliated ORNs. Therefore, I characterized multiple genetic mutants at 4 dpf in order to identify whether primary and/or motile cilia were affected and establish which mutants would be appropriate for future research. All mutations in genes important for cilia function affect development and generate a curved body axis, which prevent any larvae from becoming more than 5-6 days old.

Elipsa and *oval* mutants lack all ciliated cells in the olfactory pit, including ORNs. This makes them valuable to study the importance of both primary and motile cilia. *Ift172* have cilia present in the olfactory pit, but lack of ciliary beating is not consistent.*Foxj1a-del5*, generated in our laboratory, have a normal distribution of cilia in the olfactory pit, but cilia beat with a higher frequency and lower amplitude than controls. Lastly, the *smh* mutation affect only the motility of the cilia, without affecting the morphology and physiology of ORNs.This makes *smh* suitable for investigation of early developmental defects solely induced by lack of motility of cilia in the MCCs of the olfactory pit. *Smh* expressing GcAMP6s in neurons are currently being used to investigate whether loss of ciliary beating influences odor responses. This will be measured by the amount of Ca^{2+} activity in the ORNs in response to odors, particularly looking at the amplitude as well as the time of onset and offset. Wild-type larvae with normal ciliary activity will be compared to *smh*, which do not possess motile cilia. The experiments are conducted in the laboratory in collaboration with another researcher. However, no clear results have been generated by these experiments yet.

Chapter 5.

Conclusion

The aim of this thesis was twofold. First, to provide new insights in ciliary biology by investigation of cilia morphology and physiology of the zebrafish olfactory pit at 4 dpf, and second, to provide future research with tools to further investigate the physiological role of motile cilia. To address these questions, we developed and automated a method that allows CBF analysis from high-speed digital recordings that is cheap, easily used and highly efficient.

I provide by this thesis an extended study addressing the morphology and physiology of MCCs located in the olfactory pit of 4 dpf zebrafish larvae. My findings show that, at 4 dpf, the olfactory pit is shaped as a hollow cup with motile cilia lining the rim of the opening. They beat in the characteristic whip-like pattern that has been shown in other MCCs, and with a relatively similar frequency, normally distributed between 18.9-29.5 Hz. The beat is consistently directed outward of the pit, which may indicate that a propulsive flow generated by motile cilia is necessary to regulate the exchange of water in the pit. Moreover, my findings suggest that the ciliary beating of MCCs of the zebrafish olfactory epithelium is actively regulated and affected by various environmental factors. A markedly increase in CBF was observed upon increased temperatures and an induced flow, indicating that motile cilia of the olfactory pit are able to respond to mechanical stimuli, and also to stimuli which are not related to shear stress. The mechanisms behind ciliary regulation is still not known, but currently addressed in the laboratory. My findings suggest that CBF is not regulated by Ca^{2+}, as opposed to what has been shown for many other MCCs. As no response in CBF was detected upon treatment with forskolin, ciliary beating of MCCs in the olfactory pit is presumably not regulated by cAMP either.

The close proximity of MCCs and sensory neurons makes the olfactory pit well suited to study potential interactions between them, and specifically address the function and importance of motile cilia in olfactory physiology. No positive results were generated regarding communicative interactions between MCCs and ORNs within the work of this thesis. However,

the characterization of mutants established the *smh* mutant as well suited for future studies addressing the role of motile cilia. Ongoing work in the laboratory is now using *smh* to investigate the function of beating cilia in the olfactory pit. This ciliopathy mutant can be used in future research not only to address olfaction, but also other early developmental effects solely induced by motile cilia. In the long term, the findings presented in this thesis together with the ongoing research in our laboratory will hopefully lead forth to the establishment of zebrafish mutants as a tool for identifying small molecules curing ciliopathies. For instance, *in vivo* drug screening with the mutant *smh* could identify molecules and pathways rescuing dynein arm activity and, eventually, ciliary beating.

.

Bibliography

AFZELIUS, B. A. 1988. On the numbering of peripheral doublets in cilia and flagella. *Tissue Cell,* 20**,** 473-5.

AKERBOOM, J., CHEN, T. W., WARDILL, T. J., et al. 2012. Optimization of a GCaMP calcium indicator for neural activity imaging. *J Neurosci,* 32**,** 13819-40.

ALTUN, Z. F. H., D.H. 2010. Nervous system, neuronal support cells.

ANDRADE, Y. N., FERNANDES, J., VAZQUEZ, E., FERNANDEZ-FERNANDEZ, J. M., ARNIGES, M., SANCHEZ, T. M., VILLALON, M. & VALVERDE, M. A. 2005. TRPV4 channel is involved in the coupling of fluid viscosity changes to epithelial ciliary activity. *Journal of Cell Biology,* 168**,** 869-874.

BACHMANOV, A. A. & BEAUCHAMP, G. K. 2007. Taste receptor genes. *Annu Rev Nutr,* 27**,** 389-414.

BADURA, A., SUN, X. R., GIOVANNUCCI, A., LYNCH, L. A. & WANG, S. S. 2014. Fast calcium sensor proteins for monitoring neural activity. *Neurophotonics,* 1**,** 025008.

BARBAR, E., KLEINMAN, B., IMHOFF, D., LI, M., HAYS, T. S. & HARE, M. 2001. Dimerization and folding of LC8, a highly conserved light chain of cytoplasmic dynein. *Biochemistry,* 40**,** 1596-605.

BAYLY, R. & AXELROD, J. D. 2011. Pointing in the right direction: new developments in the field of planar cell polarity. *Nat Rev Genet,* 12**,** 385-91.

BEALES, P. & JACKSON, P. K. 2012. Cilia - the prodigal organelle. *Cilia,* 1**,** 1.

BELLMANN, D., RICHARDT, A., FREYBERGER, R., NUWAL, N., SCHWARZEL, M., FIALA, A. & STORTKUHL, K. F. 2010. Optogenetically Induced Olfactory Stimulation in Drosophila Larvae Reveals the Neuronal Basis of Odor-Aversion behavior. *Front Behav Neurosci,* 4**,** 27.

BERRIDGE, M. J., LIPP, P. & BOOTMAN, M. D. 2000. The versatility and universality of calcium signalling. *Nat Rev Mol Cell Biol,* 1**,** 11-21.

BLOODGOOD, R. A. 2010. Sensory reception is an attribute of both primary cilia and motile cilia. *Journal of Cell Science,* 123**,** 505-509.

BONINI, N. M. & NELSON, D. L. 1988. Differential Regulation of Paramecium Ciliary Motility by Camp and Cgmp. *Journal of Cell Biology,* 106**,** 1615-1623.

BORNENS, M. 2008. Organelle positioning and cell polarity. *Nat Rev Mol Cell Biol,* 9**,** 874-86.

BRAIMAN, A., ZAGOORY, O. & PRIEL, Z. 1998. PKA induces Ca^{2+} release and enhances ciliary beat frequency in a Ca^{2+}-dependent and -independent manner. *American Journal of Physiology-Cell Physiology,* 275**,** C790-C797.

BRAUBACH, O. R., WOOD, H. D., GADBOIS, S., FINE, A. & CROLL, R. P. 2009. Olfactory conditioning in the zebrafish (Danio rerio). *Behav Brain Res,* 198**,** 190-8.

BREUNIG, J. J., ARELLANO, J. I. & RAKIC, P. 2010. Cilia in the brain: going with the flow. *Nat Neurosci,* 13**,** 654-5.

BROOKS, E. R. & WALLINGFORD, J. B. 2014. Multiciliated cells. *Curr Biol,* 24**,** R973-82.

BUFFONE, M. G., WERTHEIMER, E. V., VISCONTI, P. E. & KRAPF, D. 2014. Central role of soluble adenylyl cyclase and cAMP in sperm physiology. *Biochim Biophys Acta,* 1842**,** 2610-20.

BUSH, A., CHODHARI, R., COLLINS, N., COPELAND, F., HALL, P., HARCOURT, J., HARIRI, M., HOGG, C., LUCAS, J., MITCHISON, H. M., O'CALLAGHAN, C. &

PHILLIPS, G. 2007. Primary ciliary dyskinesia: current state of the art. *Arch Dis Child,* 92**,** 1136-40.

CAMALET, S. & JULICHER, F. 2000. Generic aspects of axonemal beating. *New Journal of Physics,* 2**,** 241-2423.

CELIK, A., FUSS, S. H. & KORSCHING, S. I. 2002. Selective targeting of zebrafish olfactory receptor neurons by the endogenous OMP promoter. *Eur J Neurosci,* 15**,** 798-806.

CHILVERS, M. A. & O'CALLAGHAN, C. 2000. Local mucociliary defense mechanisms. *Paediatr Respir Rev,* 1**,** 27-34.

CHOKSI, S. P., LAUTER, G., SWOBODA, P. & ROY, S. 2014. Switching on cilia: transcriptional networks regulating ciliogenesis. *Development,* 141**,** 1427-41.

CLARY-MEINESZ, C., MOUROUX, J., COSSON, J., HUITOREL, P. & BLAIVE, B. 1998. Influence of external pH on ciliary beat frequency in human bronchi and bronchioles. *Eur Respir J,* 11**,** 330-3.

CLARY-MEINESZ, C. F., COSSON, J., HUITOREL, P. & BLAIVE, B. 1992. Temperature effect on the ciliary beat frequency of human nasal and tracheal ciliated cells. *Biol Cell,* 76**,** 335-8.

COLE, D. G. 2003. The intraflagellar transport machinery of Chlamydomonas reinhardtii. *Traffic,* 4**,** 435-442.

COLE, D. G., DIENER, D. R., HIMELBLAU, A. L., BEECH, P. L., FUSTER, J. C. & ROSENBAUM, J. L. 1998. Chlamydomonas kinesin-II-dependent intraflagellar transport (IFT): IFT particles contain proteins required for ciliary assembly in Caenorhabditis elegans sensory neurons. *J Cell Biol,* 141**,** 993-1008.

CONDUCTIER, G., BRAU, F., VIOLA, A., LANGLET, F., RAMKUMAR, N., DEHOUCK, B., LEMAIRE, T., CHAPOT, R., LUCAS, L., ROVERE, C., MAITRE, P., HOSSEINY, S., PETIT-PAITEL, A., ADAMANTIDIS, A., LAKAYE, B., RISOLD, P. Y., PREVOT, V., MESTE, O., NAHON, J. L. & GUYON, A. 2013. Melanin-concentrating hormone regulates beat frequency of ependymal cilia and ventricular volume. *Nat Neurosci,* 16**,** 845-7.

DAWE, H. R., FARR, H. & GULL, K. 2007. Centriole/basal body morphogenesis and migration during ciliogenesis in animal cells. *J Cell Sci,* 120**,** 7-15.

DEANE, J. A., COLE, D. G., SEELEY, E. S., DIENER, D. R. & ROSENBAUM, J. L. 2001. Localization of intraflagellar transport protein IFT52 identifies basal body transitional fibers as the docking site for IFT particles. *Current Biology,* 11**,** 1586-1590.

DECAEN, P. G., DELLING, M., VIEN, T. N. & CLAPHAM, D. E. 2013. Direct recording and molecular identification of the calcium channel of primary cilia. *Nature,* 504**,** 315-8.

DELLING, M., INDZHYKULIAN, A. A., LIU, X., LI, Y., XIE, T., COREY, D. P. & CLAPHAM, D. E. 2016. Primary cilia are not calcium-responsive mechanosensors. *Nature,* 531**,** 656-60.

DELMOTTE, P. & SANDERSON, M. J. 2006. Ciliary beat frequency is maintained at a maximal rate in the small airways of mouse lung slices. *Am J Respir Cell Mol Biol,* 35**,** 110-7.

DI BENEDETTO, G., MAGNUS, C. J., GRAY, P. T. & MEHTA, A. 1991. Calcium regulation of ciliary beat frequency in human respiratory epithelium in vitro. *J Physiol,* 439**,** 103-13.

DIRKSEN, E. R. & SANDERSON, M. J. 1990. Regulation of ciliary activity in the mammalian respiratory tract. *Biorheology,* 27**,** 533-45.

DOERNER, J. F., DELLING, M. & CLAPHAM, D. E. 2015. Ion channels and calcium signaling in motile cilia. *Elife,* 4.

DRUMMOND, I. 2009. Studying cilia in zebrafish. *Methods Cell Biol,* 93**,** 197-217.

DRUMMOND, I. A., MAJUMDAR, A., HENTSCHEL, H., ELGER, M., SOLNICA-KREZEL, L., SCHIER, A. F., NEUHAUSS, S. C., STEMPLE, D. L., ZWARTKRUIS, F., RANGINI, Z., DRIEVER, W. & FISHMAN, M. C. 1998. Early development of the zebrafish pronephros and analysis of mutations affecting pronephric function. *Development,* 125**,** 4655-67.

EATON, R. C., LEE, R. K. & FOREMAN, M. B. 2001. The Mauthner cell and other identified neurons of the brainstem escape network of fish. *Prog Neurobiol,* 63**,** 467-85.

EISEN, J. S. & SMITH, J. C. 2008. Controlling morpholino experiments: don't stop making antisense. *Development,* 135**,** 1735-43.

ELGETI, J. & GOMPPER, G. 2013. Emergence of metachronal waves in cilia arrays. *Proceedings of the National Academy of Sciences of the United States of America,* 110**,** 4470-4475.

EMDE, G. M., J; B.G. KAPOOR 2012. *The Senses of Fish: Adaptations for the Reception of Natural Stimuli*, Springer Science & Business Media.

ESSNER, J. J., AMACK, J. D., NYHOLM, M. K., HARRIS, E. B. & YOST, J. 2005. Kupffer's vesicle is a ciliated organ of asymmetry in the zebrafish embryo that initiates left-right development of the brain, heart and gut. *Development,* 132**,** 1247-1260.

FIMIA, G. M. & SASSONE-CORSI, P. 2001. Cyclic AMP signalling. *J Cell Sci,* 114**,** 1971-2.

FLIEGAUF, M., BENZING, T. & OMRAN, H. 2007a. Mechanisms of disease - When cilia go bad: cilia defects and ciliopathies. *Nature Reviews Molecular Cell Biology,* 8**,** 880-893.

FLIEGAUF, M., BENZING, T. & OMRAN, H. 2007b. When cilia go bad: cilia defects and ciliopathies. *Nat Rev Mol Cell Biol,* 8**,** 880-93.

FUNFAK, A., FISCH, C., ABDEL MOTAAL, H. T., DIENER, J., COMBETTES, L., BAROUD, C. N. & DUPUIS-WILLIAMS, P. 2015. Paramecium swimming and ciliary beating patterns: a study on four RNA interference mutations. *Integr Biol (Camb),* 7**,** 90-100.

GERMINO, G. G. 2005. Linking cilia to Wnts. *Nat Genet,* 37**,** 455-7.

GIBBONS, I. R. 1961. Relationship between Fine Structure and Direction of Beat in Gill Cilia of a Lamellibranch Mollusc. *Journal of Biophysical and Biochemical Cytology,* 11**,** 179-&.

GUIRAO, B. & JOANNY, J. F. 2007. Spontaneous creation of macroscopic flow and metachronal waves in an array of cilia. *Biophys J,* 92**,** 1900-17.

GUIRAO, B., MEUNIER, A., MORTAUD, S., AGUILAR, A., CORSI, J. M., STREHL, L., HIROTA, Y., DESOEUVRE, A., BOUTIN, C., HAN, Y. G., MIRZADEH, Z., CREMER, H., MONTCOUQUIOL, M., SAWAMOTO, K. & SPASSKY, N. 2010. Coupling between hydrodynamic forces and planar cell polarity orients mammalian motile cilia. *Nature Cell Biology,* 12**,** 341-U86.

HAMASAKI, T., BARKALOW, K., RICHMOND, J. & SATIR, P. 1991. Camp-Stimulated Phosphorylation of an Axonemal Polypeptide That Copurifies with the 22s Dynein Arm Regulates Microtubule Translocation Velocity and Swimming Speed in Paramecium. *Proceedings of the National Academy of Sciences of the United States of America,* 88**,** 7918-7922.

HANSEN, A. & ZEISKE, E. 1993. Development of the Olfactory Organ in the Zebrafish, Brachydanio-Rerio. *Journal of Comparative Neurology,* 333**,** 289-300.

HANSEN, A. & ZEISKE, E. 1998. The peripheral olfactory organ of the zebrafish, Danio rerio: an ultrastructural study. *Chemical Senses,* 23**,** 39-48.

HELLMAN, N. E., LIU, Y., MERKEL, E., AUSTIN, C., LE CORRE, S., BEIER, D. R., SUN, Z., SHARMA, N., YODER, B. K. & DRUMMOND, I. A. 2010. The zebrafish foxj1a transcription factor regulates cilia function in response to injury and epithelial stretch. *Proc Natl Acad Sci U S A,* 107**,** 18499-504.

HIRANO-OHNISHI, J. & WATANABE, Y. 1989. Ca^{2+}/calmodulin-dependent phosphorylation of ciliary beta-tubulin in Tetrahymena. *J Biochem,* 105**,** 858-60.

HORANI, A., BRODY, S. L. & FERKOL, T. W. 2014. Picking up speed: advances in the genetics of primary ciliary dyskinesia. *Pediatr Res,* 75**,** 158-64.

HOWE, K., CLARK, M. D., TORROJA, C. F., et al. 2013. The zebrafish reference genome sequence and its relationship to the human genome. *Nature,* 496**,** 498-503.

HUANGFU, D., LIU, A., RAKEMAN, A. S., MURCIA, N. S., NISWANDER, L. & ANDERSON, K. V. 2003. Hedgehog signalling in the mouse requires intraflagellar transport proteins. *Nature,* 426**,** 83-7.

JAIN, B., RUBINSTEIN, I., ROBBINS, R. A., LEISE, K. L. & SISSON, J. H. 1993. Modulation of Airway Epithelial-Cell Ciliary Beat Frequency by Nitric-Oxide. *Biochemical and Biophysical Research Communications,* 191**,** 83-88.

JAIN, R., JAVIDAN-NEJAD, C., ALEXANDER-BRETT, J., HORANI, A., CABELLON, M. C., WALTER, M. J. & BRODY, S. L. 2012. Sensory functions of motile cilia and implication for bronchiectasis. *Front Biosci (Schol Ed),* 4**,** 1088-98.

JANSEN, V., ALVAREZ, L., BALBACH, M., STRUNKER, T., HEGEMANN, P., KAUPP, U. B. & WACHTEN, D. 2015. Controlling fertilization and cAMP signaling in sperm by optogenetics. *Elife,* 4.

JI, G., FELDMAN, M. E., DENG, K. Y., GREENE, K. S., WILSON, J., LEE, J. C., JOHNSTON, R. C., RISHNIW, M., TALLINI, Y., ZHANG, J., WIER, W. G., BLAUSTEIN, M. P., XIN, H. B., NAKAI, J. & KOTLIKOFF, M. I. 2004. Ca^{2+}-sensing transgenic mice: postsynaptic signaling in smooth muscle. *J Biol Chem,* 279**,** 21461-8.

JOHNSON, N. T., VILLALON, M., ROYCE, F. H., HARD, R. & VERDUGO, P. 1991. Autoregulation of beat frequency in respiratory ciliated cells. Demonstration by viscous loading. *Am Rev Respir Dis,* 144**,** 1091-4.

KAWAKAMI, K. 2007. Tol2: a versatile gene transfer vector in vertebrates. *Genome Biol,* 8 Suppl 1**,** S7.

KERMEN, F., FRANCO, L. M., WYATT, C. & YAKSI, E. 2013. Neural circuits mediating olfactory-driven behavior in fish. *Front Neural Circuits,* 7**,** 62.

KIM, W., HAN, T. H., KIM, H. J., PARK, M. Y., KIM, K. S. & PARK, R. W. 2011. An Automated Measurement of Ciliary Beating Frequency using a Combined Optical Flow and Peak Detection. *Healthc Inform Res,* 17**,** 111-9.

KING, S. M. 2010. Axonemal dyneins winch the cilium. *Nat Struct Mol Biol,* 17**,** 673-4.

KORNGREEN, A. & PRIEL, Z. 1994. Simultaneous measurement of ciliary beating and intracellular calcium. *Biophys J,* 67**,** 377-80.

KOZMINSKI, K. G., JOHNSON, K. A., FORSCHER, P. & ROSENBAUM, J. L. 1993. A Motility in the Eukaryotic Flagellum Unrelated to Flagellar Beating. *Proceedings of the National Academy of Sciences of the United States of America,* 90**,** 5519-5523.

KULTGEN, P. L., BYRD, S. K., OSTROWSKI, L. E. & MIGRAM, S. L. 2002. Characterization of an A-kinase anchoring protein in human ciliary axonemes. *Molecular Biology of the Cell,* 13**,** 4156-4166.

LANSLEY, A. B. & SANDERSON, M. J. 1999. Regulation of airway ciliary activity by Ca^{2+}: simultaneous measurement of beat frequency and intracellular Ca^{2+}. *Biophys J,* 77**,** 629-38.

LANSLEY, A. B., SANDERSON, M. J. & DIRKSEN, E. R. 1992. Control of the beat cycle of respiratory tract cilia by Ca^{2+} and cAMP. *Am J Physiol,* 263**,** L232-42.

LARDNER, A. 2001. The effects of extracellular pH on immune function. *J Leukoc Biol,* 69**,** 522-30.

LECHTRECK, K. F., SANDERSON, M. J. & WITMAN, G. B. 2009. High-speed digital imaging of ependymal cilia in the murine brain. *Methods Cell Biol,* 91**,** 255-64.

LEE, R. E. & KUGRENS, P. 1992. Relationship between the Flagellates and the Ciliates. *Microbiological Reviews,* 56**,** 529-542.

LEE, R. J., XIONG, G., KOFONOW, J. M., CHEN, B., LYSENKO, A., JIANG, P., ABRAHAM, V., DOGHRAMJI, L., ADAPPA, N. D., PALMER, J. N., KENNEDY, D. W., BEAUCHAMP, G. K., DOULIAS, P. T., ISCHIROPOULOS, H., KREINDLER, J. L., REED, D. R. & COHEN, N. A. 2012. T2R38 taste receptor polymorphisms underlie susceptibility to upper respiratory infection. *J Clin Invest,* 122**,** 4145-59.

LINCK, R. W., CHEMES, H. & ALBERTINI, D. F. 2016. The axoneme: the propulsive engine of spermatozoa and cilia and associated ciliopathies leading to infertility. *J Assist Reprod Genet,* 33**,** 141-56.

LINDEMANN, C. B. & LESICH, K. A. 2010. Flagellar and ciliary beating: the proven and the possible. *J Cell Sci,* 123**,** 519-28.

LINDSAY, S. M. & VOGT, R. G. 2004. Behavioral responses of newly hatched zebrafish (Danio rerio) to amino acid chemostimulants. *Chemical Senses,* 29**,** 93-100.

LOOGER, L. L. & GRIESBECK, O. 2012. Genetically encoded neural activity indicators. *Curr Opin Neurobiol,* 22**,** 18-23.

LUNT, S. C., HAYNES, T. & PERKINS, B. D. 2009. Zebrafish ift57, ift88, and ift172 intraflagellar transport mutants disrupt cilia but do not affect hedgehog signaling. *Dev Dyn,* 238**,** 1744-59.

LYONS, R. A., SARIDOGAN, E. & DJAHANBAKHCH, O. 2006. The reproductive significance of human Fallopian tube cilia. *Hum Reprod Update,* 12**,** 363-72.

MACRAE, C. A. & PETERSON, R. T. 2015. Zebrafish as tools for drug discovery. *Nature Reviews Drug Discovery,* 14**,** 721-731.

MANGOLINI, A., DE STEPHANIS, L. & AGUIARI, G. 2016. Role of calcium in polycystic kidney disease: From signaling to pathology. *World J Nephrol,* 5**,** 76-83.

MANNOWETZ, N., WANDERNOTH, P. M. & WENNEMUTH, G. 2012. Glucose is a pH-Dependent Motor for Sperm Beat Frequency during Early Activation. *Plos One,* 7.

MARSHALL, W. F. 2010. Cilia self-organize in response to planar cell polarity and flow. *Nature Cell Biology,* 12**,** 314-315.

MESTE, O., BRAU, F. & GUYON, A. 2015. Robust estimation of the motile cilia beating frequency. *Med Biol Eng Comput,* 53**,** 1025-35.

MILLER, D. J. 2004. Sydney Ringer; physiological saline, calcium and the contraction of the heart. *J Physiol,* 555**,** 585-7.

MIZUNO, K., SHIBA, K., OKAI, M., TAKAHASHI, Y., SHITAKA, Y., OIWA, K., TANOKURA, M. & INABA, K. 2012a. Calaxin drives sperm chemotaxis by Ca^{2+}-

mediated direct modulation of a dynein motor. *Proceedings of the National Academy of Sciences of the United States of America,* 109**,** 20497-20502.

MIZUNO, K., SHIBA, K., OKAI, M., TAKAHASHI, Y., SHITAKA, Y., OIWA, K., TANOKURA, M. & INABA, K. 2012b. Calaxin drives sperm chemotaxis by Ca(2)(+)-mediated direct modulation of a dynein motor. *Proc Natl Acad Sci U S A,* 109**,** 20497-502.

MOTOKAWA, T. & SATIR, P. 1975. Laser-induced spreading arrest of Mytilus gill cilia. *J Cell Biol,* 66**,** 377-91.

MUELLER, B. H., PARK, Y., DAUDT, D. R., MA, H. Y., AKOPOVA, I., STANKOWSKA, D. L., CLARK, A. F. & YORIO, T. 2013. Sigma-1 receptor stimulation attenuates calcium influx through activated L-type Voltage Gated Calcium Channels in purified retinal ganglion cells. *Experimental Eye Research,* 107**,** 21-31.

MUHAMMAD, H., RAIS, Y., MIOSGE, N. & ORNAN, E. M. 2012. The primary cilium as a dual sensor of mechanochemical signals in chondrocytes. *Cellular and Molecular Life Sciences,* 69**,** 2101-2107.

MUKHERJEE, S., JANSEN, V., JIKELI, J. F., HAMZEH, H., ALVAREZ, L., DOMBROWSKI, M., BALBACH, M., STRUNKER, T., SEIFERT, R., KAUPP, U. B. & WACHTEN, D. 2016. A novel biosensor to study cAMP dynamics in cilia and flagella. *Elife,* 5.

NAITO, Y. & KANEKO, H. 1972. Reactivated triton-extracted models o paramecium: modification of ciliary movement by calcium ions. *Science,* 176**,** 523-4.

NAKAI, J., OHKURA, M. & IMOTO, K. 2001. A high signal-to-noise $Ca^{(2+)}$ probe composed of a single green fluorescent protein. *Nat Biotechnol,* 19**,** 137-41.

NGUYEN, T., CHIN, W. C., O'BRIEN, J. A., VERDUGO, P. & BERGER, A. J. 2001. Intracellular pathways regulating ciliary beating of rat brain ependymal cells. *J Physiol,* 531**,** 131-40.

O'CALLAGHAN, C. 1998. Brain ependymal cilia. *Thesis submitted for the degree of Doctor of Philosophy at the University of Leicester*.

O'CALLAGHAN, C., SIKAND, K. & CHILVERS, M. A. 2012. Analysis of ependymal ciliary beat pattern and beat frequency using high speed imaging: comparison with the photomultiplier and photodiode methods. *Cilia,* 1**,** 8.

O'CALLAGHAN, C., SIKAND, K. & RUTMAN, A. 1999. Respiratory and brain ependymal ciliary function. *Pediatr Res,* 46**,** 704-7.

O'CALLAGHAN, C. L., SIKAND, K., RUTMAN, A. & HIRST, R. A. 2008. The effect of viscous loading on brain ependymal cilia. *Neurosci Lett,* 439**,** 56-60.

OMORI, Y., ZHAO, C. T., SARAS, A., MUKHOPADHYAY, S., KIM, W., FURUKAWA, T., SENGUPTA, P., VERAKSA, A. & MALICKI, J. 2008. elipsa is an early determinant of ciliogenesis that links the IFT particle to membrane-associated small GTPase Rab8. *Nature Cell Biology,* 10**,** 437-U140.

PAN, J., WANG, Q. & SNELL, W. J. 2005. Cilium-generated signaling and cilia-related disorders. *Lab Invest,* 85**,** 452-63.

PANIZZI, J. R., BECKER-HECK, A., OMRAN, H. & DRUMMOND, I. A., et al. 2012. CCDC103 mutations cause primary ciliary dyskinesia by disrupting assembly of ciliary dynein arms. *Nat Genet,* 44**,** 714-9.

PATTON, E. E. & ZON, L. I. 2001. The art and design of genetic screens: zebrafish. *Nat Rev Genet,* 2**,** 956-66.

PAZOUR, G. J., DICKERT, B. L., VUCICA, Y., SEELEY, E. S., ROSENBAUM, J. L., WITMAN, G. B. & COLE, D. G. 2000. Chlamydomonas IFT88 and its mouse

homologue, polycystic kidney disease gene tg737, are required for assembly of cilia and flagella. *J Cell Biol,* 151**,** 709-18.

PEARSON, C. G. & WINEY, M. 2009. Basal body assembly in ciliates: the power of numbers. *Traffic,* 10**,** 461-71.

PEDERSEN, L. B., SCHRODER, J. M., SATIR, P. & CHRISTENSEN, S. T. 2012. The ciliary cytoskeleton. *Compr Physiol,* 2**,** 779-803.

PEREZ-CEREZALES, S., BORYSHPOLETS, S. & EISENBACH, M. 2015. Behavioral mechanisms of mammalian sperm guidance. *Asian J Androl,* 17**,** 628-32.

QUARMBY, L. M. & PARKER, J. D. 2005. Cilia and the cell cycle? *J Cell Biol,* 169**,** 707-10.

RIDGES, S., HEATON, W. L., JOSHI, D., et al. 2012. Zebrafish screen identifies novel compound with selective toxicity against leukemia. *Blood,* 119**,** 5621-31.

RILEY, B. B., ZHU, C., JANETOPOULOS, C. & AUFDERHEIDE, K. J. 1997. A critical period of ear development controlled by distinct populations of ciliated cells in the zebrafish. *Dev Biol,* 191**,** 191-201.

ROBERTS, A. J., KON, T., KNIGHT, P. J., SUTOH, K. & BURGESS, S. A. 2013. Functions and mechanics of dynein motor proteins. *Nat Rev Mol Cell Biol,* 14**,** 713-26.

ROHATGI, R. & SNELL, W. J. 2010. The ciliary membrane. *Curr Opin Cell Biol,* 22**,** 541-6.

ROSENBAUM, J. L. & WITMAN, G. B. 2002. Intraflagellar transport. *Nat Rev Mol Cell Biol,* 3**,** 813-25.

RUBIN, R. W. & FILNER, P. 1973. Adenosine 3',5'-cyclic monophosphate in Chlamydomonas reinhardtii. Influence on flagellar function and regeneration. *J Cell Biol,* 56**,** 628-35.

RYSER, M., BURN, A., WESSEL, T., FRENZ, M. & RICKA, J. 2007. Functional imaging of mucociliary phenomena: high-speed digital reflection contrast microscopy. *Eur Biophys J,* 37**,** 35-54.

SALATHE, M. 2007. Regulation of mammalian ciliary beating. *Annu Rev Physiol,* 69**,** 401-22.

SALATHE, M. & BOOKMAN, R. J. 1999. Mode of Ca^{2+} action on ciliary beat frequency in single ovine airway epithelial cells. *J Physiol,* 520 Pt 3**,** 851-65.

SANDER, J. D. & JOUNG, J. K. 2014. CRISPR-Cas systems for editing, regulating and targeting genomes. *Nat Biotechnol,* 32**,** 347-55.

SANDERSON, M. J. & SLEIGH, M. A. 1981. Ciliary activity of cultured rabbit tracheal epithelium: beat pattern and metachrony. *J Cell Sci,* 47**,** 331-47.

SATIR, P. & MATSUOKA, T. 1989. Splitting the ciliary axoneme: implications for a "switch-point" model of dynein arm activity in ciliary motion. *Cell Motil Cytoskeleton,* 14**,** 345-58.

SAWAMOTO, K., WICHTERLE, H., GONZALEZ-PEREZ, O., CHOLFIN, J. A., YAMADA, M., SPASSKY, N., MURCIA, N. S., GARCIA-VERDUGO, J. M., MARIN, O., RUBENSTEIN, J. L., TESSIER-LAVIGNE, M., OKANO, H. & ALVAREZ-BUYLLA, A. 2006. New neurons follow the flow of cerebrospinal fluid in the adult brain. *Science,* 311**,** 629-32.

SHAH, A. S., BEN-SHAHAR, Y., MONINGER, T. O., KLINE, J. N. & WELSH, M. J. 2009. Motile cilia of human airway epithelia are chemosensory. *Science,* 325**,** 1131-4.

SILVERMAN, M. A. & LEROUX, M. R. 2009. Intraflagellar transport and the generation of dynamic, structurally and functionally diverse cilia. *Trends Cell Biol,* 19**,** 306-16.

SISSON, J. H., STONER, J. A., AMMONS, B. A. & WYATT, T. A. 2003. All-digital image capture and whole-field analysis of ciliary beat frequency. *J Microsc,* 211**,** 103-11.

SLEIGH, M. A. 1989. Adaptations of ciliary systems for the propulsion of water and mucus. *Comp Biochem Physiol A Comp Physiol,* 94**,** 359-64.

SMITH, C. M., DJAKOW, J., FREE, R. C., DJAKOW, P., LONNEN, R., WILLIAMS, G., POHUNEK, P., HIRST, R. A., EASTON, A. J., ANDREW, P. W. & O'CALLAGHAN, C. 2012. ciliaFA: a research tool for automated, high-throughput measurement of ciliary beat frequency using freely available software. *Cilia,* 1**,** 14.

SMITH, E. F. & YANG, P. F. 2004. The radial spokes and central apparatus: Mechano-chemical transducers that regulate flagellar motility. *Cell Motility and the Cytoskeleton,* 57**,** 8-17.

SNELL, W. J., PAN, J. & WANG, Q. 2004. Cilia and flagella revealed: from flagellar assembly in Chlamydomonas to human obesity disorders. *Cell,* 117**,** 693-7.

SOROKIN, S. P. 1968. Reconstructions of Centriole Formation and Ciliogenesis in Mammalian Lungs. *Journal of Cell Science,* 3**,** 207-&.

SPEEDIE, N. & GERLAI, R. 2008. Alarm substance induced behavioral responses in zebrafish (Danio rerio). *Behav Brain Res,* 188**,** 168-77.

SPENCE, R., GERLACH, G., LAWRENCE, C. & SMITH, C. 2008. The behaviour and ecology of the zebrafish, Danio rerio. *Biol Rev Camb Philos Soc,* 83**,** 13-34.

STACEY, N. E. & KYLE, A. L. 1983. Effects of Olfactory Tract Lesions on Sexual and Feeding-Behavior in the Goldfish. *Physiology & Behavior,* 30**,** 621-628.

STEPANYAN, Z., KOCHARYAN, A., PYRSKI, M., HUBSCHLE, T., WATSON, A. M., SCHULZ, S. & MEYERHOF, W. 2003. Leptin-target neurones of the rat hypothalamus express somatostatin receptors. *J Neuroendocrinol,* 15**,** 822-30.

STERN, H. M. & ZON, L. I. 2003. Cancer genetics and drug discovery in the zebrafish. *Nat Rev Cancer,* 3**,** 533-9.

STREISINGER, G., WALKER, C., DOWER, N., KNAUBER, D. & SINGER, F. 1981. Production of Clones of Homozygous Diploid Zebra Fish (Brachydanio-Rerio). *Nature,* 291**,** 293-296.

SUGINO, K. & NAITOH, Y. 1982. Simulated Cross-Bridge Patterns Corresponding to Ciliary Beating in Paramecium. *Nature,* 295**,** 609-611.

SUTTO, Z., CONNER, G. E. & SALATHE, M. 2004. Regulation of human airway ciliary beat frequency by intracellular pH. *J Physiol,* 560**,** 519-32.

SVARTENGREN, K., WIMAN, L. G., THYBERG, P. & RIGLER, R. 1989. Laser light scattering spectroscopy: a new method to measure tracheobronchial mucociliary activity. *Thorax,* 44**,** 539-47.

SZYMANSKA, K. & JOHNSON, C. A. 2012. The transition zone: an essential functional compartment of cilia. *Cilia,* 1**,** 10.

TAKAHASHI, A., CAMACHO, P., LECHLEITER, J. D. & HERMAN, B. 1999. Measurement of intracellular calcium. *Physiol Rev,* 79**,** 1089-125.

TAMM, S. 1994. Ca^{2+} channels and signalling in cilia and flagella. *Trends Cell Biol,* 4**,** 305-10.

TASH, J. S., KRINKS, M., PATEL, J., MEANS, R. L., KLEE, C. B. & MEANS, A. R. 1988. Identification, characterization, and functional correlation of calmodulin-dependent protein phosphatase in sperm. *J Cell Biol,* 106**,** 1625-33.

TOLEDO-PEREYRA, L. H. 2009. The strange little animals of Antony van Leeuwenhoek surgical revolution. *J Invest Surg,* 22**,** 4-8.

TRAVIS, S. M. & NELSON, D. L. 1988. Regulation of axonemal Mg^{2+}-ATPase from Paramecium cilia: effects of Ca^{2+} and cyclic nucleotides. *Biochim Biophys Acta,* 966**,** 84-93.

TSIEN, R. Y. 1980. New calcium indicators and buffers with high selectivity against magnesium and protons: design, synthesis, and properties of prototype structures. *Biochemistry,* 19**,** 2396-404.

TSUJIKAWA, M. & MALICKI, J. 2004. Intraflagellar transport genes are essential for differentiation and survival of vertebrate sensory neurons. *Neuron,* 42**,** 703-16.

TUSON, M., HE, M. & ANDERSON, K. V. 2011. Protein kinase A acts at the basal body of the primary cilium to prevent Gli2 activation and ventralization of the mouse neural tube. *Development,* 138**,** 4921-4930.

VERDUGO, P., JOHNSON, N. T. & TAM, P. Y. 1980. beta-Adrenergic stimulation of respiratory ciliary activity. *J Appl Physiol Respir Environ Exerc Physiol,* 48**,** 868-71.

VINCENSINI, L., BLISNICK, T. & BASTIN, P. 2011. 1001 model organisms to study cilia and flagella. *Biol Cell,* 103**,** 109-30.

VOLFF, J. N. 2005. Genome evolution and biodiversity in teleost fish. *Heredity (Edinb),* 94**,** 280-94.

WEBBER, W. A. & LEE, J. 1975. Fine structure of mammalian renal cilia. *Anat Rec,* 182**,** 339-43.

WEISS, T., GHEBER, L., SHOSHAN-BARMATZ, V. & PRIEL, Z. 1992. Possible mechanism of ciliary stimulation by extracellular ATP: involvement of calcium-dependent potassium channels and exogenous Ca^{2+}. *J Membr Biol,* 127**,** 185-93.

WERNER, M. E. & MITCHELL, B. J. 2013. Using Xenopus Skin to Study Cilia Development and Function. *Cilia, Pt B,* 525**,** 191-217.

WESSELY, O. & OBARA, T. 2008. Fish and frogs: models for vertebrate cilia signaling. *Front Biosci,* 13**,** 1866-80.

WHEATLEY, D. N., WANG, A. M. & STRUGNELL, G. E. 1996. Expression of primary cilia in mammalian cells. *Cell Biol Int,* 20**,** 73-81.

WHITLOCK, K. E. & WESTERFIELD, M. 1998. A transient population of neurons pioneers the olfactory pathway in the zebrafish. *Journal of Neuroscience,* 18**,** 8919-8927.

WIRSCHELL, M., OLBRICH, H., WERNER, C., TRITSCHLER, D., BOWER, R., SALE, W. S., LOGES, N. T., PENNEKAMP, P., LINDBERG, S., STENRAM, U., CARLEN, B., HORAK, E., KOHLER, G., NURNBERG, P., NURNBERG, G., PORTER, M. E. & OMRAN, H. 2013. The nexin-dynein regulatory complex subunit DRC1 is essential for motile cilia function in algae and humans. *Nat Genet,* 45**,** 262-8.

WODARCZYK, C., ROWE, I., CHIARAVALLI, M., PEMA, M., QIAN, F. & BOLETTA, A. 2009. A Novel Mouse Model Reveals that Polycystin-1 Deficiency in Ependyma and Choroid Plexus Results in Dysfunctional Cilia and Hydrocephalus. *Plos One,* 4.

WYATT, C., BARTOSZEK, E. M. & YAKSI, E. 2015. Methods for studying the zebrafish brain: past, present and future. *Eur J Neurosci,* 42**,** 1746-63.

WYATT, T. A., FORGET, M. A., ADAMS, J. M. & SISSON, J. H. 2005. Both cAMP and cGMP are required for maximal ciliary beat stimulation in a cell-free model of bovine ciliary axonemes. *American Journal of Physiology-Lung Cellular and Molecular Physiology,* 288**,** L546-L551.

WYATT, T. A., FORGET, M. A. & SISSON, J. H. 2003. Ethanol stimulates ciliary beating by dual cyclic nucleotide kinase activation in bovine bronchial epithelial cells. *American Journal of Pathology,* 163**,** 1157-1166.

YODER, B. K. 2007. Role of primary cilia in the pathogenesis of polycystic kidney disease. *J Am Soc Nephrol,* 18**,** 1381-8.

YOSHIHARA, Y. 2009. Molecular genetic dissection of the zebrafish olfactory system. *Results Probl Cell Differ,* 47**,** 97-120.

ZAGOORY, O., BRAIMAN, A., GHEBER, L. & PRIEL, Z. 2001. Role of calcium and calmodulin in ciliary stimulation induced by acetylcholine. *American Journal of Physiology-Cell Physiology,* 280**,** C100-C109.

ZHAO, C. T. & MALICKI, J. 2007. Genetic defects of pronephric cilia in zebrafish. *Mechanisms of Development,* 124**,** 605-616.

ZHU, G., INVESTIGATORS, I., GULSVIK, A., BAKKE, P., GHATTA, S., ANDERSON, W., LOMAS, D. A., SILVERMAN, E. K. & PILLAI, S. G. 2009. Association of TRPV4 gene polymorphisms with chronic obstructive pulmonary disease. *Hum Mol Genet,* 18**,** 2053-62.

ZON, L. I. & PETERSON, R. T. 2005. In vivo drug discovery in the zebrafish. *Nat Rev Drug Discov,* 4**,** 35-44.